AN ANALYSIS OF OLFACTORY CORTICAL BEHAVIOR AND FUNCTION USING COMPUTER SIMULATION TECHNIQUES

Thesis by

Matthew A. Wilson

In Partial Fulfillment of the Requirements

for the Degree of

Doctor of Philosophy

California Institute of Technology

Pasadena, California

1991

(Submitted September 25, 1990)

ACKNOWLEDGMENTS

This work would not have been possible without the contributions of numerous people over the years. Therefore, I would like to express my thanks to these individuals. To Jim Bower for his guidance, support, and vision. Through his commitment, what were once only ideas are now realities. To Mark Nelson and Upinder Bhalla for their invaluable contributions to the Genesis project, and their invaluable contributions as friends and peers. To Dave Bilitch for his unerring advice and support on software design – a resource which I hope I did not exploit too often. To John Uhley, who made sure the computers always worked as smoothly as he did. To Lew Haberly and Josh Chover who were there at the beginning and whose dedication continues to inspire me to further achivements. To John Thomson and Pat Monaghan, for being there as only friends can be. And, of course, to Janice, Robby, and Scotty, who made everything worthwhile – and always will.

ABSTRACT

This thesis presents the results of computer simulations of olfactory cortex designed to explore the role of biological mechanisms in the behavior and function of cerebral cortical networks.

Chapter 1 provides the basic description of the model of piriform cortex including simulation methodology and parameters. The results of network simulations which reproduce three characteristic macroscopic evoked cortical responses are described with the suggestion that the simulated temporal dynamics which underlie these responses may reflect the operation of a fundamental computational strategy used in the storage and retrieval of olfactory information.

Using both single cell and network simulations, chapter 2 looks in detail at the patterns of synaptic currents produced along the dendritic tree of single cells and compares simulated results with actual experimental measurements. This technique provides the means to identify the relative synaptic contributions and provides an important constraint on the selection of synaptic weight distribution parameters in the network model. The results identify the sources of synaptic inputs underlying characteristic macroscopic evoked events and thus provide additional insights into the results of chapter 1.

Using the basic model outlined in chapter 1, chapter 3 explores the effects of incorporating a mechanism for activity dependent modification of synaptic

weights along selected interconnection pathways. This is done in the context of storage and retrieval of patterned inputs to the model intended to simulate the patterns of activity which represent actual olfactory input. The results indicate that the basic model which reproduces known physiological responses can also be made to store and retrieve patterned input indicating that the dynamics of the simulated cortex are compatible with a continuous mechanism of Hebbian synaptic plasticity.

In chapter 4 the structure of the basic piriform cortex model is modified slightly to reflect more neocortical-like features. The dynamics of this modified network are compared with experimental observations of coherent oscillatory behavior in primary visual cortex. These simulations indicate that the observed behavior are characteristic of the network architecture and do not necessarily represent the encoding of stimulus specific information.

Chapter 5 provides a general overview of the simulation system used to implement all of the simulations used in this research.

Appendix 1 examines the effects of critical parameter variations on simulated EEGs.

Appendices 2 and 3 contain the complete GENESIS scripts describing the network and single cell models used in this work.

TABLE OF CONTENTS

LIST OF FIGURES

INTRODUCTION

The chemical senses may be thought of as the earliest of all sensory systems. From bacteria to primates one finds chemosensory systems designed to gather information about the environment by sampling its molecular composition (Koshland, 1980). Of the chemical senses, olfaction is one of the most sophisticated. It is found in organisms ranging from insects to mammals where it can govern a wide range of complex behaviors.

As a feat of engineering, the olfactory system remains unparalleled in its ability to detect and identify a broad range of odorants at various concentrations. While artificial systems have been designed to detect the presence of specific vaporous substances (Zarcomb and Stetter 1984), and even to discriminate from a limited number of related odorants (Persaud and Dodd, 1982; Gardner, et al. 1990), none have achieved both the sensitivity or flexibility found in biological systems. In many species, the olfactory regions of cerebral cortex are the dominant cortical structures and it has been suggested that neocortex represents an evolutionary elaboration of the basic cortical circuit established in olfactory and archicortical systems such as the hippocampus (Shepherd, 1987). Additionally, as a model system for studying sensory cortical processing, olfactory cortex is particularly attractive due to its relatively simple structure in terms of numbers of cell types, numbers of layers, and complexity of local circuits. This system is

the basis for the work to be presented in this thesis.

Olfactory overview

The process of olfaction begins with odorant molecules being drawn into the nasal cavity through inhalations which typically occur in repetitive sniffing patterns. Within the nasal cavity are a series of convoluted structures known as the nasal turbinates, which are covered by the olfactory sensory organ – the olfactory epithelium. The epithelium consists of a thin sheet of sensory cells which are covered by a mucus layer. These cells have ciliary processes which interact with odorant molecules absorbed by the mucosa. While the specific mechanism of transduction is not known, it is thought to involve the binding of odorant molecules to receptor sites located in the ciliary membrane (Lancet, 1986). This binding is believed to initiate a second messenger cascade leading to the opening of ionic channels in the cilia, depolarizing the sensory cell and producing action potentials. The responsiveness of individual sensory cells to a particular odorant is a function of the odorant quality, concentration, and flow rate, and the sensitivity and selectivity of individual sensory cells is variable. While a significant amount of current research in the field involves the classification of receptor cell response characteristics, identification of basic receptor types has been elusive. Instead it is generally observed that most cells respond to a broad range of odorants and concentrations (Moulton, 1976). Therefore,

while there does exist a small subpopulation of 'specialist' cells which are narrowly tuned to specific odorant molecules and can transmit this information in a 'labeled-line' fashion, the general process of olfactory detection and discrimination undoubtedly involves the integration of information obtained from large numbers of broadly-tuned sensory cells.

The first stage of this integration occurs in the olfactory bulb which is the cortical relay center for receptor cell input. The circuitry of this system is dominated by local excitatory and inhibitory interactions and has been compared in structure and function to the mammalian retina. Response characteristics of mitral cells in the olfactory bulb indicate that while some increase in odor specificity may occur at this level, cells remain broadly tuned to many odorants.

The next stage of integration occurs in the olfactory cortex which receives projections from the olfactory bulb. The olfactory cortex itself is made up of a number of distinct cortical areas. Among the most prominent of these areas are the anterior olfactory nucleus (AON), the olfactory tubercle (OT), amygdala, and the piriform cortex (PC). Of these areas the piriform cortex is of particular interest and is the focus of this thesis. This region is believed to be involved in discrimination of complex odors and occupies a position close to both the periphery and limbic structures which have been implicated in general memory processes, such as entorhinal cortex, and hippocampus. This structure is also

accessible for modeling due to its relatively simple structure and the availability of experimental data describing its behavior under various conditions.

Olfactory research

Research in the area of computational neuroscience can be seen as an effort, not simply to find solutions to difficult problems which have been solved by biological systems, but rather to use knowledge regarding the problems that must be solved and the constraints under which the solution must operate to understand the mechanisms which realize the desired solution. In the case of the olfactory system the problem can be initially defined as the necessity to detect and identify odorants of variable composition and concentration. This basic problem is further complicated by the need to identify specific odorants from background compositions based on context dependent saliency and to make rapid, permanent behavioral associations given brief exposures to odorants.

Efforts to understand the mechanisms of olfaction have involved psychophysical, neurophysiological, and neuroanatomical approaches. The results of these experiments have provided vast amounts of descriptive data. Interpretation of the functional significance of this data requires a framework which can consolidate known information while providing the basis for formulation and testing of new hypotheses. Modeling has been successfully used by many researchers to provide such a framework (Koch and Segev, 1989).

Models can be broadly grouped into two categories: type 1 approaches (structural modeling), in which basic function is constrained by known structure (physiology and anatomy), and type 2 approaches (functional modeling), in which basic structure is dictated by presumed function. In both cases the objective is to understand function, and the role of structure in realizing that function. Type 1 systems take advantage of experimental data but must rely on structural constraints to provide novel intuitions concerning basic function. Type 2 systems are effective at testing functional hypotheses but they typically do not take full advantage of biological systems as a source of intuition for these hypotheses.

An example of type 1 modeling is work by Traub (1989) in which he has constructed hippocampal networks, using observable physiological data as a constraint for parameter selection, in order to explore the dependence of epileptiform activity on network and single cell properties. A type 2 approach has been taken by Granger et al. (1989) in which a high-level functional hypothesis is used as a constraint for parameter selection and the resulting system is used to interpret the role of system features in that function. Poggio et al. (1985) used the type 2 approach to construct solutions to problems of early vision, and Freeman (1975) has employed both type 1 and type 2 constraints in his work in the olfactory system.

In neurobiology, one of the most successful applications of the type 1 modeling framework has been the work of Hodgkin and Huxley (1952) in which they were able to describe the behavior of excitable membranes using a concise mathematical description as manifested in quantitative which reproduced observable phenomena while capturing the qualitative features of the underlying physical mechanisms. Subsequent to this initial verification, the model provided a framework around which experiments could be designed to test system behavior based on basic model assumptions.

The modeling presented in this thesis represents a similar attempt to organize a framework for describing, not the behavior of single neurons, but rather the behavior of networks of neurons using basic mathematical descriptions of the known components of the system. The first objective of this type of modeling is, therefore, to reproduce observed phenomena and describe these phenomena as a function of modeled components. This "curve fitting" phase is greatly enhanced by the incorporation of multiple response constraints which exercise different aspects of model behavior. The olfactory literature contains many types of data which can be used for this purpose including EEG, evoked potential, intracellular recording, and current source density measurements. This provided the basis for the work presented in the early chapters. In chapter 1, observable phenomena in the form of evoked and spontaneous macroscopic field potentials

are related to the synaptic events at single cells and the timings introduced by network circuitry and interconnection patterns. Complementing these network simulation results, chapter 2 utilizes current source density data which allows visualization of current distribution patterns generated by characteristic evoked responses. In this case, the model relates the observed current source patterns to synaptic inputs with particular temporal and spatial characteristics. Together, these chapters relate a variety of experimental measurements to basic structural features governing network interactions in a coherent view of the organization of synaptic events in the olfactory cortex.

Learning

Interest in the application of neural computational principles to the solution of complex knowledge-bound problems has spawned new research in artificial neural networks which seek to understand the representation, storage and retrieval of information in parallel distributed systems such as the brain. In this abstract approach, vastly simplified networks of interconnected processing units are used to solve a wide range of pattern recognition problems. While models in this area are typically of the type 2 variety, the type 1 approach is also capable of addressing computational issues, particularly those related to biological systems.

Piriform cortex is of particular interest as a model for associative memory

function in cerebral cortex. The extensive system of association fibers which serve to interconnect pyramidal cells within the cortex are similar to patterns of connections within more abstract associative memory networks (Hopfield 1984). These abstracted systems demonstrate a number of properties which are presumably essential for any robust distributed memory system. Among these are the ability to establish multiple stable representations which can be recalled given degraded or noisy input. Establishing these properties involves procedures in which the weight, or efficacy, of synaptic transmission between units is altered according to a synaptic modification rule.

Chapter 3 describes simulations using the basic model piriform cortex which were used to investigate the behavior of the system in the presence of a postulated mechanism governing synaptic plasticity. The principle objective of this work was to determine how a system such as the piriform cortex could perform basic associative memory functions, and whether a simple, biologically plausible synaptic modification rule would operate properly in the context of actual cortical dynamics. To explore these questions, the model was presented with spatially and temporally patterned input intended to represent odor specific activity in the olfactory bulb. Sparse synaptic connections were made between pyramidal cells and from the input onto pyramidal cells and the weight of these connections was allowed to change based on pre and post synaptic activity. Un-

der these conditions, a stable spatial pattern of pyramidal cell rapidly emerged in response to patterned stimulation. This pattern could later be recalled using a partial version of the original input.

A consequence of this work was the prediction of the model that robust information storage and retrieval required the differentiation of synaptic plasticity between different interconnection pathways. Subsequent work has, in fact, provided evidence for differential pharmacological effects across these pathways (Hasselmo and Bower 1990).

This work demonstrates the ability of a continuous Hebbian mechanism to operate in the context of actual cortical dynamics to successfully store and retrieve patterned information, thus relating mechanisms of cortical behavior with properties of cortical function.

Cortical oscillations

Adrian in 1942 was the first to observe the characteristic oscillations present in the EEG of the olfactory cortex. Since that time, considerable progress has been made in relating properties of the oscillations to behavioral variables, yet the role of detailed structural mechanisms has not been demonstrated. Recent work in visual cortex uncovered similar oscillatory behavior (Gray and Singer, 1989). In this case, as well, the mechanisms governing the oscillatory properties were not understood. The model, therefore, provided an

ideal foundation for exploring the mechanisms underlying oscillations in both systems. The central question taken up in chapter 4 was the extent to which intrinsic mechanisms which result in oscillatory behavior in piriform cortex could be used to explain the behavior of other cortical systems. To study visual cortical oscillations, the model of piriform cortex was slightly modified to reflect more neocortical-like structure. Simulations of piriform cortex had revealed the importance of horizontal excitatory connections in establishing oscillatory phase relationships in that structure and, therefore, was the focus of attention in the visual cortical model. Simulations of this basic model reproduced coherent oscillatory behavior observed experimentally in visual cortex using a mechanism dependent on lateral excitatory connections. These results indicated that the phenomenon may emerge as a property of intrinsic circuitry rather than being extrinsically imposed as a computational mechanism. Here, as in piriform cortex the model served to clarify the relationship between mechanisms of cortical behavior, and proposed mechanisms of cortical function.

Summary of thesis contributions

In summary, this research has contributed a number of insights into the nature of olfactory cortical processing. These contributions are summarized below.

The network simulations of the piriform cortex revealed novel interac-

tions which were found to underlie basic cortical responses. These interactions were a consequence of complementary network and single cell parameters which resulted in characteristic dynamic behavior. These interactions were demonstrated to be consistent with known current source density measurements.

Single cell simulations which examined the contribution of specific synaptic inputs revealed the generator mechanisms underlying characteristic evoked field potentials and provided correlation between current source density measurements and synaptic inputs. The simulations also demonstrated that the known laminar distribution of inputs contributes to a differentiation of influence on cellular integration. These results suggest unique roles of these inputs in modulation of unit activity as well as mechanisms of plasticity.

Simulations which incorporated synaptic plasticity demonstrated the first successful use of a continuous Hebbian algorithm operating in the context of known cortical dynamics to store and retrieve patterned information.

The results of simulations of visual cortex demonstrated a plausible mechanism for establishing observed coherent oscillatory based soley on intrinsic network structure.

The simulation system developed during the course of this research has proven to be a valuable tool for simulation of a wide range of neurobiological systems from single cells to large scale networks and is currently in use at a

number of academic institutions.

Overall, this work represents an attempt to demonstrate the use of modeling as a tool for testing hypotheses concerning cortical function based on constraints imposed by known cortical structure.

REFERENCES

Adrian, E.D. Olfactory reactions in the brain of the hedgehog. *J. Physiol. (Lond.)* **100**, 459-472, 1942.

Freeman, W.J. *Mass action in the nervous system.* New York, Academic Press. 1975.

Gardner, J.W., Hines, E.L., Wilkinson, M. Application of artificial neural networks to an electronic olfactory system. *Meas. Sci. Technol.* **1**, 446-451, 1990.

Granger, R., Ambros-Ingerson,J., Lynch,G. Derivation of encoding characteristics of layer II cerebral cortex. *J. Cog. Neurosci.* **1**, 61-87, 1989.

Gray, C.M., Singer, W. Stimulus-specific neuronal oscillations in orientation columns of cat visual cortex. *Proc. Natl. Acad. Sci. USA* **86**, 1698-1702, 1989.

Hasselmo, M.E., Bower, J.M. Afferent and association fiber differences in short-term potentiation in piriform (olfactory) cortex. *J. Neurophysiol.* 1990.

Hodgkin, A.L., Huxley, A.F. A quantitative description of membrane current and its application to conduction and excitation in nerve. *J. Physiol. (Lond.)* **117**, 500-544, 1952.

Hopfield,J.J. Neural networks and physical systems with emergent collective computational abilities. *Proc. Natl. Acad. Sci. USA* **79**, 2554-2558, 1982.

Koch, C., Segev, I. eds. *Methods in Neural Modeling: from Synapses to Networks*, Cambridge: MIT Press, 1989.

Koshland, D.E. Bacterial chemotaxis in relation to neurobiology. *Ann. Rev. Neurosci.* **3**, 43-76, 1980.

Lancet, D. Vertebrate olfactory reception *Ann. Rev. Neurosci.* **9**, 329-355, 1986.

Moulton, D.G. Spatial patterning of response to odors in the peripheral olfactory system *Physiol. Rev.* **56**, 578-593, 1976.

Persaud, K., Dodd, G.H. Analysis of discrimination mechanisms in the mammalian olfactory system using a model nose. *Nature*, **299**, 352-355, 1982.

Poggio,T., Torre, V., Koch, C. Computational vision and regularization theory. *Nature* **317**, 314-319, 1985.

Shepherd, G.M., The basic circuit for cortical organization. In *Perspectives in Memory Research*, ed. M.S. Gazzaniga, Cambridge, MA: MIT. 1987.

Traub, R.D., Miles, R., Wong, R.K. Model of the origin of rhythmic population oscillations in the hippocampal slice. *Science* **243**, 1319-1325, 1989.

Zarcomb,S., Stetter, J.R. *Sens. Actuators* **6**, 225-243, 1984.

Cortical oscillations and temporal interactions in a computer simulation of piriform cortex

Matthew A. Wilson and James M. Bower [1]

SUMMARY AND CONCLUSIONS

1. A large-scale computer model of the piriform cortex was constructed based on the known anatomical and physiological organization of this region.

2. The oscillatory field potential and EEG activity generated by the model was compared with actual physiological results. The model was able to produce patterns of activity similar to those recorded physiologically in response to both weak and strong electrical shocks to the afferent input. The model also generated activity patterns similar to EEGs recorded in behaving animals.

3. In addition to replicating known physiological responses it has been possible to use the simulations to explore the interactions of network components which might underly these responses. This analysis suggests that the physiological properties of the cortex are dependent on the complex interaction of both network and cellular properties. In particular, we have found that the relationship between conduction velocities in intrinsic cortical fiber systems and the time constants of excitatory and inhibitory effects are critical for replicating physiological results.

[1]The authors are members of the Computation and Neural Systems Program, California Institute of Technology, Pasadena, CA 91125.

4. Analysis of the model also suggests a correspondence between the 40 Hz oscillatory patterns of activity induced by low levels of odor-like stimulation and oscillatory patterns seen in lightly anesthetized cortex in response to weak electrical shocks to the afferent fiber system.

5. The specific relationships we have found between the different components of the model also support several speculations on their functional significance. The simulations suggest that during each 40 Hz cycle of EEG activity there is a convergence in rostral cortex of afferent information from the olfactory bulb and recurrent association fiber information from caudal cortex. This convergence could underly an iterative process central to the recognition of complex olfactory stimuli.

INTRODUCTION

The study of the dynamical properties of neural and neural-like systems is rapidly becoming an important area of research within computational neurobiology (46). Recently, this interest has increased with the finding that the oscillatory properties of groups of neurons in primary visual cortex reflect specific properties of visual stimuli (9,12). For the last several years we have been exploring the general oscillatory properties of cerebral cortical networks within the context of the piriform (olfactory) cortex which is known to produce rapid periodic variations in electrical activity (5). We have used computer simulations to explore the possible cortical mechanisms responsible for these oscillatory properties as well as their potential functional significance. The simulations are based on a large-scale network model containing known features of the anatomy and physiology of the piriform cortex (50). As reported in this paper, these simulations suggest specific cellular mechanisms and network properties that could underlie the oscillatory behavior of this cortex. Further, analysis of the simulations also suggests possible functional roles for these oscillatory patterns in olfactory processing which could also be relevent to the function of cerebral cortical networks in general.

Piriform cortex

The piriform cortex is the primary olfactory cerebral cortical region in all mammals, and is believed to be involved in the recognition of complex olfactory stimuli (14,20,43,45,51). Functionally, piriform cortex is unique for a cerebral cortical structure in that it is closely tied to both the sensory periphery and to deeper cortical structures believed to be involved in fundamental aspects of learning and memory (20). Sensory input comes directly from the olfactory bulb which itself receives direct projections from olfactory receptors. Cortical output projects to limbic structures such as entorhinal cortex (23,25,30) which, in turn, project to areas such as the hippocampus (44). Thalamic pathways have also been found which directly link olfactory cortex to neocortical regions (6,29). Structurally, this cortex is also very attractive in that it is highly laminar and has a relatively small number of different cell types when compared to neocortical areas (14). These characteristics have considerably simplified the study of its anatomical and physiological organization (20).

Structure of the model

The model to be described is meant to realistically simulate the behavior of neurons across the full extent of the actual piriform cortex (approximately

10 mm x 6 mm) which contains on the order of 10^7 neurons, with approximately 5-10 different cell types (14,15). To accomplish this we have simulated 1500 cells (50x30) in each of three principle categories: excitatory pyramidal cells, feedforward inhibitory neurons, and feedback inhibitory neurons. Given the limited number of cells which can be simulated, a cell at a given array location must be representive of all cells of that type which would occupy that area in the actual cortex. The relative density of the individual cell types is reflected in the relative strength of synaptic connection between the cell types. The current model therefore simplifies the cortex to a total of 4500 cortical cells with 100 cells representing the input to the cortex from the olfactory bulb. As in the case of total cell number, the model also greatly simplifies the representation of the neurons themselves. Pyramidal cells are modeled as five coupled membrane compartments, while inhibitory neurons are represented as a single compartment. Connections between modeled cells are made by axons with finite conduction velocities which simulate the propagation of all or none action potentials using simple delay lines. No explicit axonal membrane properties are included. Synaptic activity is produced by simulating the action-potential triggered release of presynaptic transmitter. The release of transmitter induces conductance changes in channels contained within the membranes of postsynaptic cells allowing the flow of transmembrane current. Each channel is described

by parameters which govern the time course and amplitude of synaptically activated conductance changes. The membranes of modeled neurons include Na+, Cl-, and K+ ionic channels as well as a characteristic membrane capacitance and resistance. The compartmental models of the cells integrate the transmembrane and axial currents to produce transmembrane voltages. Excursions of the cell body membrane potential above a specified threshold trigger conductances which produce an action potential waveform. Intrinsic after hyperpolarizing potentials (AHPs) are not included in the model consistent with observations of actual piriform cortex layer II pyramidal cells (48).

The simulation has been designed to generate intracellular potentials, extracellular spike trains, extracellular field potentials, and EEG type recordings. The last two measures of model behavior are calculated using the three-dimensional spatial distribution of pyramidal cell membrane currents (50).

Figure 1 about here

As shown in Fig. 1, the model is based on anatomical and physiological properties of the piriform cortex itself. Parameter values are based on measure-

ments taken from the opossum and rat. While the current description of this anatomy and physiology will be limited to those features essential for understanding the model, readers interested in a more complete description of the cortex are referred to a recent review by Haberly (14). Technical details concerning the model implementation and nominal parameter values used are given in appendices A and B.

Axonal input from the olfactory bulb is delivered to the cortex via a fiber bundle known as the lateral olfactory tract (LOT). This tract projects across the surface of the cortex making sparsely distributed (8), non-topographic (24), excitatory (21,36), synaptic connections with pyramidal cells and inhibitory interneurons (19) (Fig. 1A). Conduction velocities along these axons vary with the axonal type (16,18). For example, action potentials travel along the main fiber tract towards caudal cortex at a speed of 7.0 m/s (18), while collaterals which leave the main fiber tract at a 45 degree angle (8,41) have a conduction velocity of 1.6 m/s (18). In the actual cortex there is a diminution of afferent input to pyramidal cells moving from rostral to caudal that is reflected anatomically in the number of synaptic terminals (40), and physiologically in the amplitude of shock evoked potentials mediated by the afferent system (18,36). To simulate this effect in the model, the number of afferent synaptic contacts is exponentially attenuated with increased distance from the rostral site of stimulation.

In addition to the afferent input from the olfactory bulb, a system of association fibers arising from the principle cortical cells, the pyramidal cells, also makes sparse, distributed excitatory connections with other pyramidal cells in both rostral and caudal directions (Fig. 1B) (16,21,22,23). These fibers spread out radially from the originating cell with a rostrally directed velocity of 1.0 m/s, and caudally directed velocity of 0.5 m/s (16,18). In the model, as in the cortex, there is no apparent point-to-point topography in this projection (23,33). The broad organization of association fiber projections along medial/lateral and rostral/caudal dimensions observed by Haberly, Luskin and Price (23,33) is not incorporated into the model.

In addition to these excitatory systems, there are also inhibitory feedforward and feedback circuits associated with intrinsic cortical inhibitory interneurons (Fig. 1C). Both types of inhibition observed physiologically in the pyramidal cells of piriform cortex are incorporated into the model (48). A Cl- mediated feedback inhibition is generated by local interneurons receiving input primarily from local pyramidal cell association fibers as well as some afferent fibers (2,3,17,21,22,37,38,48). The outputs of these inhibitory interneurons feed back to nearby pyramidal cells where significant conductance increases result in a relatively short lasting current shunting inhibitory effect (Fig. 1D) (21,38,39,48). In addition to this shunting type inhibition, a K+ mediated inhibition is gen-

erated by local interneurons receiving primarily direct afferent input from the LOT as well as some associational input from pyramidal cells (38,48). The outputs of these interneurons generate a long latency, long duration hyperpolarizing inhibitory potential in nearby pyramidal cells (Fig. 1D) (21,37,38,48).

As described above, most of the principle parameters of the model are highly constrained by experimental data. However, a significant parameter which is only loosely constrained is the actual distribution of synaptic weights. To compensate for modeling many fewer than the total number of actual neurons found in this cortex, pyramidal cells are fully interconnected and the strengths of individual connections are unrealistically strong. This is likely to be particularly true of the caudal to rostral association fiber system which has been clearly shown to exist (16,21,23,33,34) but which appears to be weaker than its rostral to caudal counterpart (23,33). Simulations which incorporate this feature, however, show the same qualitative patterns of activity described below.

Simulation Results

It has been shown experimentally that weak electrical shocks of the LOT in lightly anesthetized animals produce damped oscillatory evoked potentials (Fig. 2B) (10). In contrast, strong shocks to the LOT produce a simple biphasic

response (Fig. 2A) (10). It is also known that under awake behaving conditions, EEG activity recorded from the surface of piriform cortex is oscillatory with characteristic frequency components in the 3-10 Hz and 35-85 Hz range (Fig. 2C) (4). As shown in Fig. 2 and described below, our model of piriform cortex is capable of reproducing these responses while only varying parameters related to actual experimental or stimulus conditions.

Figure 2 about here

LOT shock response. Figure 3 shows the principle events underlying the simulated responses to LOT stimulation shown in Fig. 2A,B. Specifically, Fig. 3 contrasts simulated cortical activity at the same post-stimulus times, for both strong (upper panels) and weak (lower panels) LOT stimulation. In both weak and strong shocks all afferent fibers are synchronously activated to produce a single spike along each fiber. The amplitude of this spike is set to 1.0 for the strong shock and 0.4 for the weak shock. As described below, the simulation suggests that essential differences in the responses of the cortex to weak versus strong shocks result from differences in the relative timing of network events. To

understand these interactions, it will be necessary to examine these responses in some detail.

The first two vertical set of panels in Fig. 3 demonstrate that, with both types of shocks, a sweep of afferent LOT activation into the cortex activates excitatory conductances in the distal-most apical dendrite of rostral pyramidal cells (top panel), depolarizing them to threshold and initiating action potentials (fourth panel from top). The output of these pyramidal cells is distributed in all directions along the association fiber system (panels 2 and 3) both to other pyramidal cells as well as to local inhibitory feedback neurons. These inhibitory neurons, in turn, reciprocally inhibit nearby pyramidal cells (bottom panel). Inhibition from modeled feedforward inhibitory interneurons is not shown in this figure.

Figure 3 about here

While the first set of panels look similar for both shock intensities, the second set of panels show marked differences in the model behavior in each case. Specifically, at 10 msec following a strong shock, neurons have already

spiked across a large region of the cortex. With weak shocks, however, spiking activity at 10 msec is still largely confined to rostral cortex. In the model, this trend continues so that by 15 msec, afferent activity resulting from the strong shock has driven cells to spike across the full rostral to caudal extent of the cortex, while the weak shock does not activate caudal cortex until 25 msec after the shock is delivered.

Analysis of the behavior of the model shows that these differences in the spread of activity across the cortex are a direct result of the number of afferent fibers activated by the two shocks. With strong shocks, the larger number of active afferent fibers makes total afferent activity strong enough to directly drive neuronal spiking in most cortical neurons whether they are found in rostral or caudal cortex. This rapid, afferent driven activation of the cortex generates a narrow, brief latency peak in overall association fiber activity as well as a large inhibitory response. The model suggests that this combination is particularly significant in rostral cortex where the resulting superposition of a large current shunting inhibition with association fiber inputs greatly reduces the effectiveness of the excitatory association fiber system. As a consequence, cells in rostral cortex have only a single phase of increased firing in response to large LOT shocks and the resulting evoked potential has a simple biphasic waveform (Fig. 2A).

The lower set of panels in Fig. 3 demonstrates that a quite different pattern of activity results from a low amplitude shock to the LOT. In this case, afferent activity is only strong enough to produce spiking in rostral neurons. The spread of activity across the cortex results principally from the delayed arrival of association fiber activity secondary to afferent activation of rostral cells. As discussed in the description of the model, this fiber system is known to have a much lower conduction velocity than the LOT fibers (16,18). In addition, the dependence of spread on polysynaptic effects further delays caudal spread of activation. The slow spread of activity across the cortex, and the resulting delay in spiking of caudal neurons broadens activity in the association fiber system. Additionally, the smaller number of cells initially activated by low afferent stimulus intensities results in weaker inhibitory input to pyramidal cells throughout the cortex. Thus, when delayed association fiber activity reaches rostral cortex, local inhibition as a result of the initial activation of rostral cells is greatly diminished. The broadening of association fiber activity coupled with this reduced inhibition allows rostral cells to repolarize and reactivate. If the reactivation is strong enough, a new sweep of activity into caudal cortex is initiated. As a consequence, the cortical evoked potential can have multiple repeated phases of activity reflecting these additional rostral to caudal sweeps of cortical activation.

Additional manipulations were performed to examine the sensitivity of this response to variation in certain key parameters. Reduction of association fiber strength resulted in diminished oscillatory response, while increasing association strength enhanced both amplitude and duration of the response. Similarly, increasing inhibitory strength produced increased damping of the oscillatory response. Oscillatory behavior was quite sensitive to variations in association fiber velocities. Reduction of association fiber velocity reduced the frequency of and amplitude of oscillation while increasing association velocity altered the timing of the recurrent reactivation and thus eliminated multiple oscillatory periods.

In summary, these simulations suggest that the shock strength dependence of cortical evoked potentials may be related to the interplay of local properties, such as the time course of local feedback inhibition, with network properties, such as the conduction velocities of the intrinsic fiber systems mediating intracortical communication.

EEG oscillations

A similar, but more complex sequence of events results when the model is presented with LOT activity intended to more closely approximate natural patterns of stimulation. Initially, the model was given inputs with behavior derived from

the temporal activity patterns recorded in the olfactory bulbs of behaving animals (4). Given that activity in the bulb is characterized by oscillations at frequencies similar to naturally occurring cortical oscillations (4,5), it was, perhaps, to be expected that the simulated cortex generated the appropriate EEG patterns. Of more interest, however, was the behavior of the model when oscillatory input patterns were replaced by continuous random input. This input was constructed by generating independent random spikes for each afferent fiber with a poisson rate parameter of 0.5/msec. The amplitudes of each spike event were uniformly distributed over the range of 0.5 to 1. This produced afferent input with a broad distribution of energy over the range of 0-100 Hz. The EEG response of the model under these conditions displayed the same basic frequency components as the actual cortical response to periodic bulbar input (Figs. 2C and 4).

Figure 4 about here

Figure 4 displays the response of the model to the presentation of continuous random LOT input. The resulting EEG is seen to contain both the low

frequency (3-10 Hz) theta type activity as well as the higher frequency 40 Hz activity, characteristic of actual cortical EEGs (Fig. 2C). The arrows indicate the point in the EEG cycle at which data displayed in each vertical set of three panels was obtained. Notice that at the beginning of each higher frequency cycle of EEG oscillation, cells in rostral cortex are firing (second panel in each case). If the intervening data were displayed (e.g., between 0 and 33 msec), it would be possible to see that each initiation of firing in rostral cortex was followed by a sweep of activity to caudal cortex very reminiscent of the response of the cortex to weak shocks of the LOT (Fig. 3). The bottom panel in Fig. 4 details the spatial distribution of feedback inhibitory input to pyramidal cells, and indicates that, as in the case of LOT shock stimulation, feedback inhibition is also an important component in the regulation of reactivation of rostral cells in the EEG. In fact, the model suggests that the general characteristics of cortical behavior underlying the higher frequency component of the EEG are essentially the same as those seen in response to low amplitude LOT shocks.

In addition to the high frequency component of the EEG, continuous random input to the model also produces oscillations in the lower frequency theta range. The top-most panel in each column of Fig. 4 reveals the mechanism responsible for this lower frequency EEG activity in the model. These panels detail the build up of input from the feedforward class of inhibitory neurons

onto pyramidal cells over the course of the response. As described earlier, this inhibitory influence has a delayed onset, prolonged hyperpolarizing effect. As these inhibitory cells are activated by continuous afferent input and pyramidal cell feedback, their influence on pyramidal cells continues to build up until it is large enough to shut down activity in these cells. The subsequent reduction of pyramidal cell input to the feedforward inhibitory neurons over time reduces the overall level of feedforward inhibition, allowing pyramidal cell activity to eventually resume. In the model, this produces the 3-10 Hz component of the EEG response to continuous input.

DISCUSSION

Role of inhibitory neurons

While the behavior of the simulations just described is dependent on many of its structural components, results from both simulated LOT shock evoked potentials and EEGs suggest important roles for inhibition in regulating the temporal dynamics of this network. Further, simulations of the EEG suggest that the two distinct frequency components of olfactory cortical oscillation may each be regulated by a different population of inhibitory neurons. Feedforward interneurons activate a gradual, long duration, K+ mediated IPSP which result in tuning in the 3-10 Hz theta range. Feedback interneurons which mediate

a rapid, short duration Cl- based IPSP provide tuning in the 35-85 Hz range. Thus the time constants associated with the inhibitory effects of these cells are essential in the model for regulating the oscillatory properties of the network. The dispersion of frequencies modulated by these inhibitory events over a range of values despite the uniform time constants associated with the unitary events is a consequence of the distribution of synaptic strengths and thresholds within both the inhibitory and excitatory populations.

While our results certainly do not dispute the possible role of inhibitory neurons in such classic information processing functions as surround inhibition, they do suggest that the role of these cells in the regulation of cortical dynamics should also be carefully considered. Work by Freeman in modeling olfactory oscillations using a control systems approach (11) has also demonstrated the potential role of multiple inhibitory mechanisms in producing these responses. In simulations of hippocampal oscillatory behavior, Traub et al. (47) also noted the importance of inhibitory time constants in shaping periodic activity. More abstracted models of neural population behavior have also explored the role of inhibitory mechanisms in network dynamics (26,49).

Interactions among components

While inhibition clearly plays an important role in regulating the oscillatory

properties of the simulated cortex, these effects are also dependent on interactions with other components of the model. Examples include the conduction velocities of intrinsic fiber systems, the degree of excitatory coupling, the relative influence of different fiber systems in different parts of the cortex, and the spatial extent of the cortex itself. The simulations suggest that these and other components of this network may be tuned to support the oscillatory behavior observed. Recent results, suggesting that cortical neurons may oscillate intrinsically at 40 Hz (32), are consistent with this idea. Similarly, results in hippocampus indicating that stimulation at theta rhythms is optimal for generating long term potentiation (31,42), reinforce the idea that many components of a given network may be tuned to operate at particular frequencies.

General functional significance for piriform cortex

With respect to the functional significance of oscillations for the processing of olfactory information, it is important to note that this model does not include many features known to be involved in the simulated responses. For example, the olfactory bulb in this simulation is modeled as 100 neurons with no intrinsic connections and with no feedback from the cortex. However, recent experiments using current source density measurements have shown a significant periodic influence of the bulb on patterns of activity evoked in piriform cortex by low

amplitude shocks of the LOT (27). The cortex is also known to provide feedback to the bulb (7,23) which may significantly influence the input the cortex itself receives (13). For these reasons we are in the process of expanding the cortical model to include a realistic simulation of the olfactory bulb (1).

Even at its current level of detail, however, these simulations have suggested several ideas concerning the possible significance of oscillatory cortical behavior for the actual processing of olfactory information. First, it is known that the 3-10 Hz theta frequencies of the EEG oscillations are correlated with the sniffing cycle of the animal (28,35). The simulations indicate that the cortex itself may intrinsically gate activity at these behaviorally relevant frequencies. Perhaps more interesting is the behavior of the simulated network during one of these sniff related periods of high frequency EEG activity. In Fig. 4 it can be seen that during these episodes, the system periodically initiates sweeps of activity across the cortex. As described in the results, the components of the response for each sweep of activity are very similar to those underlying the damped oscillatory evoked potentials seen in response to weak shocks (Fig. 3). Closer examination of this activity pattern within a cycle suggests an interesting interpretation of the significance of the 25 msec time interval representing the dominant 40 Hz component of the EEG. Specifically, in our model this is the length of time it takes for association fiber activity arising in rostral cortex

to sweep to caudal cortex, activate caudal pyramidal cells, and then have the resulting association fiber activity project back to rostral cortex (Fig. 3). This suggests that during a burst, each reactivation of rostral cortex takes place only after adequate time has transpired for information from the rest of the cortex to converge back on rostral cells (Fig. 4). In this context the high frequency oscillation can be seen as reflecting the gating of an intrinsic network integration interval. It is interesting to note that the half-cycle time of the 40 Hz oscillation (12.5 msec) is also in the range of the estimated integration time constant for cortical pyramidal cells of 10-15 msec (14,21) suggesting a tuning might exist between the time constants of single cells and the timing relationships of network activity.

Figure 4 also demonstrates that, in simulations, the cycle of rostral to caudal activity is repeated multiple times during each EEG burst. One question raised by the occurence of this repeated activation response is what is gained by waiting until information from across the cortex has converged on rostral cells before initiating a subsequent sweep of cell firing. We suggest that by superimposing activity evoked in a previous sweep of cortical firing onto afferent information arriving from the bulb, the network might facilitate its convergence to a stable spatial pattern of activity over the course of one sniff. It is also possible that changes in the spatial pattern of cortical activity over a sniff cycle

are used to encode information. In either case, the simulations suggest that the higher frequency oscillations in the EEG could reflect the regulation of an iterative process operating at a fundamental interval of 25 msec. More generally, the modeling results are consistent with the idea that the cortex is not performing a passive integration of sensory information over the course of sensory sampling periods (sniffs), but is dynamically altering the cortical conditions under which incoming sensory information is processed.

ACKNOWLEDGMENTS

We would like to acknowledge L. Haberly and J. Chover who were instrumental in the early stages of our modeling efforts. We would also like to recognize M. Nelson and U. Bhalla for there continuing contributions to this research. Finally, we would also like to thank D. Bilitch, J. Uhley, and S. Kallenbach for their technical assistance. This work was supported by the NSF (EET-8700064), the ONR (Contract N00014-88-K-0513), the Lockheed corporation, and the Joseph Drown Foundation.

REFERENCES

1. Bhalla, U.S., Wilson, M.A., and Bower, J.M. Integration of computer simulations and multiunit recording in the rat olfactory system. *Soc. Neurosci. Abstr.* 14:1188, 1988.

2. Biedenbach, M.A. and Stevens, C.F. Electrical activity in cat olfactory cortex produced by synchronous orthodromic volleys. *J.Neurophysiol.* 32:193-203, 1969a.

3. Biedenbach, M.A. and Stevens, C.F. Synaptic organization of the cat olfactory cortex as revealed by intracellular recording. *J. Neurophysiol.* 32:204-214, 1969b.

4. Bressler, S.L. Spatial organization of EEGs from olfactory bulb and cortex. *Electroenceph. Clin. Neurophysiol.* 57:270-276, 1984.

5. Bressler, S.L. and Freeman, W.J. Frequency analysis of olfactory system EEG in cat, rabbit and rat. *Electroenceph. Clin. Neurophysiol.* 50:19-24, 1980.

6. Cinelli, A.R., Ferreyra-Moyano, H., and Barragan, E. Reciprocal functional connections of the olfactory bulbs and other olfactory related areas with the prefrontal cortex. *Brain Res. Bull.* 19:651-661, 1987.

7. Davis, B.J. and Macrides, F. The organization of centrifugal projections from the anterior olfactory nucleus, ventral hippocampal rudiment and piriform cortex to the main olfactory bulb in the hamster: An autoradiographic study. *J. Comp. Neurol.* 203:475-493, 1981.

8. Devor, M. Fiber trajectories of olfactory bulb efferents in the hamster. *J. Comp. Neurol.* 166:31-48, 1976.

9. Eckhorn, R., Bauer, R., Jordan, W., Brosch, M., Kruse, W., Munk, M., and Reitboeck, H.J. Coherent oscillations: a mechanism of feature linking in the visual cortex? *Biol. Cybern.* 60:121-130, 1988.

10. Freeman, W.J. Relations between unit activity and evoked potentials in prepyriform cortex of cats. *J. Neurophysiol.* 31:337-348, 1968.

11. Freeman, W.J. A linear distributed feedback model for prepyriform cortex. *Exp. Neurol.* 10:525-547, 1964.

12. Gray, C.M., Konig, P., Engel, A.K., Singer, W. Oscillatory responses in cat visual cortex exhibit inter-columnar synchronization which reflects global stimulus properties. *Nature* 338:334-337, 1989.

13. Gray, C.M. and Skinner, J.E. Centrifugal regulation of neuronal activity in the olfactory bulb of the waking rabbit as revealed by reversible cryogenic blockade. *Exp. Brain Res.* 69:378-386, 1988.

14. Haberly, L.B. Neuronal circuitry in olfactory cortex: anatomy and func-

tional implications. *Chem. Senses* 10:219-238, 1985.

15. Haberly, L.B. Structure of the piriform cortex of the opossum. I. Description of neuron types with golgi methods. *J. Comp. Neurol.* 213:163-187,1983.

16. Haberly, L.B. Application of collision testing to investigate properties of multiple association axons originating from single cells in the piriform cortex of the rat. *Soc. Neurosci. Abstr.* 4:75, 1978.

17. Haberly, L.B. Unitary analysis of the opossum prepyriform cortex. *J. Neurophysiol.* 36:762-774, 1973a.

18. Haberly, L.B. Summed potentials evoked in opossum prepyriform cortex. *J. Neurophysiol.* 36:775-788, 1973b.

19. Haberly, L.B. and Behan, M. Structure of the piriform cortex of the opossum. III. Ultrastructural characterization of synaptic terminals of association and olfactory bulb afferent fibers. *J. Comp. Neurol.* 219:448-460, 1984.

20. Haberly, L.B. and Bower, J.M. Olfactory cortex: model circuit for study of associative memory? *Trends in Neurosci.* 12:258-264, 1989.

21. Haberly, L.B. and Bower, J.M. Analysis of association fiber system in piriform cortex with intracellular recording and staining techniques. *J. Neurophysiol.* 51:90-112, 1984.

22. Haberly, L.B. and Presto, S. Ultrastructural analysis of synaptic relationships of intracellularly stained pyramidal cell axons in piriform cortex. *J. Comp. Neurol.* 248:464-474, 1986.

23. Haberly, L.B. and Price, J.L. Association and commissural fiber systems of the olfactory cortex of the rat. I. Systems originating in the piriform cortex and adjacent areas. *J. Comp. Neurol.* 178:711-740, 1978.

24. Haberly, L.B. and Price, J.L. The axonal projection patterns of the mitral and tufted cells of the olfactory bulb in the rat. *Brain Res.* 129:152-157, 1977.

25. Insausti, R., Amaral, D.G., and Cowan, W.M. The entorhinal cortex of the monkey: II. Cortical afferents. *J. Comp. Neurol.* 264:356-395, 1987.

26. Kammen, D.M., Holmes, P.J., and Koch, C. Cortical architecture and oscillations in neuronal networks: feedback versus local coupling. In: *Models of Brain Function*, edited by R.M.J. Cotterill, Cambridge Univ. Press. 1989.

27. Ketchum, K.L. and Haberly, L.B. CSD analysis of oscillatory responses in rat piriform cortex reveals stereotyped cyclical components mediated by afferent and intrinsic association fibers. *Soc. Neurosci. Abstr.* 14:1188, 1988.

28. Komisaruk, B.R. Synchrony between limbic system theta activity and rhyth-

mical behavior in rats. *J. Comp. Physiol. Psychol.* 70:482-492, 1970.

29. Krettek, J.E. and Price, J.L. The cortical projections of the mediodorsal nucleus and adjacent thalamic nuclei in the rat. *J. Comp. Neurol.* 171:157-192, 1977a.

30. Krettek, J.E. and Price, J.L. Projections from the amygdaloid complex and adjacent olfactory structures to the entorhinal cortex and to the subiculum in the rat and cat. *J. Comp. Neurol.* 172:723-752, 1977b.

31. Larson, J. and Lynch, G. Role of N-methyl-D-aspartate receptors in the induction of synaptic potentiation by burst stimulation patterned after the hippocampal theta-rhythm. *Brain Res.* 441:111-118, 1988.

32. Llinas, R. and Grace, A.A. Intrinsic 40 Hz oscillatory properties of layer IV neurons in guinea pig cerebral cortex *in vitro*. *Soc. Neurosci. Abstr.* 15:60, 1989.

33. Luskin, M.B. and Price, J.L. The topographic organization of associational fibers of the olfactory system in the rat, including centrifugal fibers to the olfactory bulb. *J. Comp. Neurol.* 216:264-291, 1983a.

34. Luskin, M.B. and Price, J.L. The laminar distribution of intracortical fibers originating in the olfactory cortex of the rat. *J. Comp. Neurol.* 216:292-302, 1983b.

35. Macrides, F., Eichenbaum, H.B., and Forbes, W.B. Temporal relationship

between sniffing and the limbic theta rhythm during odor discrimination reversal learning. *J. Neuroscience* 2:1705-1717, 1982.

36. Rodriguez, R. and Haberly, L.B. Analysis of synaptic events in the opossum piriform cortex with improved current source-density techniques. *J. Neurophysiol.* 61:702-718, 1989.

37. Satou, M., Mori, K., Tazawa, Y., and Takagi, S.F. Interneurons mediating fast postsynaptic inhibition in pyriform cortex of the rabbit. *J. Neurophysiol.* 50:89-101, 1983.

38. Satou, M., Mori, K., Tazawa, Y., and Takagi, S.F. Two types of postsynaptic inhibition in pyriform cortex of the rabbit: fast and slow inhibitory postsynaptic potentials. *J. Neurophysiol.* 48:1142-1156, 1982.

39. Scholfield, C.N. A depolarizing inhibitory potential in neurones of the olfactory cortexs *in vitro*. *J. Physiol. (Lond.)* 279:547-557, 1978.

40. Schwob, J.E. and Price, J.L. The cortical projection of the olfactory bulb: development in fetal and neonatal rats correlated with quantitative variations in adult rats. *Brain Res.* 151:369-374, 1978.

41. Scott, J.W., Russell, R.L., and Schneider, S.P. The organization of projections from the olfactory bulb to the piriform cortex and olfactory tubercle in the rat. *J. Comp. Neurol.* 194:519-534, 1980.

42. Staubli, U. and Lynch, G. Stable hippocampal long-term potentiation

elicited by theta pattern stimulation. *Brain Res.* 435:227-234, 1987.

43. Staubli, U., Schlottler, F., and Nejat-Bina, D. Role of dorsomedial thalamic nucleus and piriform cortex in processing of olfactory information. *Behav. Brain. Res.* 25:117-129, 1987.

44. Steward, O. Topographic organization of the projections from the entorhinal area to the hippocampal formation of the rat. *J. Comp. Neurol.* 167:285-314, 1976.

45. Tanabe, T., Iino, M., and Takagi, S.F. Discrimination of odors in olfactory bulb, pyriform-amygdaloid areas and orbitofrontal cortex of the monkey. *J. Neurophysiol.* 38:1284-1296, 1975.

46. Touretzky, D. (editor). *Advances in Neural Information Processing Systems.* San Mateo: Morgan Kaufmann Publishers, 1989.

47. Traub, R.D., Miles, R., and Wong, R.K.S. Model of the origin of rhythmic population oscillations in the hippocampal slice. *Science* 243:1319-1325, 1989.

48. Tseng, G.F. and Haberly, L.B. Characterization of synaptically mediated fast and slow inhibitory processes in piriform cortex in an *in vitro* slice preparation. *J. Neurophysiol.* 59:1352-1376, 1988.

49. Wilson, H.R. and Cowan, J.D. Excitatory and inhibitory interactions in localized populations of model neurons. *Biophysical J.* 12:1-24, 1972.

50. Wilson, M.A. and Bower, J.M. The simulation of large-scale neural networks. In:*Methods in Neuronal Modeling: From Synapses to Networks*, edited by C. Koch and I. Segev, Cambridge: MIT Press, p.291-334, 1989.

51. Wilson, M.A. and Bower, J.M. A computer simulation of olfactory cortex with functional implications for storage and recognition of olfactory information. In:*Neural Information Processing Systems* edited by D.Z. Anderson, New York: AIP Press, p. 114-126, 1988.

FIGURE LEGENDS

Fig. 1. Schematic represention of the structural features of piriform cortex which have served as the basis for the simulations discussed in the text. (**A**) The spatial pattern of projection of lateral olfactory tract (LOT) axons into and across the cortex. Note the decrease in influence of this afferent input as the LOT courses towards the caudal end of the cortex. (**B**) The excitatory connections made by LOT and intrinsic pyramidal cell axons. Note that pyramidal cell "association" connections are both local and distant. The differently shaded regions of the apical dendrite of the pyramidal cells indicate the variations in influence of each fiber system at different rostro-caudal positions in the cortex. (**C**) The basic pattern of interconnections between pyramidal cells and inhibitory interneurons. The two classes of inhibitory neurons modeled are shown. (**D**) The time course of the conductances induced by the two classes of inhibitory neurons as discussed in the text. Modified from (51).

Fig. 2. Comparison of experimentally recorded responses with those generated by our simulation. (**A**) Field potentials evoked by large amplitude shocks of the LOT. (**B**) Field potentials evoked by weak shocks (**C**) EEG recording from awake behaving animals is compared with simulated response to continuous

random input. Actual field potentials in (A) are taken from (18); those in (B) are taken from (10). EEG recordings shown in (C) are taken from (4).

Fig. 3. Comparison of the effects of weak and strong shock strengths in simulation at 5 different time steps. At each time step, 5 different features of the simulation are compared for both the high (upper panels) and low (bottom panels) shock strength conditions. Each plot represents the acitivy at each time step across the full two dimensional extent of the cortex with rostral to the left and caudal to the right. The icons at the left of the figure indicate the feature being displayed in each row of plots. The first row indicates the conductance changes due to the afferent input to the cortex. The next two rows represent conductance changes due to the influence of the rostral to caudal and caudal to rostral association fiber systems respectively. The fourth row displays the level of depolarization of the pyramidal cell somas where the size of each box indicates the level of depolarization. The last row shows conductance changes in local pyramidal cells due to the feedback inhibitory interneurons. As discussed in the text, the principal feature of interest in this figure is the reactivation found in rostral cortex at T = 35 msec in response to a weak shock strength.

Fig. 4. Patterns of pyramidal cell activity found at the beginning of each

cycle of oscillation in the simulated EEG. The arrows and lines indicate which column of plots is associated with which cycle of the EEG oscillation. The icons indicate the feature being displayed in each row of plots. The top and bottom rows indicate the conductance changes in the local pyramidal cells due to the feedforward and feedback neurons respectively. The middle row shows the depolarization of the pyramidal cells across the cortex at each time indicated. Note the changing pattern of single neuron activity associated with each cycle of the EEG.

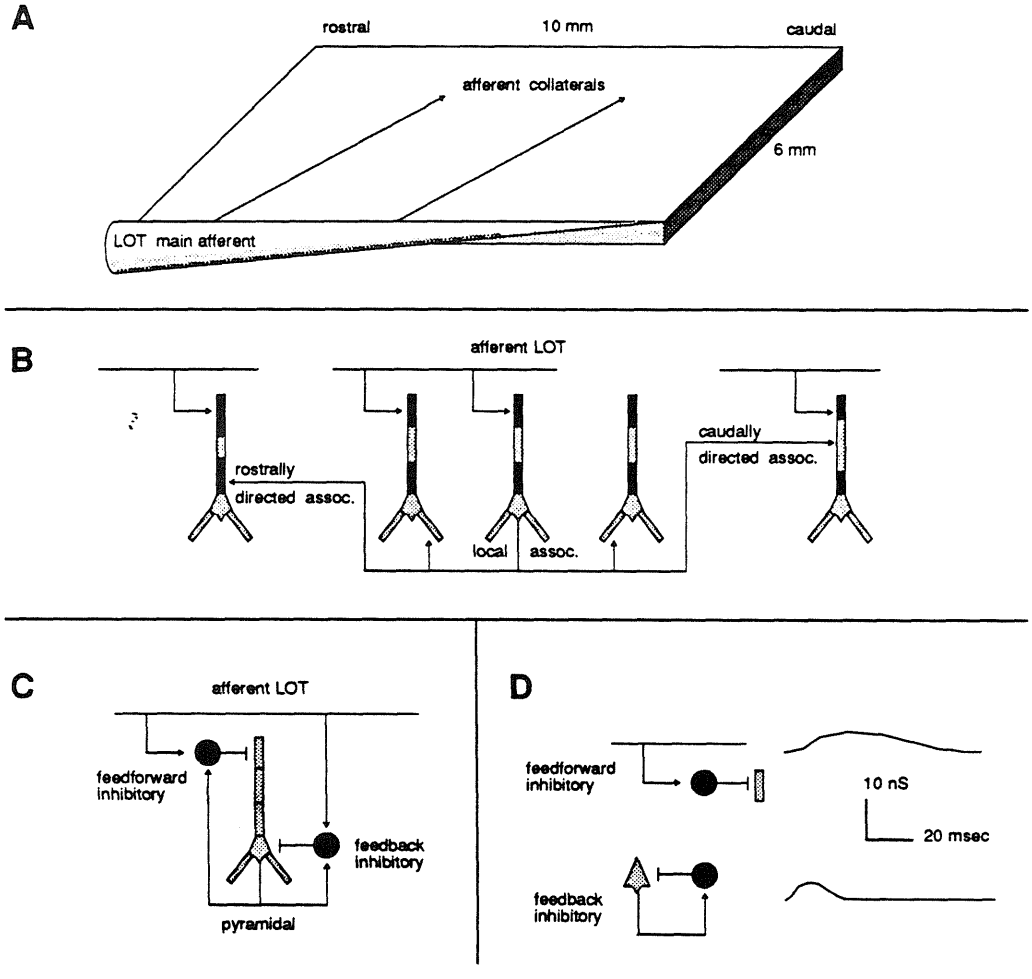
A
rostral
10 mm
caudal
afferent collaterals
6 mm
LOT main afferent
B
afferent LOT
rostrally
directed assoc.
caudally
directed assoc.
local assoc.
C
afferent LOT
feedforward
inhibitory
feedback
inhibitory
pyramidal
D
feedforward
inhibitory
10 nS
20 msec
feedback
inhibitory

FIGURE 1

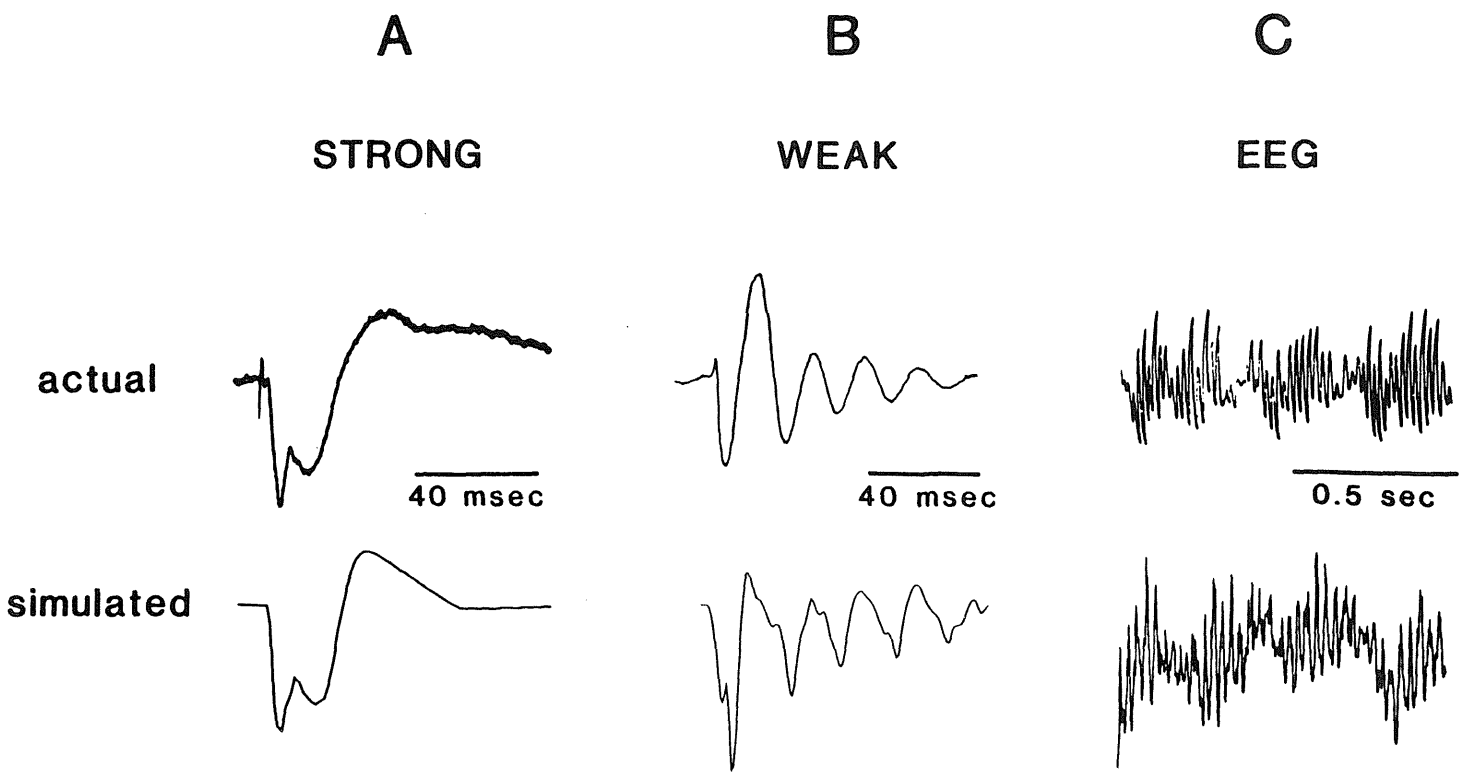

FIGURE 2

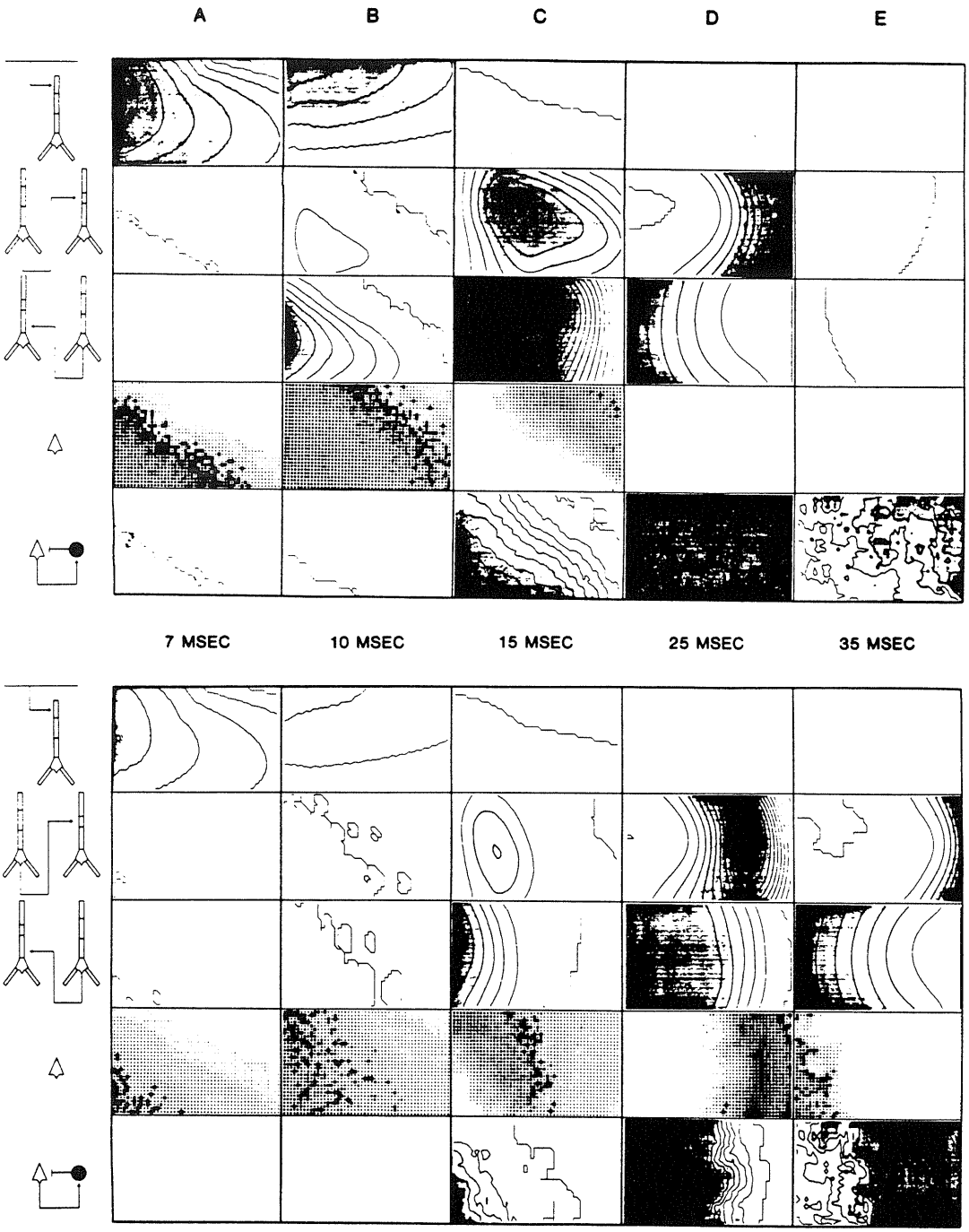

FIGURE 3

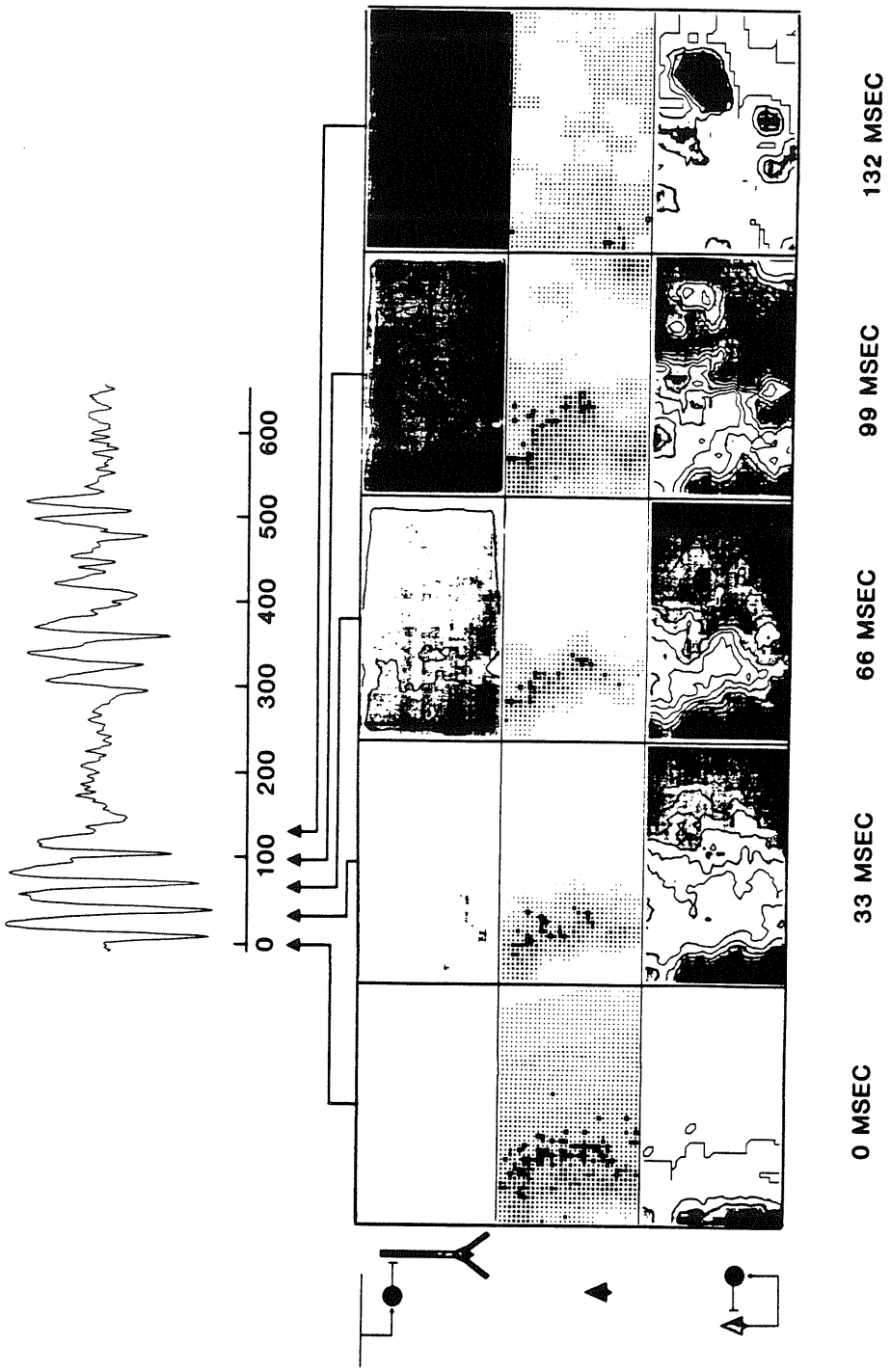

FIGURE 4

A Computer Simulation of Piriform Cortex : Synaptic Events

Matthew A. Wilson and James M. Bower [1]

SUMMARY AND CONCLUSIONS

1. Using a simple compartmental model of a single pyramidal cell, known current source density profiles from the piriform cortex of the opossum in response to shock stimuli were reproduced. Using these simulated current source profiles, depth-distributed extracellular field potentials were reconstructed and the contributions of current source components to features of the field potentials were analyzed.

2. The amplitude of the early B1 component generated by association input to proximal dendrites was found to be sensitive to the presence of the Cl- mediated shunting inhibition located near the cell body. Activation of this inhibition served to increase dipole separation of the B1 currents and therefore increase amplitude of the field potential. A smaller effect was found on the earlier A1 component due to reduced temporal overlap with the Cl- inhibitory process.

3. The period 2 component of the evoked response was found to be most sensitive to the presence of a superficial current source generated by activation of a hyperpolarizing inhibitory process. While the Cl- mediated current shunting

[1]The authors are members of the Computation and Neural Systems Program, California Institute of Technology, Pasadena, CA 91125.

inhibition located in deeper layers II and III was capable of augmenting this response, activation of the Cl- process in the absence of the superficial K+ process did not produce a significant period 2 component. Conversely, activation of the K+ process alone was sufficient to generate a significant period 2.

4. The action of shunting Cl- inhibition on dendritic and somatic membrane potential was explored. The simulated action of Cl- inhibition on intracellular membrane potentials was a current shunt which was localized to the somatic region. Integration in distal dendrites was relatively unaffected suggesting that the specific order of depth distribution and precise laminar organization of the cortex could reflect the differential action of somatic inhibitory gating.

5. Deep Ib input induced low level depolarization in both Ia dendrites and somatic regions. This is in contrast to superficial Ib input which had a potent effect on Ia depolarization. Local association fiber inputs to basal dendrites in layer III had virtually no effect on apical dendritic potentials. The segregation of inputs into distinct laminar regions may, therefore, also serve to differentiate depolarizing actions in different dendritic and somatic regions.

6. Network simulations of simple evoked shock responses were performed to determine the correspondence between the timings found to reproduce experimentally observed CSD profiles in single cell simulations and those produced by network simulation of the known circuitry. The results of these simulations

matched single cell simulations and experimental CSD profiles.

INTRODUCTION

The piriform cortex is the a primary olfactory cortical structure that has been implicated in the discrimination of complex odors (Tanabe et al., 1975; Freeman, 1978; Staubli et al., 1987ab; Boeijinga and Lopes da Silva, 1989). As a model system for studying cerebral cortex, the piriform cortex is particularly attractive due to its relatively simple structure, clear segregation of distinct synaptic pathways into well-defined laminae, the relatively planar geometry, and the availability of information concerning its anatomy and physiology.

In any cortical system, knowledge concerning the spatial and temporal structure of the input to cells becomes critical to understanding the computational properties of the network. Existing evidence suggests that the specific patterning of synaptic in the dendritic tree could have profound computational implications (Koch; Shepherd et al., 1989; Walmsley and Stuklis, 1989). The experimental techniques of intracellular and extracellular recording provide measures of state variables which only indirectly reveal the synaptic input structure. Current source density analysis of depth distributed evoked field potentials provides a more powerful tool for examining this structure (Haberly and Shepherd, 1973; Rappelsberger et al., 1981; Mitzdorf, 1985; Van Groen et al., 1987; Ferreyra-Moyano et al., 1988; Barth et al., 1989) yet successful applications of

this approach have been limited by resolution of the measurement techniques. Recently, more sophisticated CSD analyses have revealed greater detail concerning the spatial and temporal patterns of current source distribution in piriform cortex (Rodriguez and Haberly, 1989). Unfortunately, while this analysis reveals the spatial and temporal distributions of currents which give rise to observed intracellular and extracellular potentials, CSD analysis does not uniquely identify the sources of synaptic input which produce the observed patterns of current source activity.

In order to determine the patterns of synaptic inputs which could give rise to observed CSD distributions, we have used computer simulation techniques, involving compartmental models of pyramidal cells to reconstruct CSD distributions, as well as intracellular and extracellular evoked potentials in response to shock stimulation of the cortex.

Piriform cortex

The piriform cortex is a trilaminated structure. The superficial layer I contains intrinsic and extrinsic fiber pathways (layer I). The deeper layer II contains principly cell bodies of pyramidal cells. Layer III contains the basal dendrites of layer II pyramidal cell as well as cell bodies of deep pyramidal and non-pyramidal cells. Axons from the olfactory bulb travel along a pathway referred to as the lateral olfactory tract (LOT) making synaptic contact

with cells throughout the olfactory cortex. In piriform cortex these fibers terminate in a distinct superficial dendritic layer (layer Ia). In addition to the afferent input from the olfactory bulb, a system of association fibers arising from the principle cortical cells, the pyramidal cells, also makes sparse, distributed excitatory connections with other pyramidal cells in both rostral and caudal directions (fig. 1) (Haberly and Price, 1978; Haberly and Bower 1984; Haberly and Presto, 1986). These fiber systems terminate in a subregion of layer I (layer Ib) deep to the region of afferent input, with caudally directed fibers terminating more superficially in layer Ib than rostrally directed fibers. In addition to these excitatory systems, there are also inhibitory feedforward and feedback circuits associated with intrinsic cortical inhibitory interneurons (fig. 1). A Cl- mediated feedback inhibition is generated by local interneurons receiving input primarily from local pyramidal cell association fibers as well as some afferent fibers (Biedenbach 1969ab; Haberly 1973ab; Satou et al. 1982, 1983; Haberly and Bower 1984; Haberly and Presto 1986; Tseng and Haberly, 1988). The outputs of these inhibitory interneurons feed back to nearby pyramidal cells terminating primarily in layer II and superficial layer III (fig. 1) (Satou et al. 1983; Tseng and Haberly, 1988) where significant conductance increases result in a relatively short lasting current shunting inhibitory effect (Scholfield 1978; Satou et al. 1982; Haberly and Bower 1984; Tseng and Haberly 1988). In

addition to this shunting type inhibition, a K+ mediated inhibition is generated by local interneurons receiving primarily direct afferent input from the LOT as well as some associational input from pyramidal cells (fig. 1) (Satou et al. 1982; Tseng and Haberly 1988). The outputs of these interneurons generate a long latency, long duration hyperpolarizing inhibitory potential in nearby pyramidal cells (Satou et al. 1982, 1983; Haberly and Bower 1984; Tseng and Haberly 1988). These inputs are believed to terminate primarily in superficial dendrites (Haberly and Bower, 1984; Haberly et al. 1987; Tseng and Haberly, 1988).

Evoked potential

In response to a moderate strength shock stimulus to the afferent input tract of the olfactory cortex (LOT) the cortical evoked field potential has a characteristic biphasic form consisting of an initial surface negative peak lasting approximately 30 msec followed by a longer duration surface positive peak. The early surface negative peak is referred to as period I. This peak contains two characteristic subpeaks, the early A1 component and the later B1 component (fig. 2). The surface positive peak which follows is referred to as period 2 (fig. 2).

METHODS

Single cell model

In order to systematically explore the effect of particular patterns of synap-

tic input on current source density distributions and evoked potentials, a compartmental model of a pyramidal cell was constructed. Using this model, the effects of manipulations of specific inputs could be independently observed. In order to achieve high spatial resolution in the current source density profiles, the model was divided into 60 compartments each 10 um in length. To facilitate comparison of results obtained from these simulations to results obtained from network level simulations, the model consisted of a single non-branching cable which was composed of 5 distinct regions - layer Ia receiving afferent input (120 um length), superficial layer Ib receiving caudally directed association fiber input (130 um length), deep layer Ib (130 um length), layer II containing cell bodies, and layer III (100 um length) containing deep basal dendrites. To more accurately represent the distribution of current over layer II associated with the distribution of cell bodies, the layer II component was broken down into a main cell body (15 um diameter, 20 um length) and upper (10 um diam, 60 um length) and lower (10 um diam, 40 um length) segments. Parameters associated with the single cell model are given in table 1.

Synaptic input structure

Synaptic inputs were delivered to the cell according to the schedule given in table 2. Timings were selected to reproduce experimentally observed CSD events. These values are consistent with data obtained from single cell physiol-

ogy (Tseng and Haberly 1988; Haberly and Bower 1984).

Field potentials

Experimentally recorded field potentials represent the activity of cell populations. In order to reconstruct field potentials based on single cell model data a two-dimensional concentric distribution of cells (20 um spacing, radius = 2 mm) was defined. Within this population all cell bodies were placed in a single layer with dendrites perpendicular to the plane. Each cell had identical depth distributed current profiles taken from single cell simulations (see appendix A). For field potentials shown, an infinite homogeneous extracellular medium was assumed. All single cell and network simulations were carried out under the GENESIS neural simulation system (Wilson et al. 1989b) using an implicit Crank-Nicholson technique for numerical integration with an integration time step of 100 usec.

Network model

In order to evaluate results obtained from the single cell model in the context of network behavior, simulated current source profiles were generated using a network model of the cortex (Wilson and Bower 1989,1990). This model represented a 10mm x 6mm cortical area and consisted of three populations of cells – one pyramidal and two types of inhibitory interneurons (fig. 1). Each population contained 240 cells (20x12). Each pyramidal cell was modeled as a

5 compartment cable, which interneurons were represented as single compartments.

Noise

The cortex of an awake behaving animal is characterized by ongoing spontaneous activity. It has also been experimentally observed that certain evoked responses are dependent on the presence of ongoing background activation (Freeman 1968). In order to simulate the action of this steady background input in the network simulations, noise was introduced into the system by simulating the random release of transmitter at afferent and intrinsic association fiber synapses onto pyramidal cells. Transmitter pulses were of fixed amplitude with event times governed by independent poisson distributed random variables for each synaptic input. The parameters used to generate this noise are given in table 3. Spontaneous activation from inhibitory cells was not included given the purely intrinsic nature of this inhibitory activity. Instead, inhibitory cells were driven by excitatory noise input producing spontaneous inhibitory input to pyramidal cells.

Due to the high frequency of the noise (200 spikes/sec) the effect of the excitatory noise was to bias the resting potential of pyramidal cells from their nominal state of -70 mV to an average level of -55 to -60 mV. This level corresponded to a level just below the lower side of the threshold distribution for

pyramidal cells and thus produced spontaneous firing rates of 2-5 Hz. This type of noise has been examined in the acual cortex through artificial stimulation (Freeman 1968) of afferent input tracts with similar conclusions.

Noise levels on feedback inhibitory interneurons were set to provide spontaneous firing rates of 15 Hz for feedback interneurons and 1-2 Hz for feedforward interneurons. Using these levels yielded average membrane potentials of between -55 and -60 mV.

CSD profiles

The current source density (CSD) profiles shown represent the spatial distribution of transmembrane current along the z or depth axis of the cell. Membrane currents are described by their direction of flow relative to the extracellular space. Inward (extracellular to intracellular) currents are referred to as sinks and correspond to the action of depolarizing synaptic input. A distinction is made between active and passive sources and sinks. An active source is produced by the activation of a hyperpolarizing channel while an active sink corresponds to a depolarizing event. Associated with this active flow of current is a passive flow of current of equal magnitude but opposite polarity at locations distant from the site of active current flow. The locus of the active source or sink corresponds to the location of localized synaptic inputs while passive sources and sinks are distributed according to the geometry and the resistive

properties of membrane, although the location and amplitude of passive and active sources and sinks are subject to interaction.

RESULTS

Basic response

Figure 2 contains a comparison of actual depth distributed evoked field potentials with potentials produced by single cell simulations. The simulated potentials show a close correspondence between the waveforms at various recording depths. Note the correspondence of peak latencies and the latencies of zero crossings as a function of depth. The simulated fields show an A1 peak latency of 5 msec and a B1 latency of 15 msec with a period 2 peak latency of approximately 40 msec.

Figure 3 shows raster plots of membrane currents as a function of time and depth from single cell simulations and actual cortical measurements. The amplitudes and time courses of the synaptically activated conductances which produce the simulated CSD profiles and field potentials in the single cell model are shown in fig 4. The amplitude of the conductance waveforms are directly propotional to the strength of synaptic input.

A1 profile

Figure 5 shows a comparison the the current distribution associated with the A1 peak of period I. In the actual cortex, as well as in our single cell

simulations, this component consists of a current sink in layer Ia with a current source which shifts over time from a location in superficial layer Ib to layer II, extending to a lesser degree into layer III (fig 5). The shift in the current source to layer II is partially a function of activation of the shunting Cl- mediated inhibition in layer II as is seen by comparing the shift of current sources with and without the Cl- inhibitory component (fig 5).

B1 profiles

The simulated current profile associated with superficial layer Ib shows an initial passive source due to afferent activation of layer Ia. Activation of synaptic input after 6 msec results in a current sink with passive sources in layers Ia and II. This component crosses zero at approximately 25 msec latency and becomes an active source associated with the long duration K+ hyperpolarizing inhibition. The deep Ib component shows an initial passive source, due to both Ia and superficial Ib active sinks, which becomes an active sink after 8 msec. The deep component is of lower amplitude and longer duration, crossing zero between 30 and 40 msec. The B1 peak of the simulated field potential is a result of the contribution of these two components. Simulations in which the Ib inputs were suppressed show that the B1 peak is nearly completely blocked and the zero crossings to period 2 are distorted (fig 6).

Period 2 profiles

To explore the contributions of Cl- and K+ inhibitory components to period 2, simulations were performed which manipulated the relative contributions of these two inputs. Figure 7 shows the results of these manipulations. The Cl- mediated inhibition was found to have a much smaller impact on the period 2 component of the waveform than the K+ component. Supressing the K+ inhibitory input dramatically reduced period 2, while increasing amplitude and time course of Cl- input did not significantly increase period 2 amplitude (fig 7). Period 2 could be evoked in the absence of Cl- inhibitory input. The activation of the superficial K+ input alone produced a current source in superficial dendrites and a current sink distributed along deeper locations of the dendrite and into the soma.

Comparison of this response with that evoked with both Cl- and K+ components shows little difference in the period 2 components. The CSD profile for the K+ input alone shows a superficial source with the associated sinks distributed along deeper dendrites with a peak at the level of somata (layer II). This profile is quite similar to that evoked with the addition of the Cl- component. The principal effect of the Cl- inhibition is to increase the amplitude of the layer II sink.

The general shape of period 2 can be altered by adjusting the time constants of Cl- and K+ mediated inhibitory processes, although increasing the

duration of the Cl- inhibitory process in the absence of superficial K+ inhibition did not result in a significant increase in period 2 amplitude.

As in the case of the Ia sink, the Ib components are also sensitive to the activation of layer II inhibitory processes. Due to the increased temporal overlap this interaction is more prominent than that observed in layer Ia. This effect can be clearly seen in simulations in which Cl- mediated layer II inhibition was blocked showing that the B1 peak is nearly completely eliminated with no effect on the A1 peak.

Layer III profiles

The simulated layer III profile begins as a weak passive source associated with superficial Ia input which becomes an active sink after 5 msec due to excitatory input to basal dendrites. This approaches zero after approximately 25 msec and remains near zero over the course of period 2. This behavior is consistent with actual profiles (see fig. 3 for comparison).

This component has a negligible effect on the field potential as seen in fig 6 which compares simulated evoked responses with and without layer III input.

Intracellular potentials

The primary effect of the Cl- inhibition is as a current shunt which reduces the influence of excitatory inputs. This is most clearly seen in comparisons of somatic membrane potentials in which Cl- inhibition is intact with those in which

it has been blocked. The somatic membrane potential is severly attenuated in the presence of Cl- inhibition. The depolarizing potentials associated with association fiber inputs (layer Ib) are particularly affected. In contrast, potentials in distal dentrites are more insensitive to the shunting action (fig. 8). Note that because the resting potential is -70 mV which is higher than the equilibrium potential for Cl- which is taken to be -65 mV, the inhibitory influence is slightly depolarizing (Scholfield 1978).

Excitatory inputs

The contributions of the four basic excitatory inputs were explored by supressing each component and comparing the evoked and intracellular responses (figs. 6 and 9). Note that all supression effects were evaluated with inhibitory processes intact. The reduction of somatic membrane potential by suppression of Ia input lasted 10 msec following stimulation, after which normal integration of association fiber inputs occured.

Deep Ib supression had a small but long lasting affect on both dendritic (maximal difference = 5 mV) and somatic potentials (2 mV) which began at 10 msec following stimulation and lasted approximately 30 msec. Superficial Ib supression induced a pronounced reduction of superficial dendritic membrane potentials (25 mV) with a small reduction of somatic potential (4 mV). Supression of layer III input had virtually no affect on superficial dendritic potentials

(< 1 mV) and only slightly altered somatic potentials slightly (1.5 mV) over the period from 6 to 20 msec.

Blockage of afferent input completely suppressed the A1 peak but had little effect on B1 or period 2. Supression of superficial Ib input had a significant effect on the evoked field potential. The change in the evoked waveform was similar to that produced by supression of Cl- inhibitory input. Blockage of deep Ib input had very little effect on the simulated field potentials.

Modification of cellular parameters

Given the approximate nature of the geometry of single cell model the effect of modifying the electrotonic structure of the cell was explored. The diameters of the dendritic portions of the cable were varied from 2 um to 6 um and the resulting CSD profiles were compared. The effect of passive electrotonic properties had little effect on the simulated CSD distributions.

DISCUSSION

Comparison of actual and simulated CSD

The results of simulated CSD profiles indicates that the patterns of synaptic input which were selected are capable of reproducing many of the major components found in actual profiles. Despite the general agreement of results, discrepencies do arise primarily due to simplifications introduced in the model. Comparisons of simulated with actual CSD profiles show artificially distinct

boundaries between simulated sources and sinks. This is due to the complete segregation of synaptic inputs into non-overlapping dendritic regions. While introducing slightly overlapping synaptic input regions would produce more realistic profiles, it would not qualitatively change the basic results. Comparison of actual CSD profiles and simulated profiles also shows that the actual current source located in layer II which is associated with the the activation of Cl-mediated inhibition is more smoothly distributed across layers II and III (fig. 3). This does not necessarily reflect an inadequacy in the single cell model but rather the distributed nature of cell bodies over layer II in the actual cortex. The average current sources therefore become distributed over a greater depth than the space occupied by a single cell body. This could be resolved by the use of a model containing many independent cells whose cell bodies were distributed throughout the depth of layer II. While this would more accurately reproduce the more diffuse distibution of current observed experimentally, it should have no significant affect on interpretation of our results.

An additional discrepancy is found in the simulated CSD profiles which show a source appearing in layer Ia beginning at the B1 peak and continuing through period 2. The early source component observed in the simulations appears to be absent in experimentally measured CSD profiles (Rodriguez and Haberly, 1989). This difference could result from the action of several mecha-

nisms. In our simulations, the presence of the hyperpolarizing K+ inhibitory input is principly responsible for the appearance of the superficial source; therefore, increasing the latency of K+ inhibitory onset reduces the early onset of the source but also delays onset of period 2 and is not consistent with observations of intracellular latency for hyperpolarization associated with K+ inhibition. Another possible mechanism involves increasing the opening time constant for the K+ channel which diminishes the early component of the source. Shifting the distribution of K+ inhibition from layer Ia to superficial layer Ib, selectively decreasing dendritic diameter of layer Ia dendrites, and increasing overlap of association fiber inputs to layer Ia, have similar effects.

Excitatory effects

The significant variations in depolarizations introduced by different excitatory inputs in these simulations suggests that the segregation of inputs into distinct laminar regions may serve to differentiate depolarizing actions in different dendritic and somatic regions. This in in addition to its potential role in restricting pharmacological actions to particular synaptic regions for purposes of selective synaptic modulation (Hasselmo and Bower, 1990). Of particular interest was the relatively uniform depolarizing influence of rostrally directed association fiber input (deep Ib) on both dendritic and somatic areas. This is in contrast with the action of caudally directed fibers which exerted a more

powerful influence on superficial regions of afferent dendritic zones. This suggests that these caudally directed inputs may play a more significant role in modulation of activity dependent changes in afferent synapses. Conversely, the more uniform effect of deep inputs suggests a more subtle role on modulation of general activity.

The results of afferent suppression indicate that there is minimal temporal interaction between afferent and association inputs beyond intervals of 10 msec. Additionally, inputs to basal dendrites are effectively isolated from apical dendrites while still providing modest depolarization of the soma, again indicating differentiation of dendritic interactions and output modulation as a function of dendritic location.

It is important to note that while these results are suggestive of differential integrative properties present in olfactory cortical pyramidal cells, more detailed modeling of dendritic geometry is necessary to make more conclusive evaluations.

Inhibitory effects

Experimental evidence indicates that during period 2 the CSD profile shows a current sink in layer II with a corresponding source in superficial layers. The occurence of period 2 coincides with the activation of a Cl- mediated inhibition on the somata (layer II) and initial segments (layer II-II) of pyramidal

cells. It has also been demonstrated that this inhibitory event is depolarizing (-65 mV) with respect to the in vitro and suspected in vivo resting potential (-70 mV) of pyramidal cells (Haberly and Bower 1984). It has been suggested that activation of this input is primarily responsible for the observed CSD profiles and is the principal event underlying period 2 (Rodriguez and Haberly 1989). Also occuring during this period is a hyperpolarizing K+ mediated current produced by synaptic input from inhibitory interneurons. This input is primarily located on superficial dendrites and thus would produce a superficial current source which has the characteristics necessary to produce the observed surface positive period 2 waveform.

It is interesting to note that within the simulations, the principle effect of increased Cl- mediated inhibition was not on the period 2 component of the evoked response but rather on the secondary peak of the period I component. Increased Cl- inhibition increased the amplitude of the Ib peak in both superficial and deep recorded evoked responses. This follows from the shifting of the location of the current source associated with the Ib peak to layer II from more superficial locations. This has the effect of increasing the dipole separation of this component and thus increasing the associated field potential.

The relative ineffectiveness of Cl- inhibition alone in generating the period 2 field component is primarily due to the relative closeness of the Cl- equilib-

rium potential to the resting potential which accounts for the limited ability to introduce significant current flows. Additionally, in the absence of an associated superficial source, the source associated with the Cl- induced sink alone is distributed across superficial and deep dendrites which further reduces the effective dipole moment and thus the field potential.

Another consideration in assessing the impact of Cl- inhibition on the period 2 waveform is the fact that under normal conditions the cortex is subject to steady input from the olfactory bulb. This activity has the effect of biasing the membrane potential of pyramidal cells closer to the firing threshold of the cell. Network simulations have shown that steady state levels of between -55 and -60 mV are obtained given background activity levels sufficient to reproduce damped oscillatory responses associated with unanesthetized or lightly anesthetized states (unpublished observations). At the nominal resting potential of -70 mV, the Cl- mediated inhibition is slightly depolarizing, while at the presumed biased level of -60 mV the Cl- inhibitory input is hyperpolarizing therefore contributing a surface negative rather the surface positive period 2 response. Only in the presence of the superficial K+ mediated current source can the observed period 2 waveform be evoked under these conditions. It is therefore likely that the superficial source is the essential component of the period 2 response which can be enhanced by the action of the Cl- inhibitory process.

The simulated action of Cl- inhibition on intracellular membrane potentials was a current shunt which was localized to the somatic region with integration in distal dendrites relatively unaffected. The selective effect of inhibition on somatic integration of association fiber activity could have implications for the computational action of this process. As an example, dendritic interactions which govern synaptic plasticity could, in this way, proceed independently of somatic output. The distinct laminar segregation of synaptic inputs in the dendritic tree introduces the possibility of selective modulation of synaptic activity based on dendritic location. Anatomical (Luskin and Price, 1983; Haberly and Behan, 1983), physiological (Haberly and Bower, 1984; Hoffman and Haberly, 1989), and pharmacological (Collins and Howlett,1988; Ffrench-Mullen et al. 1986; Hori et al. 1982; Hasselmo and Bower, 1989, 1990) evidence has revealed differences in the properties of synapses lying within different laminae. Our results suggest that the specific order of depth distribution and precise laminar organization of the cortex could be also be based on the differential action of somatic inhibitory gating.

Network simulations

The results of network simulations show that the timing and amplitude distributions of synaptic input and depth distributed current generated by this model are consistent with results from the single cell model designed to re-

produce experimental CSD profiles. The results obtained by manipulation of individual synaptic components in the single cell simulation reveal differential contributions to integration and interactions within the dendrite which could result in differential modulation of network dynamics and modification of synaptic efficacy. Earlier network simulations revealed that the timings which produce the observed CSD profiles reflect the specific coordination of synaptic activity across the cortex within oscillatory cycles which occur during active odor discrimination. Simulations which incorporated a Hebbian mechanism for modification of synaptic efficacy demonstrated that these events were sufficient to allow storage and retrieval of patterned information encoding specific odors.

The results presented in this paper provide additional insights into the interactions between single cell biophysics and network dynamics which may underly the action of activity dependent synaptic modification and sensory discrimination in cerebral cortex. Therefore, this work represents an integral component of our efforts to construct realistic models of cortical systems capable of enabling the study of cortical computation in the context of known biological constraints.

Table 1 - pyramidal cell characteristics

Channel characteristics

channel type	equilibrium potential (mV)	tau1 (msec)	tau2 (msec)	peak conductance (mS)
Exc	0	1	3	
Cl	-65	1	18*	
K	-90	10	100	

*open time assuming light pentobarbital anesthesia

resting potential = -70 mV

Rm = 2.7e+8 Kohm-um^2

Cm = 3.0e-8 uF/um^2

Ra = 0.1e+4 Kohm-um

Rin = 38 Mohm

tau = 8.2 msec

lambda = 800 um

Input resistance (Rin) and primary membrane time constant (τ) were measured from the main soma. The space constant (λ) was evaluated by injection of current into superficial Ia and measuring resulting dc potential in the main soma.

Table 2 - synaptic input schedule

input site	channel	onset time	relative stimulus amplitude	stimulus duration (msec)	stimulus interspike decay rate (msec)	stimulus interval (msec)
Ia	Exc	1.0	6.0	10	0.1	5
supIb	Exc	6.0	1.0	20	0.5	10
deepIb	Exc	8.0	0.6	30	1.0	10
III	Exc	5.0	0.8	20	0.5	5
uppersoma	Cl	5.0	0.3	20	0.5	5
soma	Cl	5.0	0.6	20	0.5	5
lowersoma	Cl	5.0	3.0	20	0.5	5
Ia	K	5.0	0.3	20	0.5	5

Table 3 - Noise parameters

pathway	p(release/msec)	pulse amplitude
afferent	.2	700
supIb	.2	100
deepIb	.2	100
III	.2	100

Appendix A

Field potentials are generated when membrane currents generated by neurons pass through the extracellular space. These currents can be set up both by active output processes such as action potentials, as well as input processes such as synaptic currents. The field potential at any point will be composed of the linear superposition of fields generated by current sources (current from the intracellular space to the extracellular space) and sinks (current from the extracellular space into the intracellular space) distributed along multiple cells. In the following discussion the term 'current source' will be used to refer to both sources and sinks.

The value of the field potential depends on the extracellular resistivity, the location and amplitude of the current sources, and the location of the recording electrode relative to the current sources. For example, when the recording electrode is approximately equidistant from a large number of current sources

it will measure the spatially averaged field produced by these sources. This corresponds to an electrode placed on the cortical surface measuring the fields generated by a sheet of neurons beneath it (as in the EEG). As a separate example, an electrode placed very close to a smaller number of current sources would preferentially record the fields generated by those sources.

The exact contributions to the field potential by neuronal activity depend largely on the geometry of single cells and network circuitry, as well as the spatial and temporal patterns of activity both within a cell (e.g., sequence of dendritic activation), and among groups of cells (e.g., synchrony of firing).

Consider the multi-compartmental model used to generate the spatial distributions of membrane currents. The model computes a single transmembrane current I_m intended to represent the 'lumped' current across a section of membrane. If we assign each compartment an x,y,z coordinate, we can treat each lumped transmembrane current I_m as a point current source located at those coordinates.

For point current sources distributed in a linear non-capacitive medium we have (Nunez,1981)

$$V_f(t) = \frac{R_e}{4\pi} \sum_{j=1}^{n_{cells}} \sum_{k=1}^{n_{compartments}} \frac{I_{m(jk)}(t)}{r_{jk}} \qquad (1)$$

where

$$r_{jk} = \left[(x' - x_{jk})^2 + (y' - y_{jk})^2 + (z' - z_{jk})^2\right]^{\frac{1}{2}} \qquad (2)$$

The coordinates (x', y', z') give the location of the recording site. The coordinates (x^{jk}, y^{jk}, z^{jk}) give the coordinates of the compartment k in cell j. r_{jk} is the distance from compartment k in cell j to the recording site. $I_{m(jk)}$ is the transmembrane current in compartment k of cell j. R_e gives the extracellular resistivity per unit distance assuming a homogeneous extracellular medium (constant resistivity). V_f is an estimate of the extracellular field potential at (x', y', z').

Thus, in order to compute an estimate of the field potential the total transmembrane current for each compartment in each cell is summed according to the inverse distance of the current source (compartment) from the simulated recording site.

To construct the population field potential using data obtained from a single cell, we assumed a uniform concentric distribution of cells with identical response profiles. This resulted in a two-dimensional array of depth distributed current sources from which the population field could be computed using the above technique.

This research was supported by the NSF (EET-8700064), the ONR (Contract N00014-88-K-0513), and the Lockheed Corporation.

REFERENCES

Barth, D.S., Di, S., and Baumgartner, C. Laminar cortical interactions during epileptic spikes studied with principal component analysis and physiological modeling. *Brain Res.* 484:13-35, 1989.

Biedenbach, M.A. and Stevens, C.F. Electrical activity in cat olfactory cortex produced by synchronous orthodromic volleys. *J.Neurophysiol.* 32:193-203, 1969a.

Biedenbach, M.A. and Stevens, C.F. Synaptic organization of the cat olfactory cortex as revealed by intracellular recording. *J. Neurophysiol.* 32:204-214, 1969b.

Boeijinga, P.H., and Lopes da Silva, F.H. Modulations of EEG activity in the entorhinal cortex and forebrain olfactory areas during odour sampling. *Brain Res.* 478:257-268, 1989.

Collins, G.G.S., and Howlett, S.J. The pharmacology of excitatory transmission in the rat olfactory cortex slice *Neuropharmacology* 27:697-705, 1988.

Ferreyra-Moyano, H., Cinelli, A.R., Molina, J.C., and Barragan, E. Current generators and properties of late components evoked in rat olfactory cortex. *Brain Res. Bull.* 20:433-446, 1988.

Ffrench-Mullen, J.M.H., Hori, N., and Carpenter, D.O. Receptors for excitatory

amino acids on neurons in rat pyriform cortex *J. Neurophysiol.* 55:1283-1294, 1986.

Freeman, W.J. Effects of surgical isolation and tetanization on prepyriform cortex in cats. *J. Neurophysiol.* 31:349-357, 1968.

Freeman, W.J. Spatial properties of an EEG event in the olfactory bulb and cortex *Electroenceph. and clin. Neurophysiol.* 44:586-605, 1978.

Haberly, L.B. Unitary analysis of the opossum prepyriform cortex. *J. Neurophysiol.* 36:762-774, 1973a.

Haberly, L.B. Summed potentials evoked in opossum prepyriform cortex. *J. Neurophysiol.* 36:775-788, 1973b.

Haberly, L.B. and Behan, M. Struture of the piriform cortex of the opossum. III. Ultrastructural characterization of synaptic terminals of association and olfactory bulb afferent fibers. *J. Comp. Neurol.* 219:448-460, 1983.

Haberly, L.B. and Bower, J.M. Analysis of association fiber system in piriform cortex with intracellular recording and staining techniques. *J. Neurophysiol.* 51:90-112, 1984.

Haberly, L.B., Hansen, D.J., Feig, S.L., Presto, S. Distribution and ultrastructure of neurons in opossum piriform cortex displaying immunoreactivity to GABA and GAD and high-affinity tritiated GABA uptake. *J. Comp Neurol.* 266:269-290, 1987.

Haberly, L.B. and Presto, S. Ultrastructural analysis of synaptic relationships of intracellularly stained pyramidal cell axons in piriform cortex. *J. Comp. Neurol.* 248:464-474, 1986.

Haberly, L.B. and Price, J.L. Association and commissural fiber systems of the olfactory cortex of the rat. I. Systems originating in the piriform cortex and adjacent areas. *J. Comp. Neur.* 178:711-740, 1978.

Haberly, L.B. and Shepherd, G.M. Current-density analysis of summed evoked potentials in opossum prepyriform cortex. *J. Neurophysiol.* 36:789-802, 1973.

Hoffman, W.H. and Haberly, L.B. Bursting induces persistent all-or-none EPSPs by an NMDA-dependent process in piriform cortex. *J. Neuroscience* 9:206-215, 1989.

Hori, N., Auker, C.R., Braitman, D.J., and Carpenter, D.O. Pharmacologic sensitivity of amino acid responses and synaptic activation of in vitro prepyriform neurons. *J. Neurophysiol.* 48:1289-1301, 1982.

Luskin, M.B., Price, J.L. The laminar distribution of intracortical fibers originating in the olfactory cortex of the rat *J. Comp. Neurol.* 216:292-302, 1983.

Mitzdorf, U. Current source-density method and application in cat cerebral cortex: Investigation of evoked potentials and EEG phenomena. *Physiol.*

Rev. 65: 37-100, 1985.

Rappelsberger, P., Pockberger, H., and Petsche, H. Current source density analysis: Methods and application to simultaneously recorded field potentials of the rabbit's visual cortex. *Pflugers Arch.* 389:159-170, 1981.

Rodriguez, R. and Haberly, L.B. Analysis of synaptic events in the opossum piriform cortex with improved current source density techiques. *J. Neurophysiol.* 61: 702-718, 1989.

Satou, M., Mori, K., Tazawa, Y., and Takagi, S.F. Interneurons mediating fast postsynaptic inhibition in pyriform cortex of the rabbit. *J. Neurophysiol.* 50:89-101, 1983.

Satou, M., Mori, K., Tazawa, Y., and Takagi, S.F. Two types of postsynaptic inhibition in pyriform cortex of the rabbit: fast and slow inhibitory postsynaptic potentials. *J. Neurophysiol.* 48:1142-1156, 1982.

Scholfield, C.N. A depolarizing inhibitory potential in neurones of the olfactory cortexs *in vitro*. *J. Physiol. (Lond.)* 279:547-557, 1978.

Shepherd, G.M., Woolf, T.B., and Carnevale, N.T. Comparisons between active properties of distal dendritic branches and spines: Implications for neuronal computations. *J. Cog. Neurosci.* 1:273-286, 1989.

Staubli,U., Fraser, D., Faraday, R., and Lynch, G. Olfaction and the data memory system in rats. *Behav. Neurosci.* 101:757-765, 1987a.

Staubli, U., Schottler, F., and Nejat-Bina, D. Role of dorsomedial thalamic nucleus and piriform cortex in processing olfactory information. *Behav. Brain Res.* 25:117-129, 1987b.

Tanabe,T., Iino, M., and Takagi, S.F. Discrimination of odors in olfactory bulb, pyriform-amygdaloid areas, and orbitofrontal cortex of the monkey *J. Neurophysiol.* 38:1284-1296, 1975.

Tseng, G.F. and Haberly, L.B. Characterization of synaptically mediated fast and slow inhibitory processes in piriform cortex in an *in vitro* slice preparation. *J. Neurophysiol.* 59:1352-1376, 1988.

Van Groen, Th., Lopes da Silva, F.H., and Wadman, W.J. Synaptic organization of olfactory inputs and local circuits in the entrorhinal cortex: a current source density analysis in the cat. *Exp. Brain Res.* 67:615-622, 1987.

Walmsley, B. and Stuklis, R. Effects of spatial and temporal dispersion of synaptic input on the time course of synaptic potentials *J. Neurophysiol.* 61:681-687, 1989.

Wilson, M.A. and Bower, J.M.(1988) A computer simulation of olfactory cortex with functional implications for storage and retrieval of olfactory information, In: *Neural Information Processing Systems*, edited by D.Z. Anderson, New York: AIP Press, 114-126.

Wilson, M.A. and Bower, J.M. The simulation of large-scale neuronal networks,

In: *Methods in Neural Modeling: from Synapses to Networks*, edited by C.Koch and I.Segev, Cambridge: MIT Press, 291-334. 1989a.

Wilson, M.A., Bhalla, U.S., Uhley, J.D., and Bower, J.M. GENESIS: A System for Simulating Neural Networks. In D. S. Touretzky (ed.), *Advances in Neural Information Processing Systems 1.* San Mateo, CA: Morgan Kaufmann, 485-492. 1989b.

Wilson, M.A. and Bower, J.M. Cortical oscillations and temporal interactions in a computer simulation of piriform cortex. (to appear in J. Neurophysiol.)

FIGURE LEGENDS

Fig. 1. Schematic diagram of the circuitry in piriform cortex showing the laminar organization of afferent, excitatory associational, and local inhibitory inputs.

Fig. 2. Comparison of actual and simulated evoked potentials measured at different depths within the cortex in response to electrical stimulation of the LOT. (Actual measurements modified from Rodriguez and Haberly 1989).

Fig. 3. Comparison of actual and simulated current source density profiles measured at different depths within the cortex in response to electrical stimulation of the LOT. Inward currents (sinks) are indicated as positive deflections on the traces. (Actual profiles modified from Rodriguez and Haberly 1989).

Fig. 4. Top: Simulated synaptically activated conductances which produced the evoked potentials shown in figure 2 and the current source density profiles shown in figure 3. Bottom: Conductances generated by network simulation of shock response which produced evoked potentials and CSD profiles shown in figure 10.

Fig. 5. Top: Current source density profiles as a function of depth at successive times during the A1 peak showing the shift of the source associated with the A1 peak from superficial layers to layer II during the activation of the Cl- inhibitory input. Bottom: Equivalent profiles with Cl- inhibitory input blocked.

Fig. 6. Comparison of simulated evoked potentials in which individual excitatory synaptic components have been suppressed.

Fig. 7. Comparison of simulated evoked potentials in which individual inhibitory synaptic components have been suppressed.

Fig. 8. Comparison of membrane potentials along different depths of the dendritic tree in which individual excitatory synaptic components have been suppressed.

Fig. 9. Comparison of membrane potentials along different depths of the dendritic tree in which individual inhibitory synaptic components have been suppressed.

Fig. 10. Evoked potentials and current source density profiles generated by network simulation of piriform cortex.

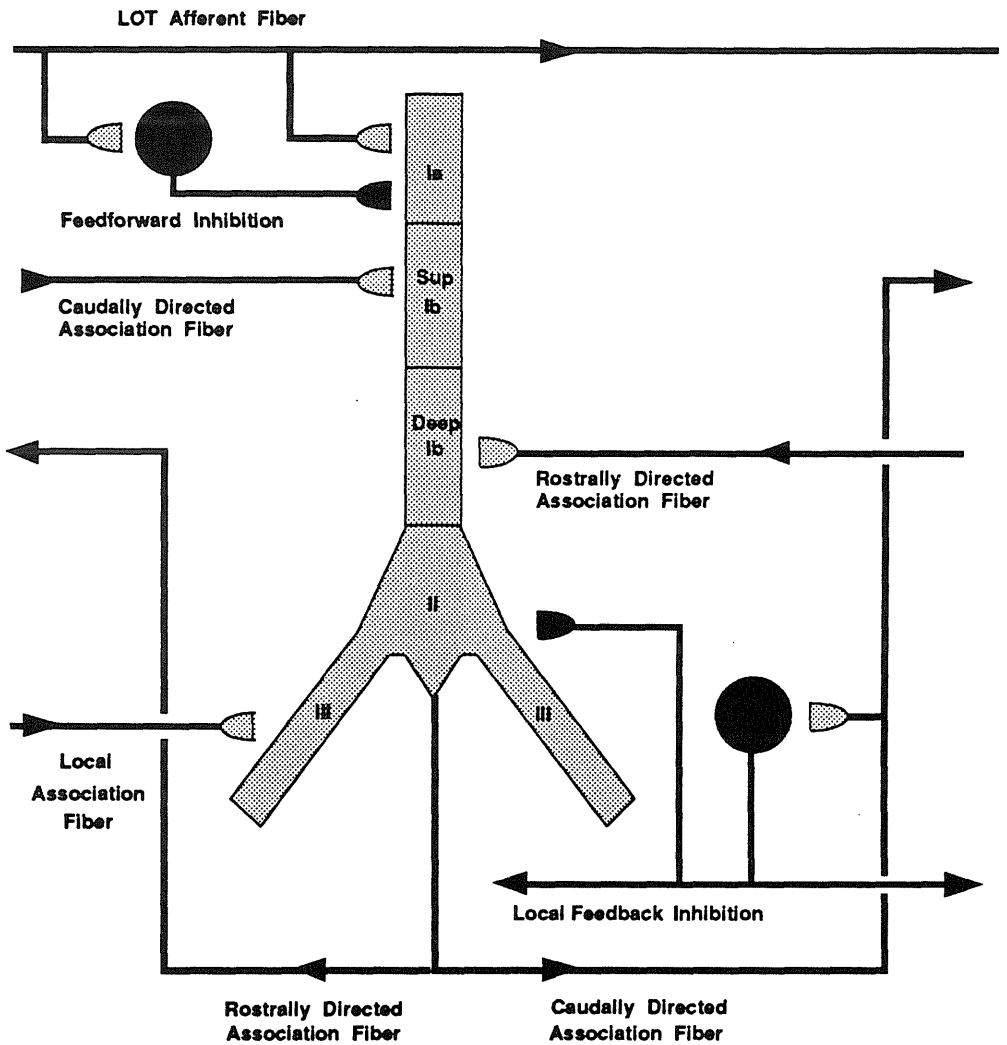
LOT Afferent Fiber
Ia
Feedforward Inhibition
Sup Ib
Caudally Directed Association Fiber
Deep Ib
Rostrally Directed Association Fiber
II
III
III
Local Association Fiber
Local Feedback Inhibition
Rostrally Directed Association Fiber
Caudally Directed Association Fiber

Figure 1

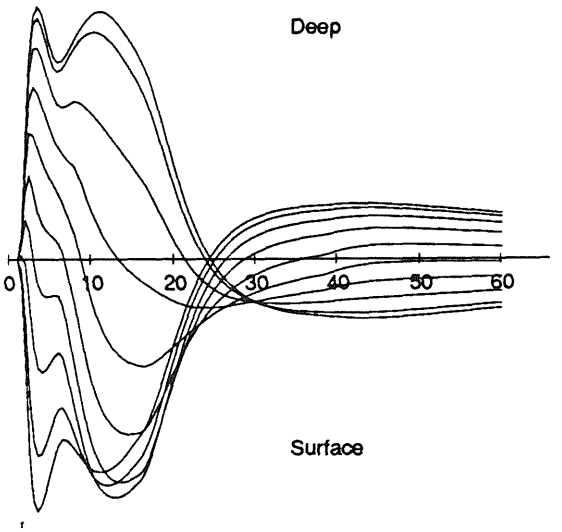

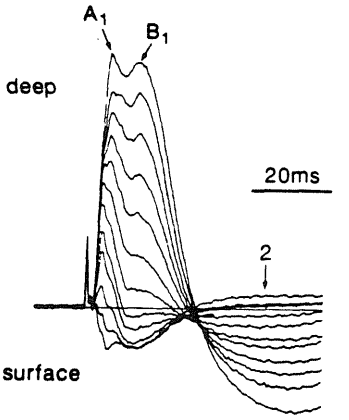

Figure 2

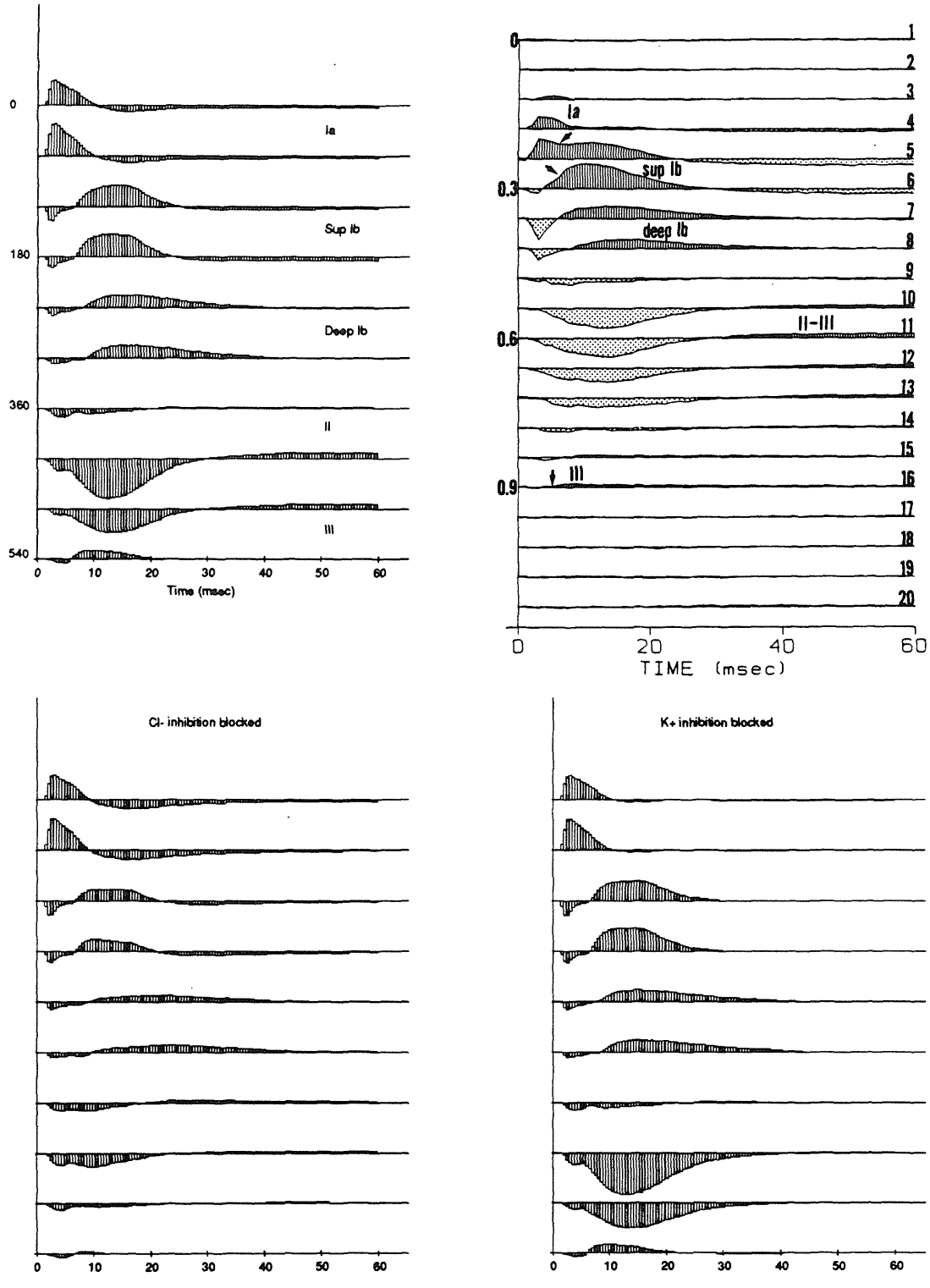
0
180
360
540
Ia
Sup Ib
Deep Ib
II
III
0 10 20 30 40 50 60
Time (msec)
0
0.3
0.6
0.9
1 2 3 4 5 6 7 8 9 10 11 12 13 14 15 16 17 18 19 20
Ia
sup Ib
deep Ib
II-III
III
0 20 40 60
TIME (msec)
Cl- inhibition blocked
K+ inhibition blocked
0 10 20 30 40 50 60
0 10 20 30 40 50 60

Figure 3

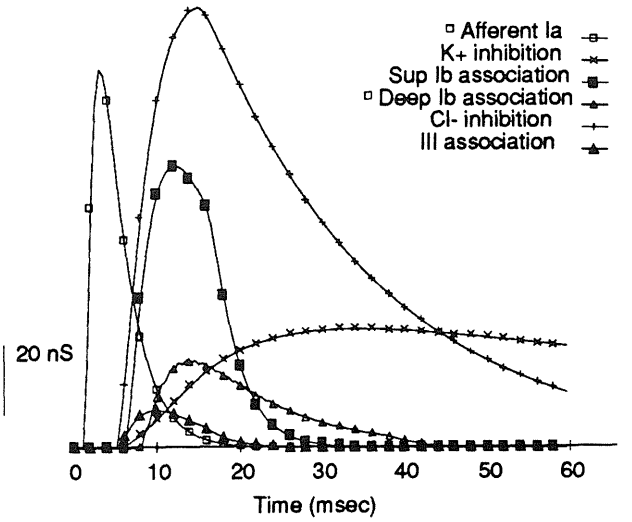
Afferent Ia
K+ inhibition
Sup Ib association
Deep Ib association
Cl- inhibition
III association
20 nS
0
10
20
30
40
50
60
Time (msec)

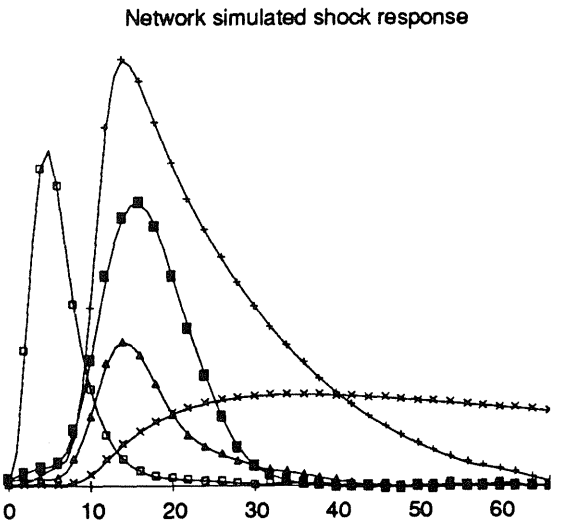
Network simulated shock response
0
10
20
30
40
50
60

Figure 4

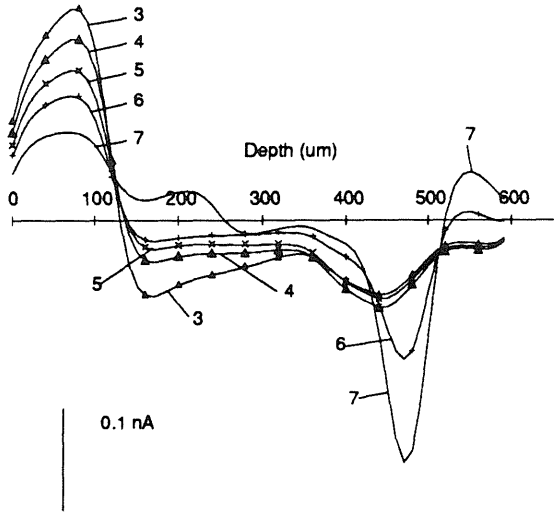
3
4
5
6
7
Depth (um)
7
0
100
200
300
400
500
600
5
4
3
6
7
0.1 nA

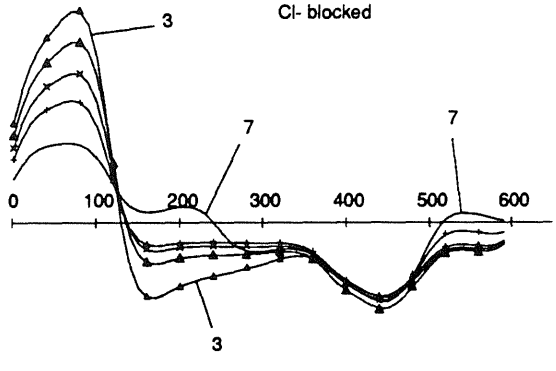
Cl- blocked
3
7
7
0
100
200
300
400
500
600
3

Figure 5

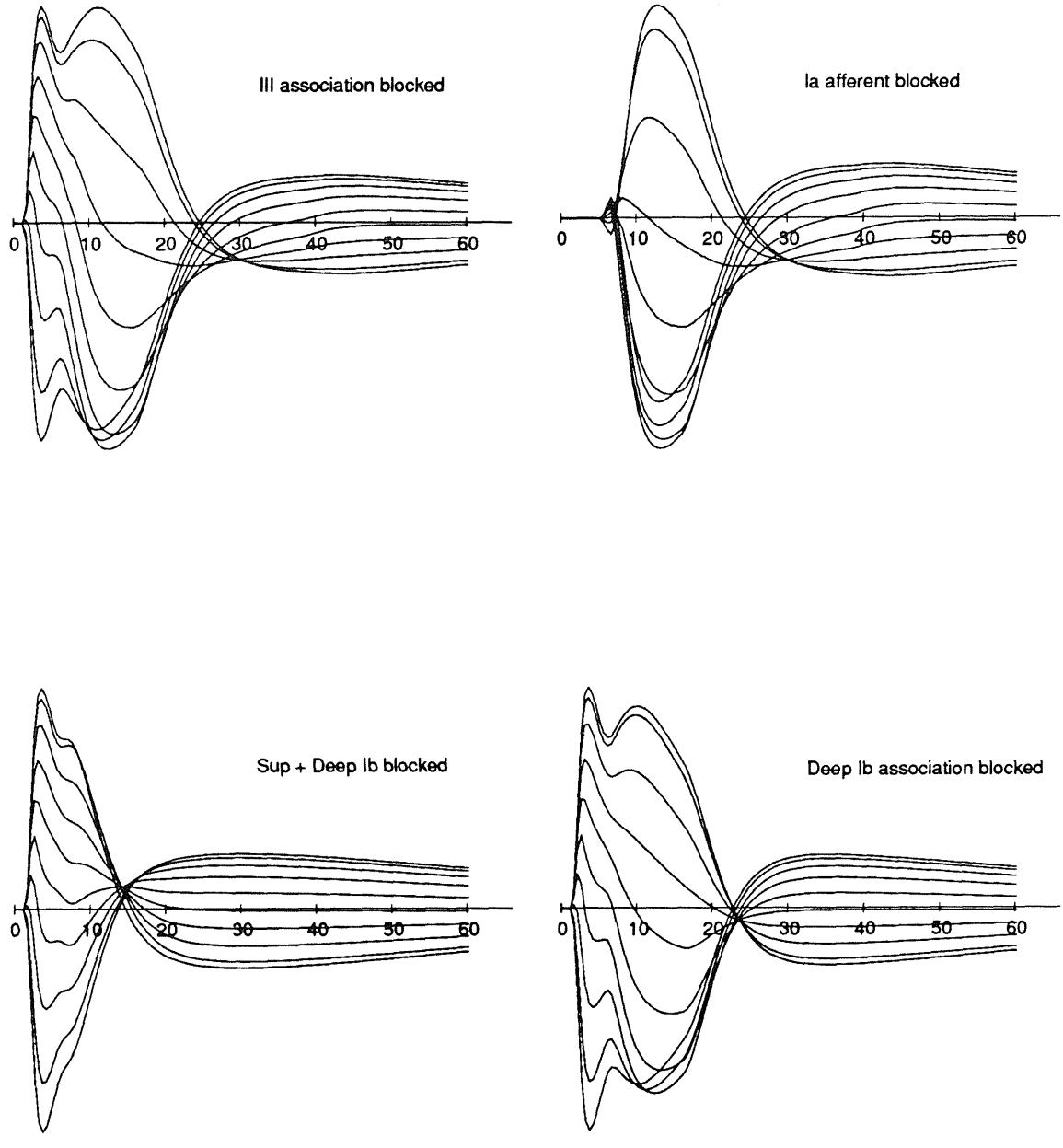
III association blocked
Ia afferent blocked
Sup + Deep Ib blocked
Deep Ib association blocked
0
10
20
30
40
50
60

Figure 6

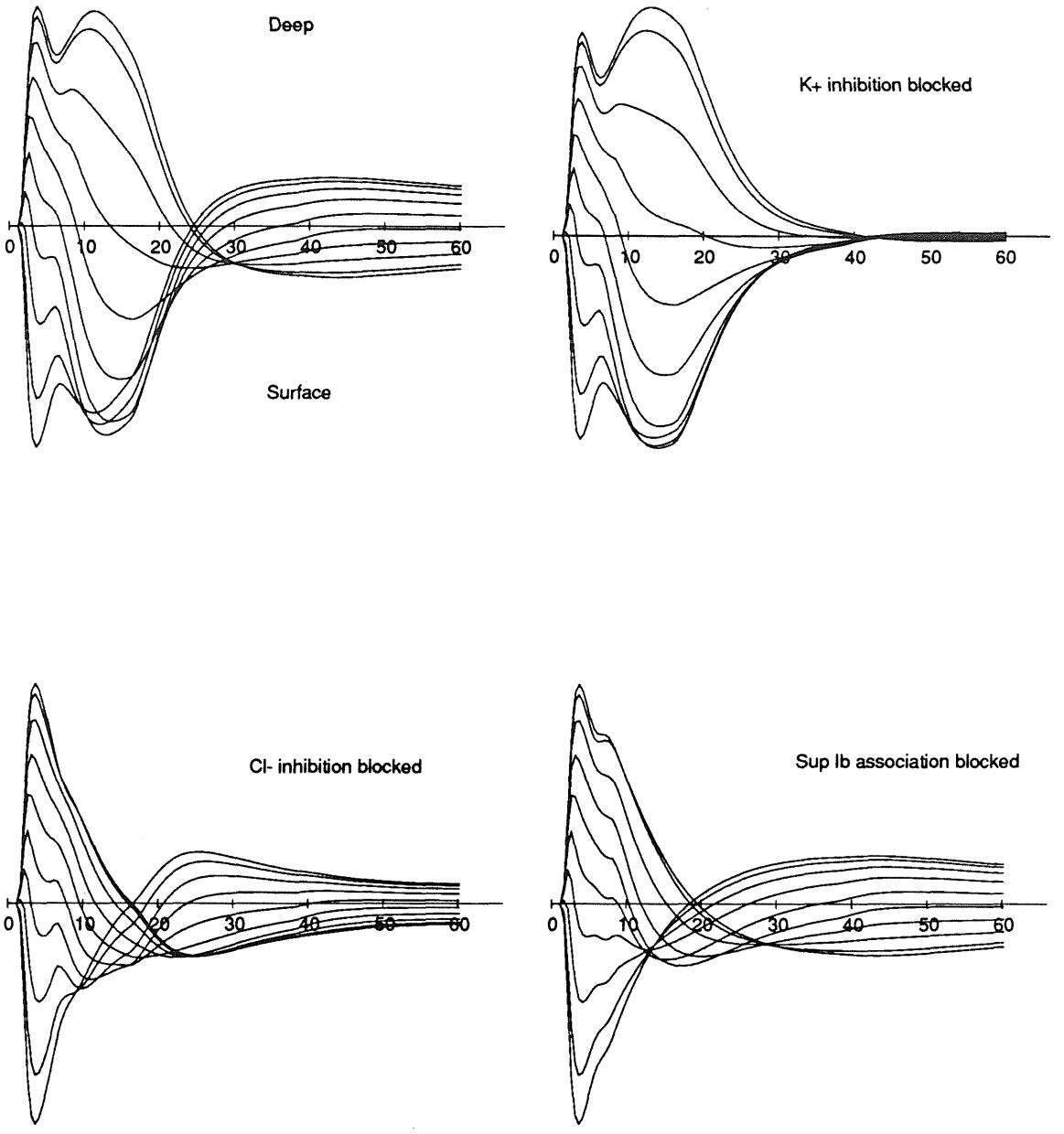
Deep
Surface
0
10
20
30
40
50
60
K+ inhibition blocked
Cl- inhibition blocked
Sup Ib association blocked

Figure 7

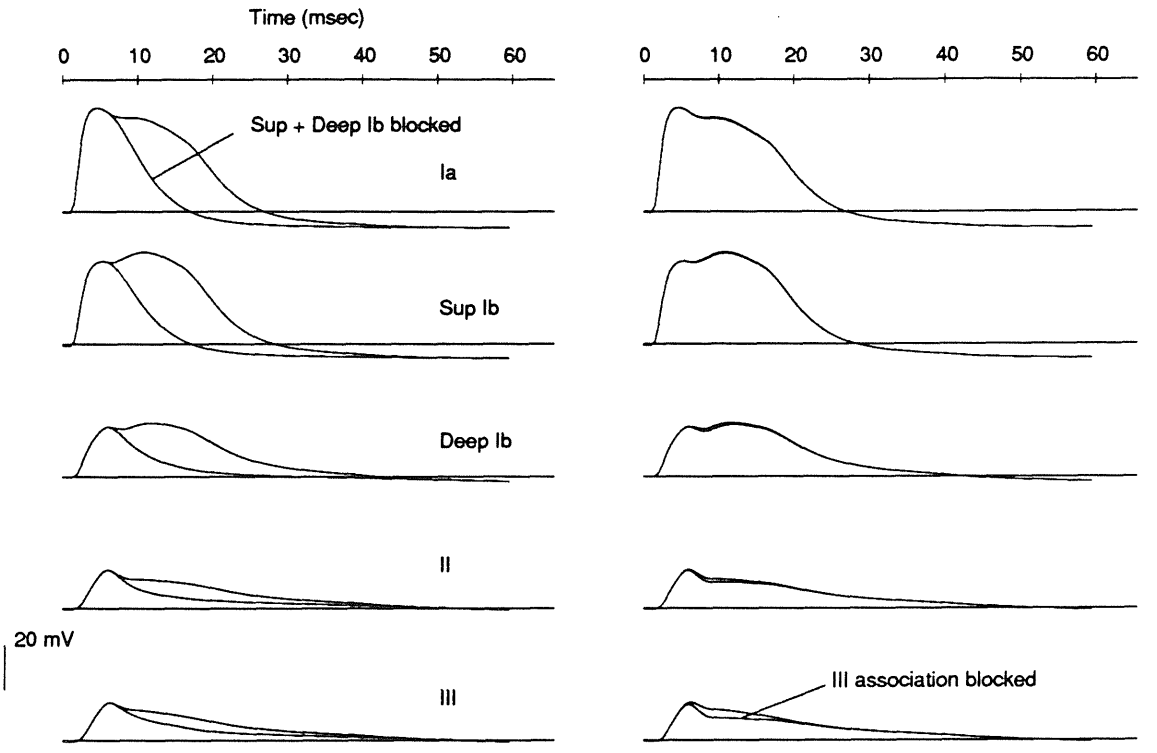
Time (msec)
0
10
20
30
40
50
60
Sup + Deep Ib blocked
Ia
Sup Ib
Deep Ib
II
20 mV
III
III association blocked

Figure 8

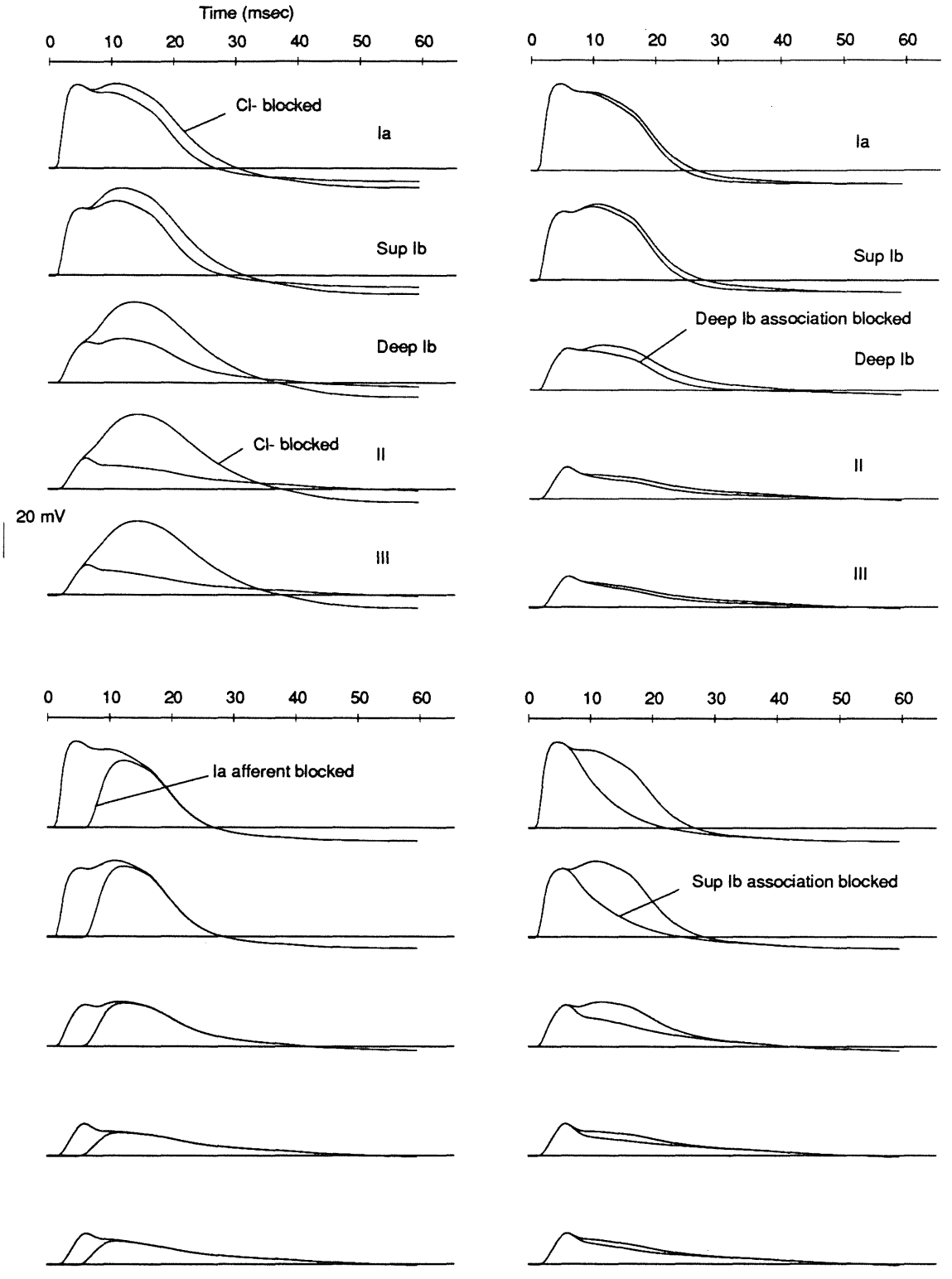
Time (msec)
0
10
20
30
40
50
60
Cl- blocked
Ia
Sup Ib
Deep Ib
Cl- blocked
II
20 mV
III
Deep Ib association blocked
Ia afferent blocked
Sup Ib association blocked

Figure 9

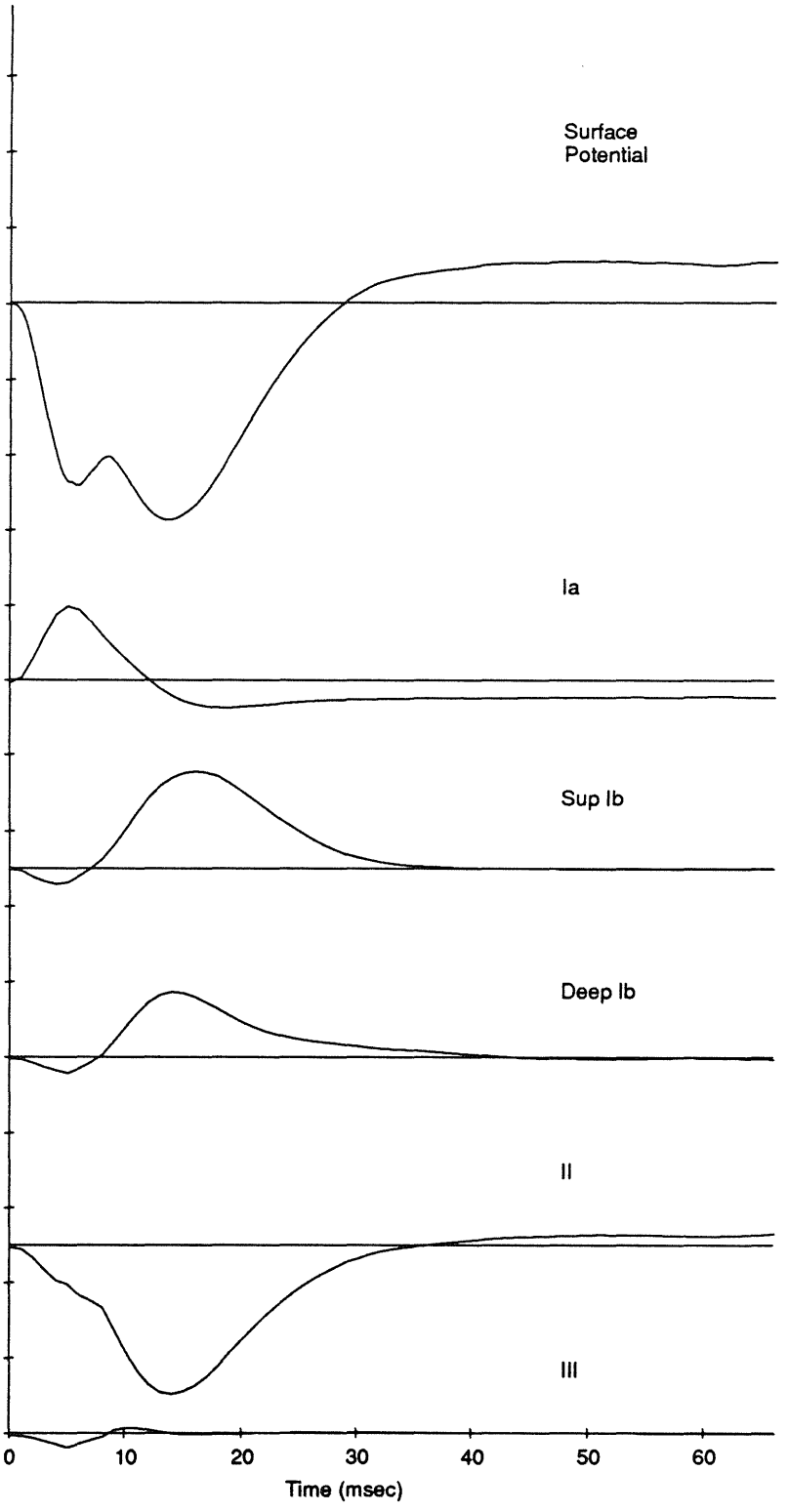
Surface
Potential
Ia
Sup Ib
Deep Ib
II
III
0
10
20
30
40
50
60
Time (msec)

Figure 10

A Computer Simulation of Olfactory Cortex With Functional Implications for Storage and Retrieval of Olfactory Information

Matthew A. Wilson and James M. Bower
Computation and Neural Systems Program
Division of Biology, California Institute of Technology, Pasadena, CA 91125

ABSTRACT

Based on anatomical and physiological data, we have developed a computer simulation of piriform (olfactory) cortex which is capable of reproducing spatial and temporal patterns of actual cortical activity under a variety of conditions. Using a simple Hebb-type learning rule in conjunction with the cortical dynamics which emerge from the anatomical and physiological organization of the model, the simulations are capable of establishing cortical representations for different input patterns. The basis of these representations lies in the interaction of sparsely distributed, highly divergent/convergent interconnections between modeled neurons. We have shown that different representations can be stored with minimal interference, and that following learning these representations are resistant to input degradation, allowing reconstruction of a representation following only a partial presentation of an original training stimulus. Further, we have demonstrated that the degree of overlap of cortical representations for different stimuli can also be modulated. For instance similar input patterns can be induced to generate distinct cortical representations (discrimination), while dissimilar inputs can be induced to generate overlapping representations (accommodation). Both features are presumably important in classifying olfactory stimuli.

INTRODUCTION

Piriform cortex is a primary olfactory cerebral cortical structure which receives second order input from the olfactory receptors via the olfactory bulb (Fig. 1). It is believed to play a significant role in the classification and storage of olfactory information[1,2,3]. For several years we have been using computer simulations as a tool for studying information processing within this cortex[4,5]. While we are ultimately interested in higher order functional questions, our first modeling objective was to construct a computer simulation which contained sufficient neurobiological detail to reproduce experimentally obtained cortical activity patterns. We believe this first step is crucial both to establish correspondences between the model and the cortex, and to assure that the model is capable of generating output that can be compared to data

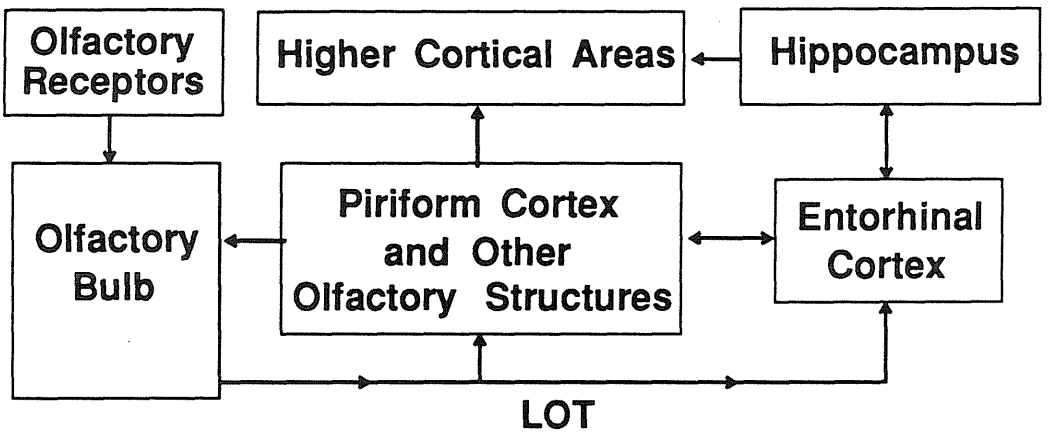

Fig. 1. Simplified block diagram of the olfactory system and closely related structures.

from actual physiological experiments. In the current case, having demonstrated that the behavior of the simulation at least approximates that of the actual cortex[4] (Fig. 3), we are now using the model to explore the types of processing which could be carried out by this cortical structure. In particular, in this paper we will describe the ability of the simulated cortex to store and recall cortical activity patterns generated by stimulus various conditions. We believe this approach can be used to provide experimentally testable hypotheses concerning the functional organization of this cortex which would have been difficult to deduce solely from neurophysiological or neuroanatomical data.

MODEL DESCRIPTION

This model is largely instructed by the neurobiology of piriform cortex[3]. Axonal conduction velocities, time delays, and the general properties of neuronal integration and the major intrinsic neuronal connections approximate those currently described in the actual cortex. However, the simulation reduces both the number and complexity of the simulated neurons (see below). As additional information concerning the these or other important features of the cortex is obtained it will be incorporated in the model. Bracketed numbers in the text refer to the relevent mathematical expressions found in the appendix.

Neurons. The model contains three distinct populations of intrinsic cortical neu-

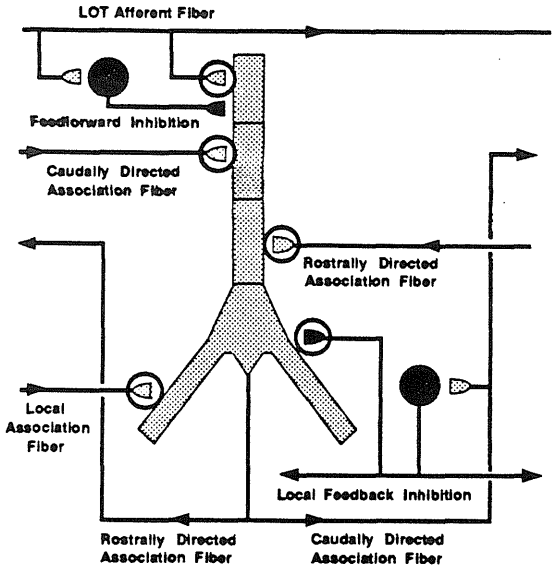

Fig. 2. Schematic diagram of piriform cortex showing an excitatory pyramidal cell and two inhibitory interneurons with their local interactions. Circles indicate sites of synaptic modifiability.

rons, and a fourth set of cells which simulate cortical input from the olfactory bulb (Fig. 2). The intrinsic neurons consist of an excitatory population of pyramidal neurons (which are the principle neuronal type in this cortex), and two populations of inhibitory interneurons. In these simulations each population is modeled as 100 neurons arranged in a 10x10 array (the actual piriform cortex of the rat contains on the order of 10^6 neurons). The output of each modeled cell type consists of an all-or-none action potential which is generated when the membrane potential of the cell crosses a threshold [2.3]. This output reaches other neurons after a delay which is a function of the velocity of the fiber which connects them and the cortical distance from the originating neuron to each target neuron [2.0, 2.4]. When an action potential arrives at a destination cell it triggers a conductance change in a particular ionic channel type in that cell which has a characteristic time course, amplitude, and waveform [2.0, 2.1]. The effect of this conductance change on the transmembrane potential is to drive it towards the equilibrium potential of that channel. Na^+, Cl^-, and K^+ channels are included in the model. These channels are differentially activated by activity in synapses associated with different cell types (see below).

Connection Patterns. In the olfactory system, olfactory receptors project to the olfactory bulb which, in turn, projects directly to the piriform cortex and other olfactory structures (Fig. 1). The input to the piriform cortex from the olfactory bulb is delivered via a fiber bundle known as the lateral olfactory tract (LOT). This fiber tract appears to make sparse, non-topographic, excitatory connections with pyramidal and feedforward inhibitory neurons across the extent of the cortex[3,6]. In the model this input is simulated as 100 independent cells each of which make random connections (p=0.05) with pyramidal and feedforward inhibitory neurons (Fig. 1 and 2).

In addition to the input connections from the olfactory bulb, there is also an extensive set of connections between the neurons intrinsic to the cortex (Fig. 2). For example, the association fiber system arises from pyramidal cells and makes sparse, distributed excitatory connections with other pyramidal cells all across the cortex[7,8,9]. In the model these connections are randomly distributed with 0.05 probability. In the model and in the actual cortex, pyramidal cells also make excitatory connections with nearby feedforward and feedback inhibitory cells. These interneurons, in turn, make reciprocal inhibitory connections with the group of nearby pyramidal cells. The primary effect of the feedback inhibitory neurons is to inhibit pyramidal cell firing through a Cl^- mediated current shunting mechanism[10,11,12]. Feedforward interneurons inhibit pyramidal cells via a long latency, long duration, K^+ mediated hyperpolarizing potential[12,13]. Pyramidal cell axons also constitute the primary output of both the model and the actual piriform cortex[7,14].

Synaptic Properties and Modification Rules. In the model, each synaptic connection has an associated weight which determines the peak amplitude of the conductance change induced in the postsynaptic cell following presynaptic activity [2.0]. To study learning in the model, synaptic weights associated with some of the fiber systems are modifiable in an activity-dependent fashion (Fig. 2). The basic modification rule in each case is Hebb-like; i.e. change in synaptic strength is proportional to presynaptic activity multiplied by the offset of the postsynaptic membrane potential from a baseline potential. This baseline potential is set slightly more positive than the Cl^- equilibrium potential associated with the shunting feedback inhibition. This means that synapses activated while a destination cell is in a depolarized or excited state are strengthened, while those activated during a period of inhibition are weak-

ened. In the model, synapses which follow this rule include the association fiber connections between excitatory pyramidal neurons as well as the connections between inhibitory neurons and pyramidal neurons. Whether these synapses are modifiable in this way in the actual cortex is a subject of active research in our lab. However, the model does mimic the actual synaptic properties associated with the input pathway (LOT) which we have shown to undergo a transient increase in synaptic strength following activation which is independent of postsynaptic potential[15]. This increase is not permanent and the synaptic strength subsequently returns to its baseline value.

Generation of Physiological Responses. Neurons in the model are represented as first-order "leaky" integrators with multiple, time-varying inputs [1.0]. During simulation runs, membrane potentials and currents as well as the time of occurence of action potentials are stored for comparison with actual data. An explicit compartmen-

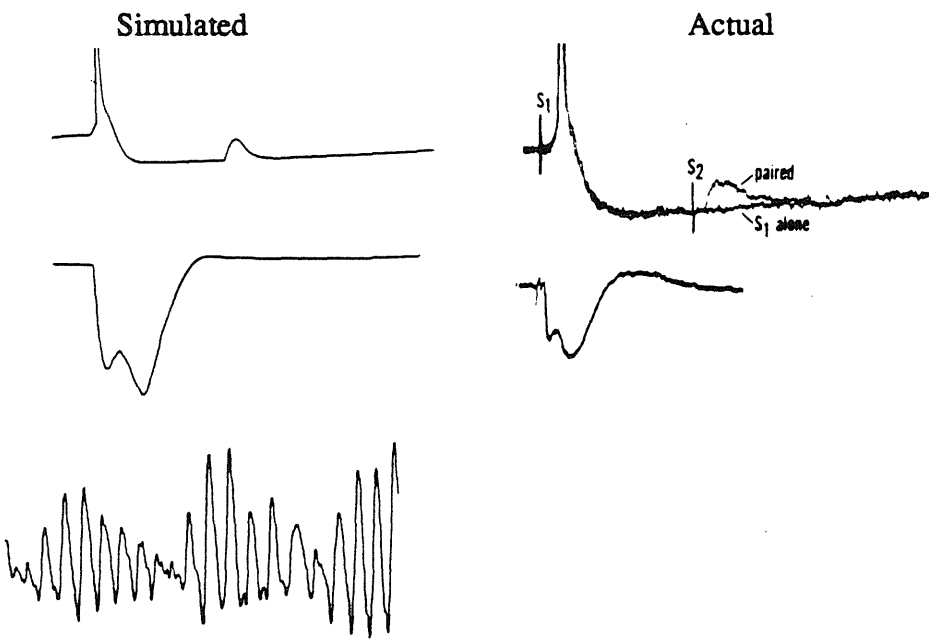

Fig. 3. Simulated physiological responses of the model compared with actual cortical responses. Upper: Simulated intracellular response of a single cell to paired stimulation of the input system (LOT) (left) compared with actual response (right) (Haberly & Bower,'84). Middle: Simulated extracellular response recorded at the cortical surface to stimulation of the LOT (left), compared with actual response (right) (Haberly,'73b). Lower: Stimulated EEG response recorted at the cortical surface to odor-like input (left), for actual EEG see Freeman 1978.

tal model (5 compartments) of the pyramidal cells is used to generate the spatial current distributions used for calculation of field potentials (evoked potentials, EEGs) [3.0, 4.0].

Stimulus Characteristics. To compare the responses of the model to those of the actual cortex, we mimicked actual experimental stimulation protocols in the simulated cortex and contrasted the resulting intracellular and extracellular records. For example, shock stimuli applied to the LOT are often used to elicit characteristic cortical evoked potentials *in vivo*[16,17,18]. In the model we simulated this stimulus paradigm by simultaneously activating all 100 input fibers. Another measure of cortical activity used most successfully by Freeman and colleagues involves recording EEG activity from piriform cortex in behaving animals[19,20]. These odor-like respons-

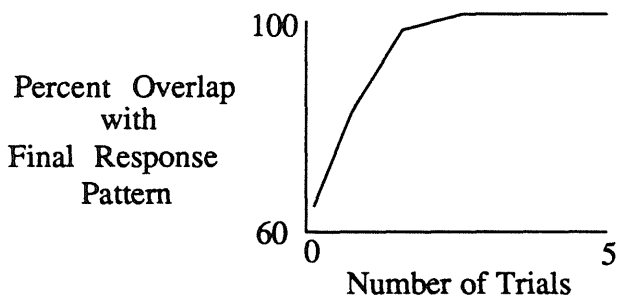

Fig. 4. Convergence of the cortical response during training with a single stimulus with synaptic modification.

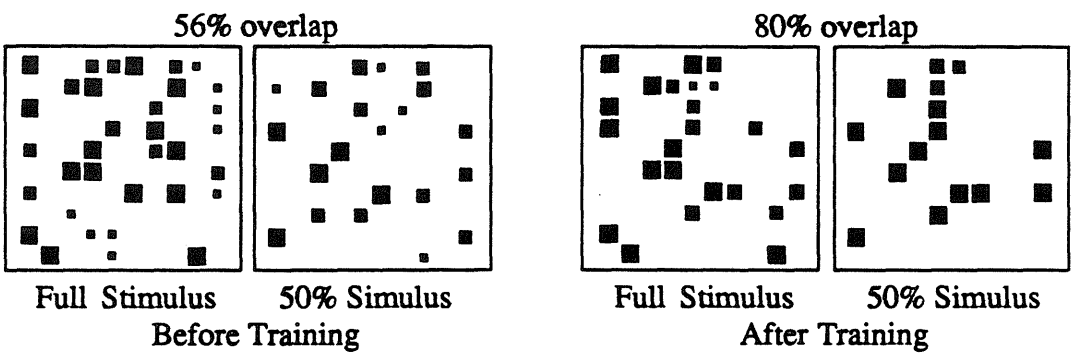

Fig. 5. Reconstruction of cortical response patterns with partially degraded stimuli. Left: Response, before training, to the full stimulus (left) and to the same stimulus with 50% of the input fibers inactivated (right). There is a 44% degradation in the response. Right: Response after training, to the full stimulus (left), and to the same stimulus with 50% of the input fibers inactivated (right). As a result of training, the degradation is now only 20%.

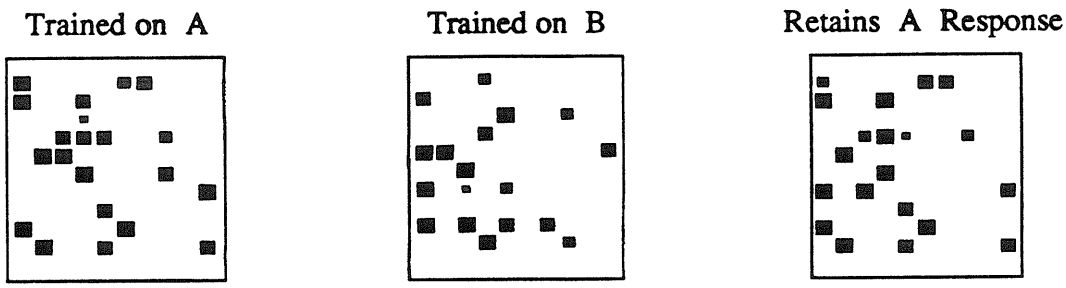

Fig. 6. Storage of multiple patterns. Left: Response to stimulus A after training. Middle: Response to stimulus B after training on A followed by training on B. Right: Response to stimulus A after training on A followed by training on B. When compared with the original response (left) there is an 85% congruence.

es were generated in the model through steady, random stimulation of the input fibers.

To study learning in the model, once physiological measures were established, it was required that we use more refined stimulation procedures. In the absence of any specific information about actual input activity patterns along the LOT, we constructed each stimulus out of a randomly selected set of 10 out of the 100 input fibers. Each stimulus episode consisted of a burst of activity in this subset of fibers with a duration of 10 msec at 25 msec intervals to simulate the 40 Hz periodicity of the actual olfactory bulb input. This pattern of activity was repeated in trials of 200 msec duration which roughly corresponds to the theta rhythm periodicity of bulbar activity and respiration[21,22]. Each trial was then presented 5 times for a total exposure time of 1 second (cortical time). During this period the Hebb-type learning rule could be used to modify the connection weights in an activity-dependent fashion.

Output Measure for Learning. Given that the sole output of the cortex is in the form of action potentials generated by the pyramidal cells, the output measure of the model was taken to be the vector of spike frequency for all pyramidal neurons over a 200 msec trial, with each element of the vector corresponding to the firing frequency of a single pyramidal cell. Figures 5 through 8 show the 10 by 10 array of pyramidal cells. The size of the box placed at each cell position represents the magnitude of the spike frequency for that cell. To evaluate learning effects, overlap comparisons between response pairs were made by taking the normalized dot product of their

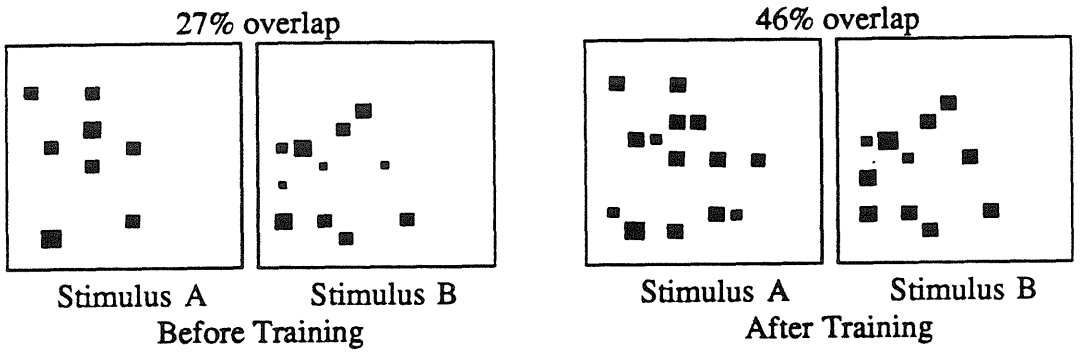

Fig. 7. Results of merging cortical response patterns for dissimilar stimuli. Left: Response to stimulus A and stimulus B before training. Stimuli A and B do not activate any input fibers in common but still have a 27% overlap in cortical response patterns. Right: Response to stimulus A and stimulus B after training in the presence of a common modulatory input E1. The overlap in cortical response patterns is now 46%.

response vectors and expressing that value as a percent overlap (Fig. 4).

Computational Requirements. All simulations were carried out on a Sun Microsystems 3/260 model microcomputer equipped with 8 Mbytes of memory and a floating point accelerator. Average time for a 200 msec simulation was 3 cpu minutes.

RESULTS

Physiological Responses

As described above, our initial modeling objective was to accurately simulate a wide range of activity patterns recorded, by ourselves and others, in piriform cortex using various physiological procedures. Comparisons between actual and simulated records for several types of responses are shown in figure 3. In general, the model replicated known physiological responses quite well (Wilson et al. in preparation describes, in detail, the analysis of the physiological results). For example, in response to shock stimulation of the input pathway (LOT), the model reproduces the principle characteristics of both the intracellular and location-dependent extracellular waveforms recorded in the actual cortex[9,17,18] (Fig. 3). Further, in response to odor-like stimulation the model exhibits 40 Hz oscillations which are characteristic of the

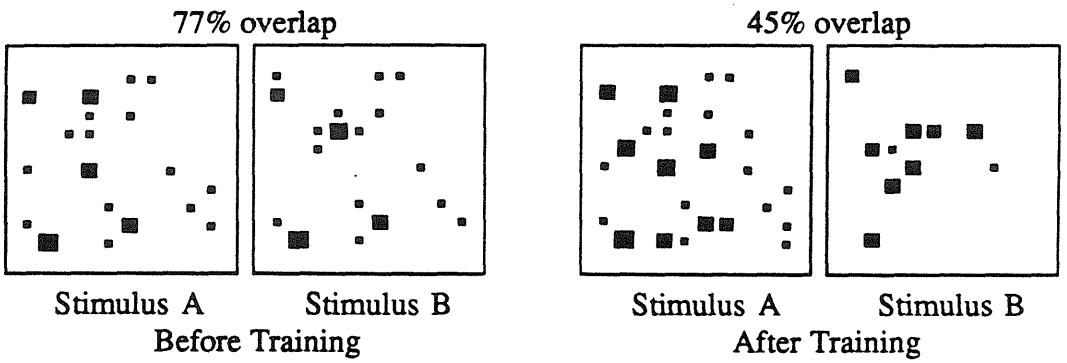

Fig. 8. Results of differentiating cortical response patterns for similar stimuli. Left: Response to stimulus A and stimulus B before training. Stimuli A and B activate 75% of their input fibers in common and have a 77% overlap in cortical response patterns. Right: Response to stimulus A and stimulus B after training A in the presence of modulatory input E1 and training B with a different modulatory input E2. The overlap in cortical response patterns is now 45%.

EEG activity in olfactory cortex in awake, behaving animals[19]. Although beyond the scope of the present paper, the simulation also duplicates epileptiform[9] and damped oscillatory[16] type activity seen in the cortex under special stimulus or pharmacological conditions[4].

Learning

Having simulated characteristic physiological responses, we wished to explore the capabilities of the model to store and recall information. Learning in this case is defined as the development of a consistent representation in the activity of the cortex for a particular input pattern with repeated stimulation and synaptic modification. Figure 4 shows how the network converges, with training, on a representation for a stimulus. Having demonstrated that, we studied three properties of learned responses - the reconstruction of trained cortical response patterns with partially degraded stimuli, the simultaneous storage of separate stimulus response patterns, and the modulation of cortical response patterns independent of relative stimulus characteristics.

Reconstruction of Learned Cortical Response Patterns with Partially Degraded

Stimuli. We were interested in knowing what effect training would have on the sensitivity of cortical responses to fluctuations in the input signal. First we presented the model with a random stimulus A for one trial (without synaptic modification). On the next trial the model was presented with a degraded version of A in which half of the original 10 input fibers were inactivated. Comparison of the responses to these two stimuli in the naive cortex showed a 44% variation. Next, the model was trained on the full stimulus A for 1 second (with synaptic modification). Again, half of the input was removed and the model was presented with the degraded stimulus for 1 trial (without synaptic modification). In this case the difference between cortical responses was only 20% (Fig. 5) showing that training increased the robustness of the response to degradation of the stimulus.

Storage of Two Patterns. The model was first trained on a random stimulus A for 1 second. The response vector for this case was saved. Then, continuing with the weights obtained during this training, the model was trained on a new non-overlapping (i.e. different input fibers activated) stimulus B. Both stimulus A and stimulus B alone activated roughly 25% of the cortical pyramidal neurons with 25% overlap between the two responses. Following the second training period we assessed the amount of interference in recalling A introduced by training with B by presenting stimulus A again for a single trial (without synaptic modification). The variation between the response to A following additional training with B and the initially saved reponse to A alone was less than 15% (Fig. 6) demonstrating that learning B did not substantially interfere with the ability to recall A.

Modulation of Cortical Response Patterns. It has been previously demonstrated that the stimulus evoked response of olfactory cortex can be modulated by factors not directly tied to stimulus qualities, such as the behavioral state of the animal[1,20,23]. Accordingly we were interested in knowing whether the representations stored in the model could be modulated by the influence of such a "state" input.

One potential role of a "state" input might be to merge the cortical response patterns for dissimilar stimuli; an effect we refer to as accommodation. To test this in the model, we presented it with a random input stimulus A for 1 trial. It was then presented with a random input stimulus B (non-overlapping input fibers). The amount of overlap in the cortical responses for these untrained cases was 27%. Next, the model

was trained for 1 second on stimulus A in the presence of an additional random "state" stimulus E1 (activity in a set of 10 input fibers distinct from both A and B). The model was then trained on stimulus B in the presence of the same "state" stimulus E1. After training, the model was presented with stimulus A alone for 1 trial and stimulus B alone for 1 trial. Results showed that now, even without the coincident E1 input, the amount of overlap between A and B responses was found to have increased to 46% (Fig 7). The role of E1 in this case was to provide a common stimulus component during learning which reinforced shared components of the responses to input stimuli A and B.

To test the ability of a state stimulus to induce differentiation of cortical response patterns for similar stimuli, we presented the model with a random input stimulus A for 1 trial, followed by 1 trial of a random input stimulus B (75% of the input fibers overlapping). The amount of overlap in the cortical responses for these untrained cases was 77%. Next, the model was trained for a period of 1 second on stimulus A in the presence of an additional random "state" stimulus E1 (a set of 10 input fibers not overlapping either A or B). It was then trained on input stimulus B in the presence of a different random "state" stimulus E2 (10 input fibers not overlapping either A, B, or E1) After this training the model was presented with stimulus A alone for 1 trial and stimulus B alone for 1 trial. The amount of overlap was found to have decreased to 45% (Fig 8). In this situation E1 and E2 provided a differential signal during learning which reinforced distinct components of the responses to input stimuli A and B.

DISCUSSION

Physiological Responses. Detailed discussion of the mechanisms underlying the simulated patterns of physiological activity in the cortex is beyond the scope of the current paper. However, the model has been of value in suggesting roles for specific features of the cortex in generating physiologically recorded activity. For example, while actual input to the cortex from the olfactory bulb is modulated into 40 Hz bursts[24], continuous stimulation of the model allowed us to demonstrate the model's capability for intrinsic periodic activity independent of the complementary pattern of stimulation from the olfactory bulb. While a similar ability has also been demonstrated by models of Freeman[25], by studying this oscillating property in the model we were able to associate these oscillatory characteristics with specific interactions of

local and distant network properties (e.g. inhibitory and excitatory time constants and trans-cortical axonal conduction velocities). This result suggests underlying mechanisms for these oscillatory patterns which may be somewhat different than those previously proposed.

Learning. The main subject of this paper is the examination of the learning capabilities of the cortical model. In this model, the apparently sparse, highly distributed pattern of connectivity characteristic of piriform cortex is fundamental to the way in which the model learns. Essentially, the highly distributed pattern of connections allows the model to develop stimulus-specific cortical response patterns by extracting correlations from randomly distributed input and association fiber activity. These correlations are, in effect, stored in the synaptic weights of the association fiber and local inhibitory connections.

The model has also demonstrated robustness of a learned cortical response against degradation of the input signal. A key to this property is the action of sparsely distributed association fibers which provide reinforcment for previously established patterns of cortical activity. This property arises from the modification of synaptic weights due to correlations in activity between intra-cortical association fibers. As a result of this modification the activity of a subset of pyramidal neurons driven by a degraded input drives the remaining neurons in the response.

In general, in the model, similar stimuli will map onto similar cortical responses and dissimilar stimuli will map onto dissimilar cortical responses. However, a presumably important function of the cortex is not simply to store sensory information, but to represent incoming stimuli as a function of the absolute stimulus qualities and the context in which the stimulus occurs. The fact that many of the structures that piriform cortex projects to (and receives projections from) may be involved in multimodal "state" generation[14] is circumstantial evidence that such modulation may occur. We have demonstrated in the model that such a modulatory input can modify the representations generated by pairs of stimuli so as to push the representations of like stimuli apart and pull the representations of dissimilar stimuli together. It should be pointed out that this modulatory input was not an "instructive" signal which explicitly directed the course of the representation, but rather a "state" signal which did not require *a priori* knowledge of the representational structure. In the model, this modulatory phenomenon is a simple consequence of the degree of overlap in the com-

bined (odor stimulus + modulator) stimulus. Both cases approached approximately 50% overlap in cortical responses reflecting the approximately 50% overlap in the combined stimuli for both cases. Of interest was the use of the model's reconstructive capabilities to maintain the modulated response to each input stimulus even in the absence of the modulatory input.

CAVEATS AND CONCLUSIONS

Our approach to studying this system involves using computer simulation to investigate mechanisms of information processing which could be implemented given what is known about biological constraints. The significance of results presented here lies primarily in the finding that the structure of the model and the parameter settings which were appropriate for the reproduction of physiological responses were also appropriate for the proper convergence of a simple, biologically plausible learning rule under various conditions. Of course, the model we have developed is only an approximation to the actual cortex limited by our knowledge of its organization and the computing power available. For example, the actual piriform cortex of the rat contains on the order of 10^6 cells (compared with 10^2 in the simulations) with a sparsity of connection on the order of $p=0.001$ (compared with $p=0.05$ in the simulations). Our continuing research effort will include explorations of the scaling properties of the network.

Other assumptions made in the context of the current model include the assumption that the representation of information in piriform cortex is in the form of spatial distributions of rate-coded outputs. Information contained in the spatio-temporal patterns of activity was not analyzed, although preliminary observation suggests that this may be of significance. In fact, the dynamics of the model itself suggest that temporally encoded information in the input at various time scales may be resolvable by the cortex. Additionally, the output of the cortex was assumed to have spatial uniformity, i.e. no differential weighting of information was made on the basis of spatial location in the cortex. But again, observation of the dynamics of the model, as well as the details of known anatomical distribution patterns for axonal connections, indicate that this is a major oversimplification. Preliminary evidence from the model would indicate that some form of hierarchical structuring of information along rostral/caudal lines may occur. For example it may be that cells found in progressively more rostral

locations would have increasingly non-specific odor responses.

Further investigations of learning within the model will explore each of these issues more fully, with attempts to correlate simulated findings with actual recordings from awake, behaving animals. At the same time, new data pertaining to the structure of the cortex will be incorporated into the model as it emerges.

ACKNOWLEDGEMENTS

We wish to thank Dr. Lewis Haberly and Dr. Joshua Chover for their roles in the development and continued support of the modeling effort. We also wish to thank Dave Bilitch for his technical assistance. This work was supported by NIH grant NS22205, NSF grant EET-8700064, the Lockheed Corporation, and a fellowship from the ARCS foundation.

REFERENCES

W. J. Freeman, J. Neurophysiol., 23, 111 (1960).

T. Tanabe, M. Iino, and S. F. Takagi, J. Neurophysiol., 38,1284 (1975).

L. B. Haberly, Chemical Senses, 10, 219 (1985).

M. Wilson, J. M. Bower, J. Chover, and L. B. Haberly, Soc. Neurosci. Abs., 12, 1358 (1986).

M. Wilson and J. M. Bower, Soc. Neurosci. Abs., 13, 1401 (1987).

M. Devor, J. Comp. Neur., 166, 31 (1976).

L. B. Haberly and J. L. Price, J. Comp. Neurol., 178, 711 (1978a).

L. B. Haberly and S. Presto, J. Comp. Neurol., 248, 464 (1986).

L. B. Haberly and J. M. Bower, J. Neurophysiol., 51, 90 (1984).

M. A. Biedenbach and C. F. Stevens, J. Neurophysiol., 32, 193 (1969).

M. A. Biedenbach and C. F. Stevens, J. Neurophysiol., 32, 204 (1969).

M. Satou, K. Mori, Y. Tazawa, and S. F. Takagi, J. Neurophysiol., 48, 1157 (1982).

G. F. Tseng and L. B. Haberly, Soc. Neurosci. Abs. 12, 667 (1986).

L. B. Luskin and J. L. Price, J. Comp. Neur., 216, 264 (1983).

J. M. Bower and L. B. Haberly,L.B., Proc. Natl. Acad. Sci. USA, 83, 1115 (1985).

W. J. Freeman, J. Neurophysiol., 31, 1 (1968).

L. B. Haberly, J. Neurophysiol., 36, 762 (1973).

L. B. Haberly, J. Neurophysiol., 36, 775 (1973).

W. J. Freeman, Electroenceph. and Clin. Neurophysiol., 44, 586 (1978).

W.J. Freeman and W. Schneider, Psychophysiology, 19, 44 (1982).

F. Macrides and S. L. Chorover, Science, 175, 84 (1972).

F. Macrides, H. B. Eigenbaum, and W. B. Forbes, J. Neurosci., 2, 12, 1705 (1982).

P. D. MacLean, N. H. Horwitz, and F. Robinson, Yale J. Biol. Med., 25, 159 (1952).

E. D. Adrian, Electroenceph. and Clin. Neurophysiol., 2, 377 (1950).

W. J. Freeman, Exp. Neurol., 10, 525 (1964).

$$\frac{dV_i}{dt} = \frac{1}{c_m}\left[\sum_{k=1}^{n_{types}} I_{ik}(t) + \frac{E_r - V_i(t)}{r_l}\right] \tag{1.0}$$

Somatic Integration

$$I_{ik}(t) = [E_k - V_i(t)]g_{ik}(t) \tag{1.1}$$

n_{types} = number of input types
$V_i(t)$ = membrane potential of i th cell
$I_{ik}(t)$ = current into cell i due to input type k
E_k = equilibrium potential associated with input type k
E_r = resting potential
r_l = membrane leakage resistance
c_m = membrane capacitance
$g_{ik}(t)$ = conductance due to input type k in cell i

$$g_{ik}(t) = \sum_{j=1}^{n_{cells}} \int_{\lambda=0}^{\lambda=d_k} F_k(\lambda)\, A_{ijk}\, W_{ij}\, S_j(t - \lambda - \frac{L_{ij}}{v_k} - \varepsilon_k)\, d\lambda \tag{2.0}$$

$$F_k(t) = \frac{t}{\tau} e^{\left(1 - \frac{t}{\tau}\right)}\left[(1 - U(t-\tau)) + U(t-\tau)\cos\left[\frac{\pi}{2}\frac{(t-\tau)}{(d_k - \tau)}\right]\right], \quad \tau = \gamma d_k \tag{2.1}$$

Spike Propagation and Synaptic Input

$$A_{ijk} = (1 - \rho_k^{min}) e^{-L_{ij}\rho_k} + \rho_k^{min} \tag{2.2}$$

$$S_j(t) = \begin{cases} 1 & V_j(t) > T_j,\ S_j(\lambda) = 0 \text{ for } \lambda = t..t - \Delta t_r \\ 0 & \text{otherwise} \end{cases} \tag{2.3}$$

$$L_{ij} = |i - j|\Delta x \tag{2.4}$$

n_{cells} = number of cells in the simulation
Δx = distance between adjacent cells
d_k = duration of conductance change due to input type k
v_k = velocity of signals for input type k
ε_k = latency for input type k
ρ_k = spatial attenuation factor for input type k
ρ_k^{min} = minimum spatial attenuation for input type k
Δt_r = refractory period
T_j = threshold for cell j
L_{ij} = distance from cell i to cell j
A_{ijk} = distribution of synaptic density for input type k
W_{ij} = synaptic weight from cell j to cell i
$g_{ik}(t)$ = conductance due to input type k in cell i
$F_k(t)$ = conductance waveform for input type k
$S_j(t)$ = spike output of cell j at time t
$U(t)$ = unit step function

Field Potentials

$$V_{ep}^j(t) = \frac{R_e}{4\pi}\sum_{i=1}^{n_{cells}}\sum_{n=1}^{n_{segs}} \frac{I_m^{in}(t)}{\left[(z_{elec} - z_n)^2 + (x_j - x_i)^2\right]^{\frac{1}{2}}} \tag{3.0}$$

n_{cells} = number of cells in the simulation
n_{segs} = number of segments in the compartmental model
$V_{ep}^j(t)$ = approximate extracellular field potential at cell j
$I_m^{in}(t)$ = membrane current for segment n in cell i
z_{elec} = depth of recording site
z_n = depth of segment n
x_j = x location of the j th cell
R_e = extracellular resistance per unit length

$$\frac{dV_n}{dt} = \frac{1}{c_m^n}\left[I_a^{n-}(t) + I_a^{n+}(t) + \frac{E_r - V_n(t)}{r_m^n} + \sum_{c=1}^{n_{conc}} [E_c - V_n(t)]g_{nc}(t)\right] \tag{4.0}$$

Dendritic Model

$$I_a^{n-}(t) = \frac{V_{n-1}(t) - V_n(t)}{r_a^{n-1} + r_a^n}, \quad I_a^{n+}(t) = \frac{V_{n+1}(t) - V_n(t)}{r_a^{n+1} + r_a^n} \tag{4.1}$$

$$I_m^n(t) = I_a^{n-}(t) + I_a^{n+}(t) \tag{4.2}$$

$$r_a^n = \frac{1}{2}\left[R_e l_n + R_i \frac{l_n}{\pi\left(\frac{d_n}{2}\right)^2}\right] \quad , \quad r_m^n = \frac{R_m}{\pi\, l_n d_n} \quad , \quad c_m^n = C_m \pi\, l_n d_n \tag{4.3}$$

n_{chan} = number of different channels per segment
$V_n(t)$ = membrane potential of n th segment
c_m^n = membrane capacitance for segment n
r_a^n = axial resistance for segment n
r_m^n = membrane resistance for segment n
$g_{nc}(t)$ = conductance of channel c in segment n
E_c = equilibrium potential associated with channel c
$I_a^{n\pm}(t)$ = axial current between segment $n\pm1$ and n
$I_m^n(t)$ = membrane current for segment n
l_n = length of segment n
d_n = diameter of segment n
R_m = membrane resistivity
R_i = intracellular resistivity per unit length
R_e = extracellular resistance per unit length
C_m = capacitance per unit surface area

A Computer Simulation of Oscillatory Behavior in Primary Visual Cortex

Matthew A. Wilson and James M. Bower

Computation and Neural Systems Program, Division of Biology, 216-76
California Institute of Technology, Pasadena, CA 91125.

Periodic variations in correlated cellular activity have been observed in many regions of the cerebral cortex. The recent discovery of stimulus dependent, spatially coherent oscillations in primary visual cortex of the cat, has led to suggestions of neural information encoding schemes based on phase and/or frequency variation. In order to explore the mechanisms underlying this behavior and their possible functional consequences, we have developed a realistic neural model, based on structural features of visual cortex, which replicates observed oscillatory phenomena. In the model, this oscillatory behavior emerges directly from the structure of the cortical network and the properties of its intrinsic neurons; however, phase coherence is shown to be an average phenomenon only seen when measurements are made over multiple trials. Because average coherence does not insure synchrony of firing over the course of single stimuli, oscillatory

phase may not be a robust strategy for directly encoding stimulus-specific information. Instead, the phase and frequency of cortical oscillations may reflect the coordination of general computational processes within and between cortical areas. Under this interpretation coherence emerges as a result of horizontal interactions which could be involved in the formation of receptive field properties.

Introduction

An obvious characteristic of the general behavior of cerebral cortex, as evident in EEG recordings, is its tendency to oscillate (Bressler and Freeman, 1980). Cortical oscillations have been observed both in the electric fields generated by populations of cells (Bressler and Freeman, 1980) as well as in the activity of single cells (Llinas, 1988). Recent observations of oscillations within visual cortex that are dependent on the nature of the visual stimulus (Gray and Singer, 1987; Eckhorn et al., 1988; Gray et al., 1989; Gray and Singer, 1989) have generated increased interest in the role of periodic behavior in cerebral cortical processing in general. These studies have shown that populations of visual cortical neurons at considerable cortical distances exhibit increased coherence in neuronal activity when the visual stimulus is a single continuous object as compared to a discontinuous object. This work represents an extension of ear-

lier work showing that the reponses of cells can be influenced by stimuli which are located beyond of the boundaries of the classical receptive field (Allman, Miezin, McGuinness, 1985), with horizontal interactions implicated in shaping these more complex receptive field properties (Tso, Gilbert, Wiesel, 1986). These recent results have led to suggestions that differences in oscillatory phase and/or frequency between cell populations in primary visual cortex could be used to label different objects in the visual scene for subsequent processing in higher visual areas (Eckhorn et al., 1988; Gray et al., 1989; Gray and Singer, 1989; Sporns et al., 1989; Kammen, Holmes, and Koch, 1989). It has further been suggested that these oscillatory patterns may rely on central, extracortical control in order to assure temporal coherence (Kammen, Holmes, and Koch, 1989).

In this paper we describe the results of simulations of a biologically realistic model of neocortical networks designed to explore the possible mechanisms underlying oscillations in visual cortex, as well as the functional significance of this oscillatory behavior. In particular we analyze the role of horizontal interactions in the establishment of coherent oscillatory behavior.

Cortical Model

The model consists of a network of three basic cell types found throughout cerebral cortex. The principal excitatory neuron, the pyramidal cell, is

modeled here as five coupled membrane compartments. In addition there are two inhibitory neurons, one principally mediating a slow K+ inhibition and one mediating a fast Cl- inhibition. Both are modeled as a single compartment. Connections between modeled cells are made by axons with finite conduction velocities, but no explicit axonal membrane properties other than delay are included. Synaptic activity is produced by simulating the action-potential triggered release of presynaptic transmitter and the resulting flow of transmembrane current through membrane channels. Each of these channels is described with parameters governing the time course and amplitude of synaptically activated conductance changes. The compartmental models of the cells integrate the transmembrane and axial currents to produce transmembrane voltages. Excursions of the cell body membrane voltage above a specified threshold trigger action potentials. Additional details of these features of the model are described in Wilson and Bower (1990).

This model is intended to represent a 10 mm x 6 mm region of visual cortex. The many millions of actual neurons in this area are represented here by 375 cells (25x15) of the three types for a total of 1125 cells. Input to the model is provided by 100 independent fibers, each making contact with a local cortical region (1 sq mm), and each reflecting the retinotopic organization of many structures in the visual system (Van Essen, 1979). The model also includes excitatory horizontal

fiber connections between pyramidal cells (Gilbert, 1983) which extend over a radius of 3 mm from each pyramidal cell. Inhibitory cells receive input from pyramidal cells within a 2 mm radius and make connections with pyramidal cells over a radius of 1 mm. The influence of each of these fiber systems falls off exponentially with a space constant of 5 mm. No effort was made to reproduce the periodic structure of actual connections or many other known features of visual cortex. Instead, our intention was to reproduce oscillations characteristic of visual cortex using a small but sufficient set of physiological and anatomical features.

Coherent Oscillations

Figure 1 shows auto and cross correlations of simulated pyramidal cell spike activity recorded from two sites in visual cortex separated by 6 mm. Total cross correlations in the modeled data were computed by averaging correlations from 50 individual 500 msec trials. Within each trial, simulated activity was generated by providing input representing bars of light at different locations in the visual field. In these cases, the model produced oscillatory auto and cross correlations with peak energy in the 30-60 Hz range, consistent with experimental data (Gray et al., 1989). As in the experimental data, the model also produced nearly synchronous oscillatory activity in groups of neurons separated by 6 mm when presented with a continuous bar (fig 1a). A broken bar which

did not stimulate the region between the recording sites produced a weaker response (fig 1b), again consistent with experimental evidence (Gray et al., 1989). Shuffling trials with respect to each other prior to calculating cross correlation functions greatly diminished or completely eliminated oscillations. The same technique applied to actual physiological data yields similar results (Gray and Singer, 1989) indicating that while the oscillations are stimulus dependent they are not stimulus locked. Simulations run in the absence of stimuli produced low baseline activity with no oscillations.

Further analysis of the models behavior revealed that the 30-60 Hz oscillations are primarily determined by the amplitude and time course of the fast feedback inhibitory input. Increasing the amplitude of the inhibitory input to pyramidal cells reduces oscillatory frequency, while reducing inhibition produces an increase in frequency. Allowing inhibitory cells to inhibit each other within a local region improved frequency locking and produced auto and cross correlations with more pronounced oscillatory characteristics.

Dependence on Horizontal Interconnections

While the frequency of oscillations was primarily due to local inhibitory circuitry, the coherence in correlated cell firing appears to be related primarily to activity in the horizontal interconnections between pyramidal cells. When all long-range (> 1 mm) horizontal fibers were eliminated, the auto correlations at

each recording site continued to show strong oscillatory behavior, but oscillations in the cross correlation function vanished (fig. 2a). Increasing the range of horizontal fibers to 2 mm restored coherent oscillatory behavior (fig 2a).

The dependence of phase coherence on horizontal connections immediately raises a number of interesting questions. First, because horizontal fibers have finite conductions velocities, it was surprising that they would produce coherence with zero phase over relatively long distances. If phase coherence was strictly a consequence of horizontal fiber coupling between the recorded cell groups, it seems reasonable to expect a phase difference related to the propagation delay. To explore this further, we reduced the propagation velocity of horizontal fibers from 0.86+-0.13 m/s to 0.43+-0.13 m/s and examined the response to a continuous bar. No effect on phase was found in the cross correlation function. If, however, the degree of horizontal fiber coupling was enhanced by increasing synaptic weights along horizontal pathways, the cortex displayed a transition from near-zero phase coherence to a phase shift consistent with the delay along the shortest horizontal interconnection path (fig. 2b).

To examine this result more closely, we analyzed the time course of phase coherence at successive time periods following stimulus onset in both the strong and weakly coupled cases. Initially, in both conditions, the synchronizing effect of the stimulus onset itself produces a tendency for zero-phase correlations

during the period from 0-125 msec (fig 2b). However, in the periods following the onset of the stimulus, when activity is dominated by horizontal fiber effects (125-500 msec), the response differs in the two cases. With enhanced horizontal fiber coupling, non-zero phase shifts emerge which reflect the propagation delays along horizontal fibers (fig. 2b). However, in the weak coupling case, zero-phase correlations persist, decaying over the entire trial interval (0-500 msec).

Mechanisms Governing Coherence

Analysis of the activity patterns generated in the weak coupling condition indicates that the mechanism that sustains the zero-phase bias between distant cell groups after stimulus onset depends on the activation of spatially intermediate cells via horizontal fibers. When this intermediate population of cells is activated by the single stimulus bar, they can activate adjacent cells through their own horizontal fibers in a phase-symmetric fashion. When these intermediate cells are not activated directly by the stimulus, as in the case of the discontinuous bar, their ability to coactivate adjacent cell populations is diminished, resulting in a reduction in observed long-range phase coherence. Increasing the strength of horizontal connections establishes a path of direct polysynaptic coupling between distant sites which gives rise to systematic phase shifts related to propagation delay.

The model's dependence on horizontal connections for phase coherence

leads directly to the prediction that the areal extent of strongest correlations should be related to the spatial spread of the horizontal fibers. This effect was demonstrated in the model by increasing the size of the stimulus bar from 6 to 12 mm in an enlarged cortical simulation in which the horizontal fibers remained at a length of 3 mm. Under these conditions, oscillatory correlations were not found between distant recording sites (1,3 in fig. 3). Interestingly, correlations were still found between recording points separated by no more than 6 mm (pairs 1,2 and 2,3 in fig. 3). This absence of transitivity demonstrates the presence of within and between-trial variations in phase relationships and suggests that the observed zero-phase phenomena may only be present in the average of multiple trials.

Overall, our simulation results suggest that the oscillatory patterns so far reported to exist in visual cortex, can be explained by mechanisms that are entirely intrinsic to the cortical region and do not require an extrinsic driving mechanism (c.f. Kammen, Holmes, Koch, 1989). In the current simulations of visual cortex, we have used long bar stimuli to make the additional prediction that the more restricted extent of horizontal connections should limit coherent correlated activity to an area twice the radius of the horizontal fibers (4-12 mm in cats and monkeys (Gilbert, 1983)). More extensive correlations within primary visual cortex would imply either an additional intrinsic mechanism (e.g.,

long distance inhibitory coupling) or a more global synchronizing mechanism (Kammen, Holmes, and Koch, 1989). Even if such mechanisms exist, it is likely that they will be coordinated with intrinsic cortical mechanisms.

Significance of Phase Relationships

Beyond providing a structural explanation for the properties of visual cortical oscillations, our results also have implications for several recently proposed functional interpretations of the observed stimulus dependent zero-phase coherence. Several researchers have proposed the use of these phase relationships as a means of cortically segmenting, or labelling, different objects in a visual scene (Eckhorn et al., 1988; Gray et al., 1989; Gray and Singer, 1989; Sporns et al., 1989; Kammen, Holmes, and Koch, 1989). Associated with this idea, models have been generated that produce the instantaneous phase effects presumably necessary for the visual system to make use of such a coding mechanism on single stimulus trials (Kammen, Holmes, and Koch, 1989). If our results are correct, however, zero-phase relationships between particular neurons should only exist on average, over multiple trials. The absence of consistent within-trial coherence over long distances would be expected to seriously confound the interpretation of fine phase differences in higher visual processing areas.

Our simulations suggest that the oscillatory behavior seen in visual cortex may be dependent on horizontal interactions which are capable of modulating

the responses of widely separated neurons. While the computational function of these types of interactions within the actual cortex is not yet understood, the lateral spread of information could be involved in reinforcing the continuity of visual objects, in modulating classical receptive field properties (Tso, Gilbert, Wiesel, 1986; Mitcheson and Crick,1982), or in establishing non-classical receptive field structure (Allman, Miezin, McGuinness, 1985). The stimulus dependence of coherence in the model is observed to result from the modulation of the magnitude of these interactions as a function of stimulus structure. Under this interpretation, phase coherence does not in itself encode information necessary for subsequent processing, but rather, phase relationships emerge as a result of the horizontal integration of information involved in the shaping of receptive field properties.

General Cerebral Cortical Processing

For the last several years we have been using biologically realistic computer simulations to study the oscillatory behavior of another primary sensory region of cerebral cortex, the olfactory, or piriform cortex (Wilson and Bower, 1988;1989; 1990). This structure is also known to generate oscillatory activity in the 40 Hz range under a variety of experimental conditions (Adrian, 1942; Freeman, 1968; 1978). It is interesting to note that the neural mechanisms that generate the oscillatory behavior described here in the visual cortex model

are also capable of reproducing the basic frequency and phase relationships of olfactory cortex. In each case inhibitory neurons govern the frequency of the oscillations while the long range horizontal connections are involved in establishing specific phase relationships. Our work in piriform cortex suggests that the 40 Hz cycle reflects a fundamental cortical processing interval while phase relationships, as in the model of visual cortex, reflect the structure of inter-cellular communication within the network (Wilson and Bower, 1990). If true, then this 40 Hz oscillatory structure may reflect very general properties of cerebral cortical function.

Acknowledgements

This research was supported by the NSF (EET-8700064), the ONR (N00014-88-K-0513), and the Lockheed Corporation. We wish to thank Christof Koch and Dan Kammen for valuable discussions.

REFERENCES

Adrian, E.D. 1942. Olfactory reactions in the brain of the hedgehog. *J. Physiol. (Lond.)* **100**, 459-472.

Allman, J., Miezin, F., and McGuinness, E. 1985. Stimulus specific responses from beyond the classical receptive field: Neurophysiological mechanisms for local-global comparisons in visual neurons. *Ann. Rev. Neurosci.* **8**,

407-430.

Bressler, S.L. and Freeman, W.J. 1980. Frequency analysis of olfactory system EEG in cat, rabbit and rat. *Electroenceph. clin. Neurophysiol.* **50**, 19-24.

Eckhorn, R., Bauer, R., Jordan, W., Brosch, M., Kruse, W., Munk, M., and Reitboeck, H.J. 1988. Coherent oscillations: A mechanism of feature linking in the visual cortex? *Biol. Cybern.* **60**, 121-130.

Freeman, W.J. 1978. Spatial properties of an EEG event in the olfactory bulb and cortex. *Electroenceph. clin. Neurophysiol.* **44**, 586-605.

Freeman, W.J. 1968. Relations between unit activity and evoked potentials in prepyriform cortex of cats. *J. Neurophysiol.* **31**, 337-348.

Gilbert, C.D. 1983. Microcircuitry of the visual cortex. *Ann. Rev. Neurosci.* **6**, 217-247.

Gray, C.M., Konig, P., Engel, A.K., Singer ,W. 1989. Oscillatory responses in cat visual cortex exhibit inter-columnar synchronization which reflects global stimulus properties. *Nature* **338**, 334-337.

Gray, C.M. and Singer,W. 1989. Stimulus specific neuronal oscillations in orientation columns of cat visual cortex. *Proc. Natl. Acad. Sci. U.S.A.* **86**, 1698-1702.

Gray, C.M. and W. Singer. 1987. Stimulus-specific neuronal oscillations in the

cat visual cortex: A cortical functional unit. *Soc. Neurosci. Abstr.* **404**, 3.

Kammen, D.M., Holmes, P.J., and Koch. C. 1989. Cortical architecture and oscillations in neuronal networks: Feedback versus local coupling. in *Models of Brain Function* (ed Cotterill, R.M.J.) (Cambridge Univ. Press).

Llinas, R. 1988. The intrinsic electrophysiological properties of mammalian neurons: Insights into central nervous system function. *Science* **242**, 1654-1664.

Mitchison, G. and Crick, F. 1982. Long axons within the striate cortex: their distribution, orientation and patterns of connection. *Proc. Natl. Acad. Sci. U.S.A.* **79**, 3661-3665.

Sporns, O., Gally, J.A., Reeke, Jr., G.N., and Edelman, G.M. 1989. Reentrant signaling simulated neuronal groups leads to coherency in their oscillatory activity. *Proc. Natl. Acad. Sci. U.S.A.* **86**, 7265-7269.

Tso, D.Y., Gilbert, C.D., and Wiesel, T.N. 1986. Relationships between horizontal interactions and functional architecture in cat striate cortex as revealed by cross-correlation analysis. *J. Neurosci.* **6**, 1160-1170.

Van Essen, D.C. 1979. Visual areas of the mammalian cerebral cortex. *Ann. Rev. Neurosci.* **2**, 227-263.

Wilson, M.A., and Bower, J.M. 1990. Cortical oscillations and temporal in-

teractions in a computer simulation of piriform cortex. (to appear in J. Neurophysiol.)

Wilson, M.A. and Bower, J.M. 1989. The simulation of large scale neuronal networks. in *Methods in Neuronal Modeling: From Synapses to Networks* (eds Koch,C. and Segev,I.) 291-334 (MIT Press, Cambridge, MA).

Wilson, M.A. and Bower, J.M. 1988. A computer simulation of olfactory cortex with functional implications for storage and retrieval of olfactory information. in *Neural Information Processing Systems*, (ed Anderson, D.Z.) (AIP Press, New York, NY).

Fig. 1. Simulated auto and cross correlations generated by presentation of a broken bar (A) and a continuous bar (B) over 500 msec. Upper diagrams show the model with the stimulus region shaded. Grid squares correspond to the location of modeled cells. The numbers indicate the location of the recording sites referred to in the auto (1-1,2-2) and cross (1-2) correlations.

METHODS: Multi-neuronal activity used to produce the correlations were summed from 9 neurons nearest each recording site. The stimulus was generated using independent poisson processes on individual input fibers. The poisson rate parameter was increased from a baseline of 20 spikes/sec to 500 spikes/sec over the onset period from 20-100 msec. The difference in phase between the firing of cells in these locations was estimated by measuring the offset of the dominant peak in the cross correlation function. These values were consistent with measurements obtained both through chi-square fitting of a modified cosine function and measurement of the phase of the peak frequency component in the correlation function power spectra.

Fig. 2. (A) Cross correlations between sites 1-2 (see fig. 1) for a continuous bar stimulus with radius of horizontal fiber coupling of 2 mm (left) and 1 mm

(right). (B) Time course of cross correlation functions taken at successive 125 intervals over the 500 msec period for relative horizontal fiber coupling strengths of 1 (left) and 1.5 (right). The bottom-most correlation function covers the entire 500 msec interval.

Fig. 3. Cross correlations between sites along a 12 mm stimulus bar.

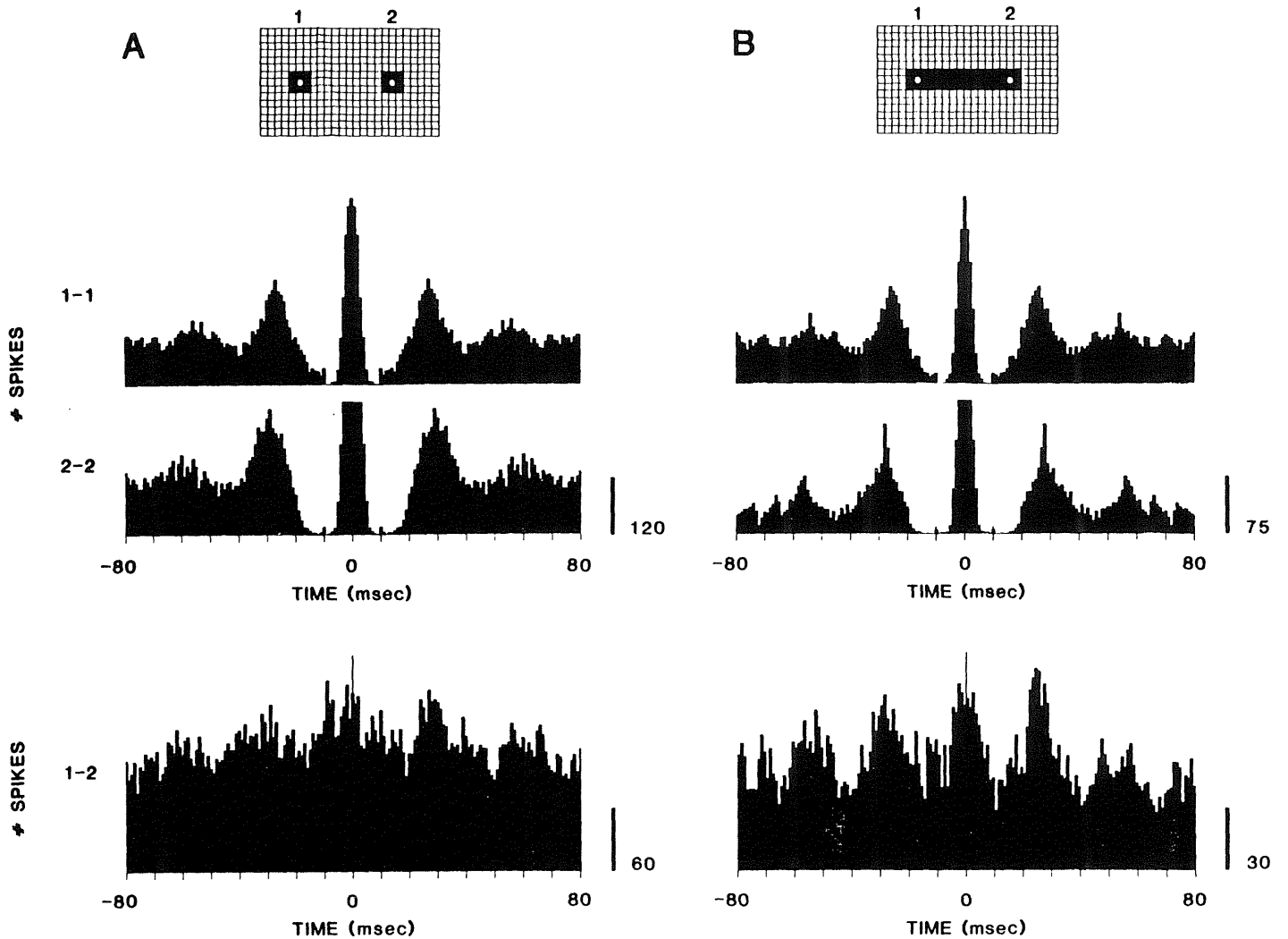
A
1
2
B
1
2
1-1
2-2
SPIKES
120
75
-80
0
80
TIME (msec)
1-2
SPIKES
60
30
-80
0
80
TIME (msec)

FIGURE 1

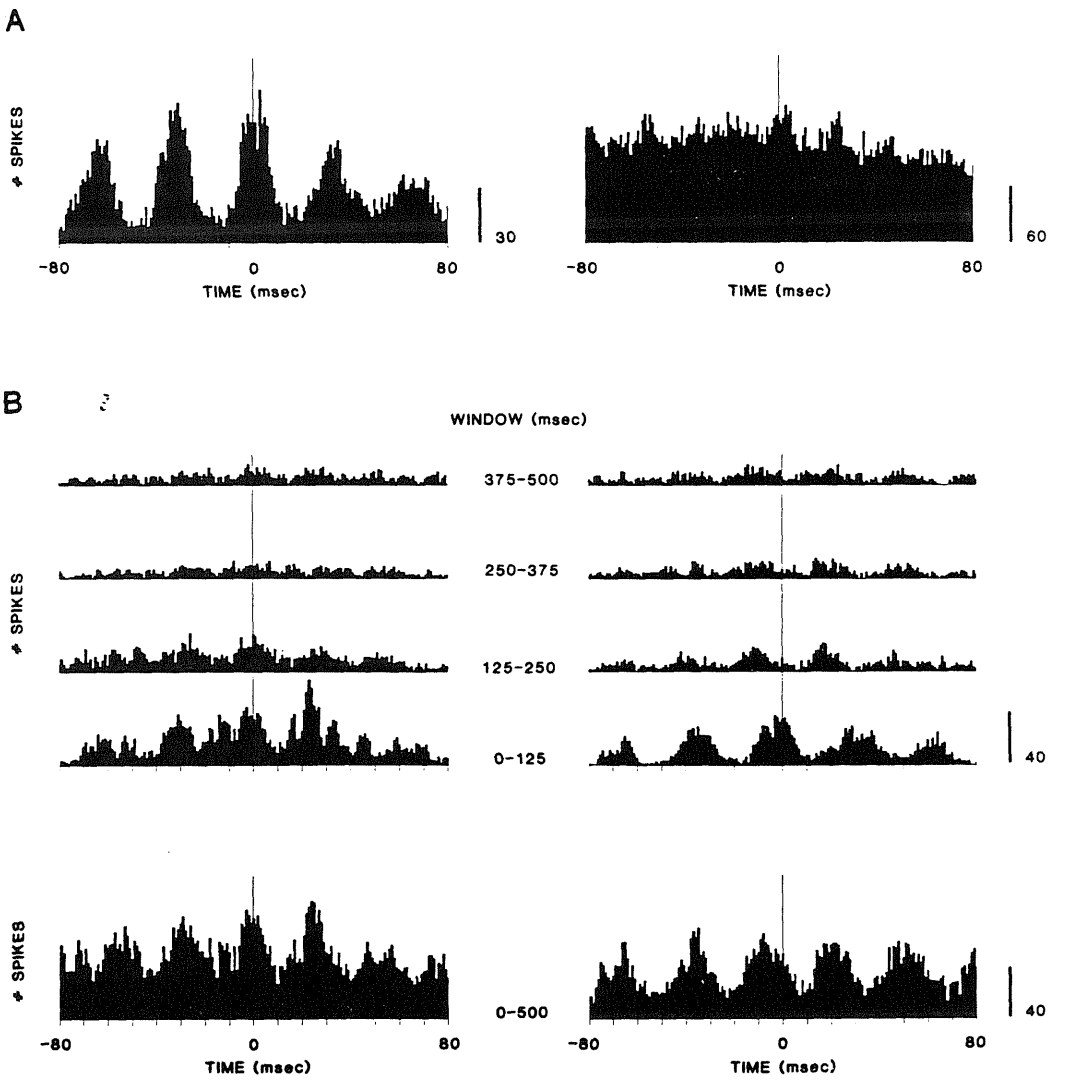
A
SPIKES
30
60
-80
0
80
TIME (msec)
B
WINDOW (msec)
375-500
250-375
125-250
0-125
0-500
40
40

FIGURE 2

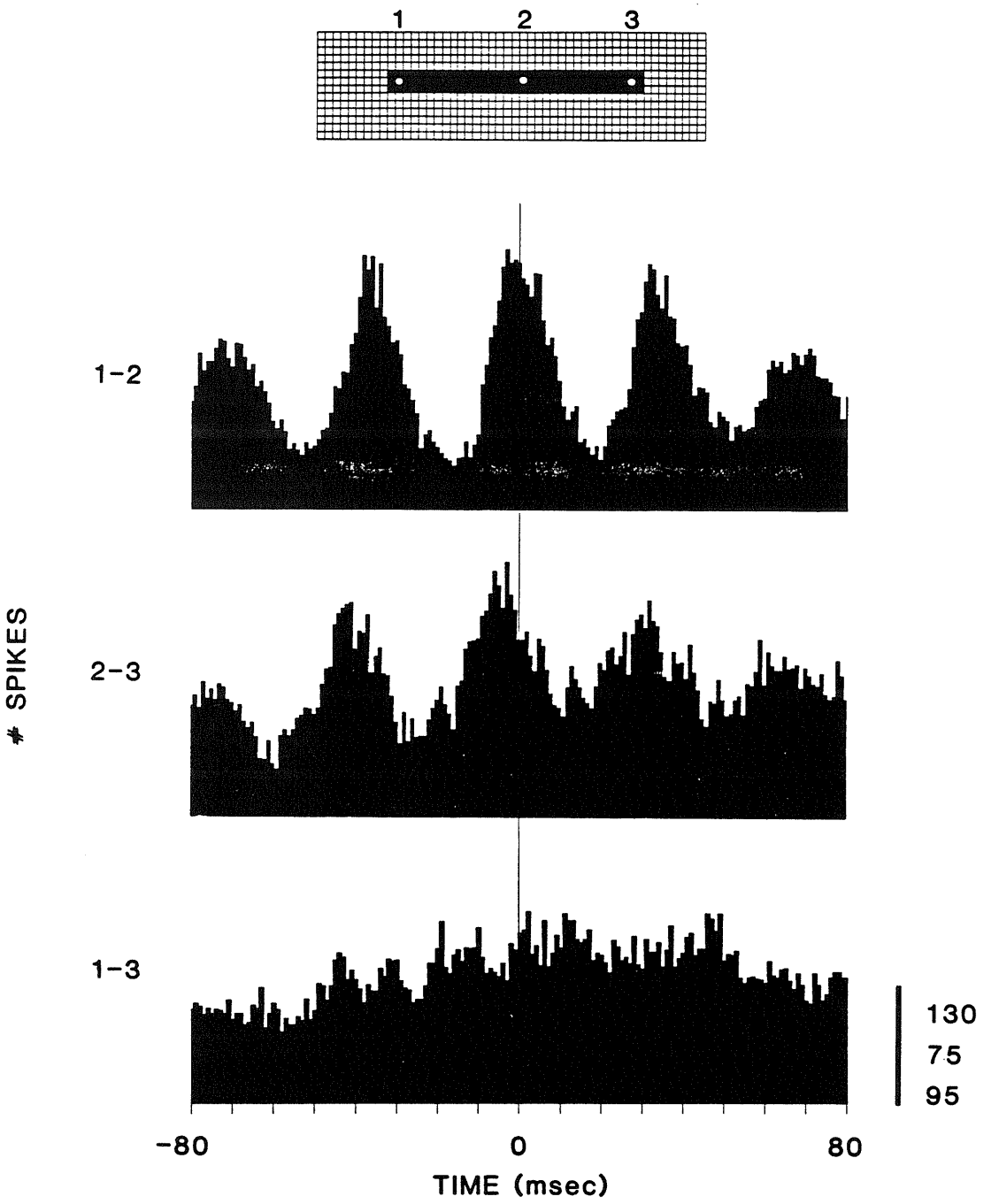

FIGURE 3

GENESIS: A SYSTEM FOR SIMULATING NEURAL NETWORKS

Matthew A. Wilson, Upinder S. Bhalla, John D. Uhley, James M. Bower.
Division of Biology
California Institute of Technology
Pasadena, CA 91125

ABSTRACT

We have developed a graphically oriented, general purpose simulation system to facilitate the modeling of neural networks. The simulator is implemented under UNIX and X-windows and is designed to support simulations at many levels of detail. Specifically, it is intended for use in both applied network modeling and in the simulation of detailed, realistic, biologically-based models. Examples of current models developed under this system include mammalian olfactory bulb and cortex, invertebrate central pattern generators, as well as more abstract connectionist simulations.

INTRODUCTION

Recently, there has been a dramatic increase in interest in exploring the computational properties of networks of parallel distributed processing elements (Rumelhart and McClelland, 1986) often referred to as "neural networks" (Anderson, 1988). Much of the current research involves numerical simulations of these types of networks (Anderson, 1988; Touretzky, 1989). Over the last several years, there has also been a significant increase in interest in using similar computer simulation techniques to study the structure and function of biological neural networks. This effort can be seen as an attempt to reverse-engineer the brain with the objective of understanding the functional organization of its very complicated networks (Bower, 1989). Simulations of these systems range from detailed reconstructions of single neurons, or even components of single neurons, to simulations of large networks of complex neurons (Koch and Segev, 1989). Modelers associated with each area of research are likely to benefit from exposure to a large range of neural network simulations. A simulation package capable of implementing these varied types of network models would facilitate this interaction.

DESIGN FEATURES OF THE SIMULATOR

We have built GENESIS (GEneral NEtwork SImulation System) and its graphical interface XODUS (X-based Output and Display Utility for Simulators) to provide a standardized and flexible means of constructing neural network simulations while making minimal assumptions about the actual structure of the neural components. The system is capable of growing according to the needs of users by incorporating user-defined code. We will now describe the specific features of this system.

Device independence.

The entire system has been designed to run under UNIX and X-windows (version 11) for maximum portability. The code was developed on Sun workstations and has been ported to Sun3's, Sun4's, Sun 386i's, and Masscomp computers. It should be portable to all installations supporting UNIX and X-11. In addition, we will be developing a parallel implementation of the simulation system (Nelson et al., 1989).

Modular design.

The design of the simulator and interface is based on a "building-block" approach. Simulations are constructed of modules which receive inputs, perform calculations on them, and generate outputs (figs. 2,3). This approach is central to the generality and flexibility of the system as it allows the user to easily add new features without modification to the base code.

Interactive specification and control.

Network specification and control is done at a high level using graphical tools and a network specification language (fig. 1). The graphics interface provides the highest and most user friendly level of interaction. It consists of a number of tools which the user can configure to suit a particular simulation. Through the graphical interface the user can display, control and adjust the parameters of simulations. The network specification language we have developed for network modeling represents a more basic level of interaction. This language consists of a set of simulator and interface functions that can be executed interactively from the keyboard or from text files storing command sequences (scripts). The language also provides for arithmetic operations and program control functions such as looping, conditional statements, and subprograms or macros. Figures 3 and 4 demonstrate how some of these script functions are used.

Simulator and interface toolkits.

Extendable toolkits which consist of module libraries, graphical tools and the simulator base code itself (fig. 2) provide the routines and modules used to construct specific simulations. The base code

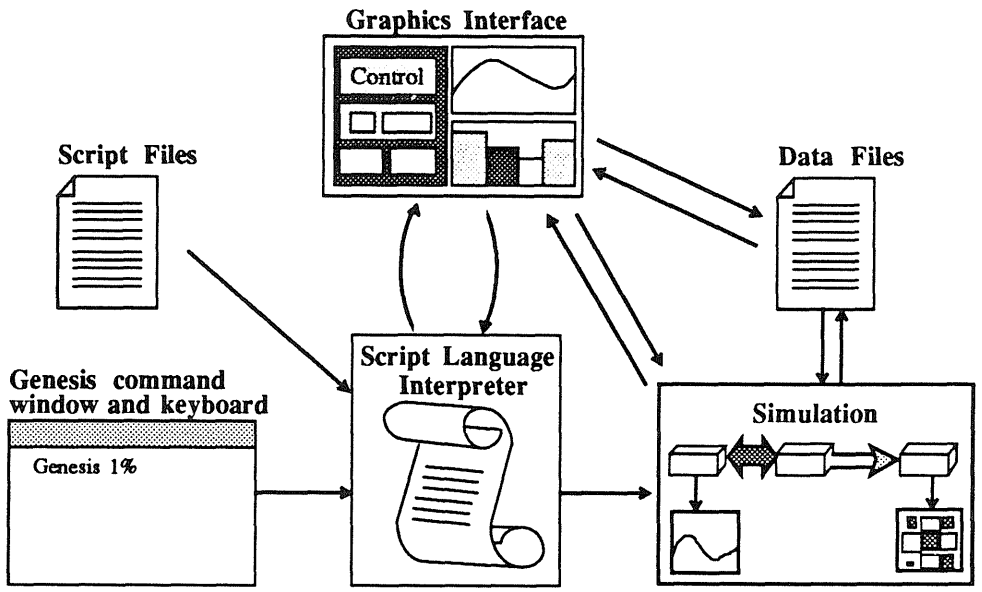

Figure 1. Levels Of Interaction With The Simulator

provides the common control and support routines for the entire system.

CONSTRUCTING SIMULATIONS

The first step in using GENESIS involves selecting and linking together those modules from the toolkits that will be necessary for a particular simulation (fig. 2,3). Additional commands in the scripting language establish the network and the graphical interface (fig. 4).

Module Classes.

Modules in GENESIS are divided into computational modules, communications modules and graphical modules. All instances of computational modules are called *elements*. These are the central components of simulations, performing all of the numerical calculations. Elements can communicate in two ways: via *links* and via *connections*. Links allow the passing of data between two elements with no time delay and with no computation being performed on the data. Thus, links serve to unify a large number of elements into a single computational unit (e.g. they are used to link elements together to form the neuron in fig. 3C). Connections, on the other hand, interconnect computational units via simulated communication channels which can incorporate time delays and perform transformations on data being transmitted (e.g. axons in fig. 3C). Graphical modules called *widgets* are used to construct the interface. These modules can issue script commands as well as

respond to them, thus allowing interactive access to simulator structures and functions.

Hierarchical organization.

In order to keep track of the structure of a simulation, elements are organized into a tree hierarchy similar to the directory structure in UNIX (fig. 3B). The tree structure does not explicitly represent the pattern of links and connections between elements, it is simply a tool for organizing complex groups of elements in the simulation.

Simulation example.

As an example of the types of modules available and the process of structuring them into a network simulation and graphical interface, we will describe the construction of a simple biological neural simulation (fig. 3). The model consists of two neurons. Each neuron contains a passive dendritic compartment, an active cell body, an axonal output, and a synaptic input onto the dendrite. The axon

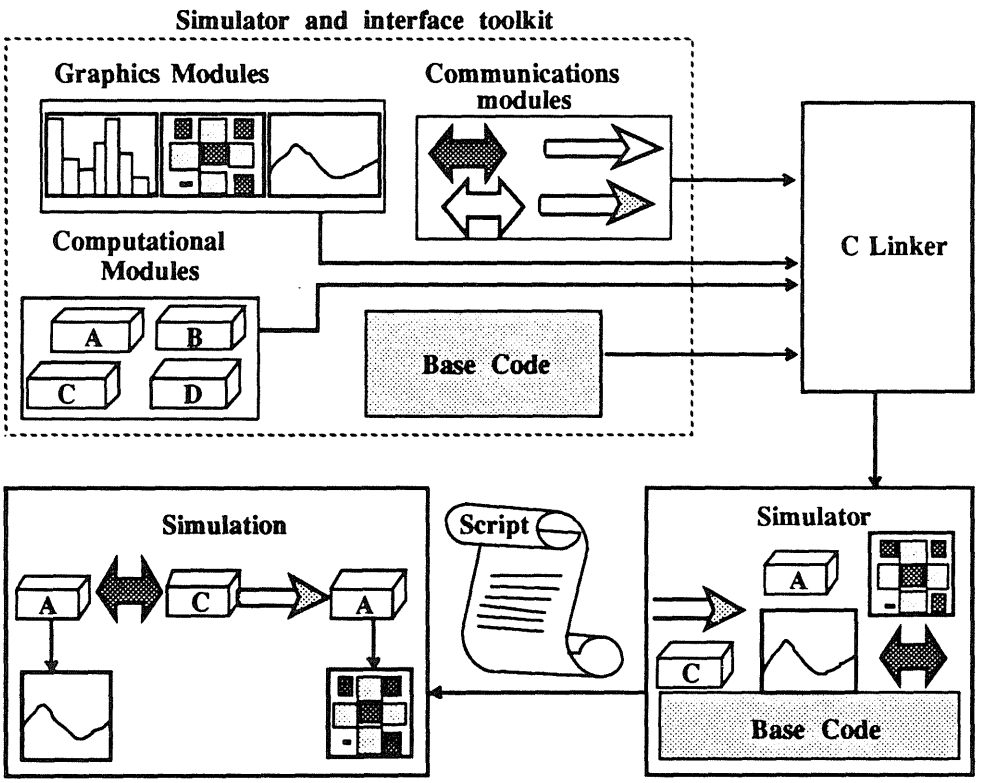

Figure 2. Stages In Constructing A Simulation.

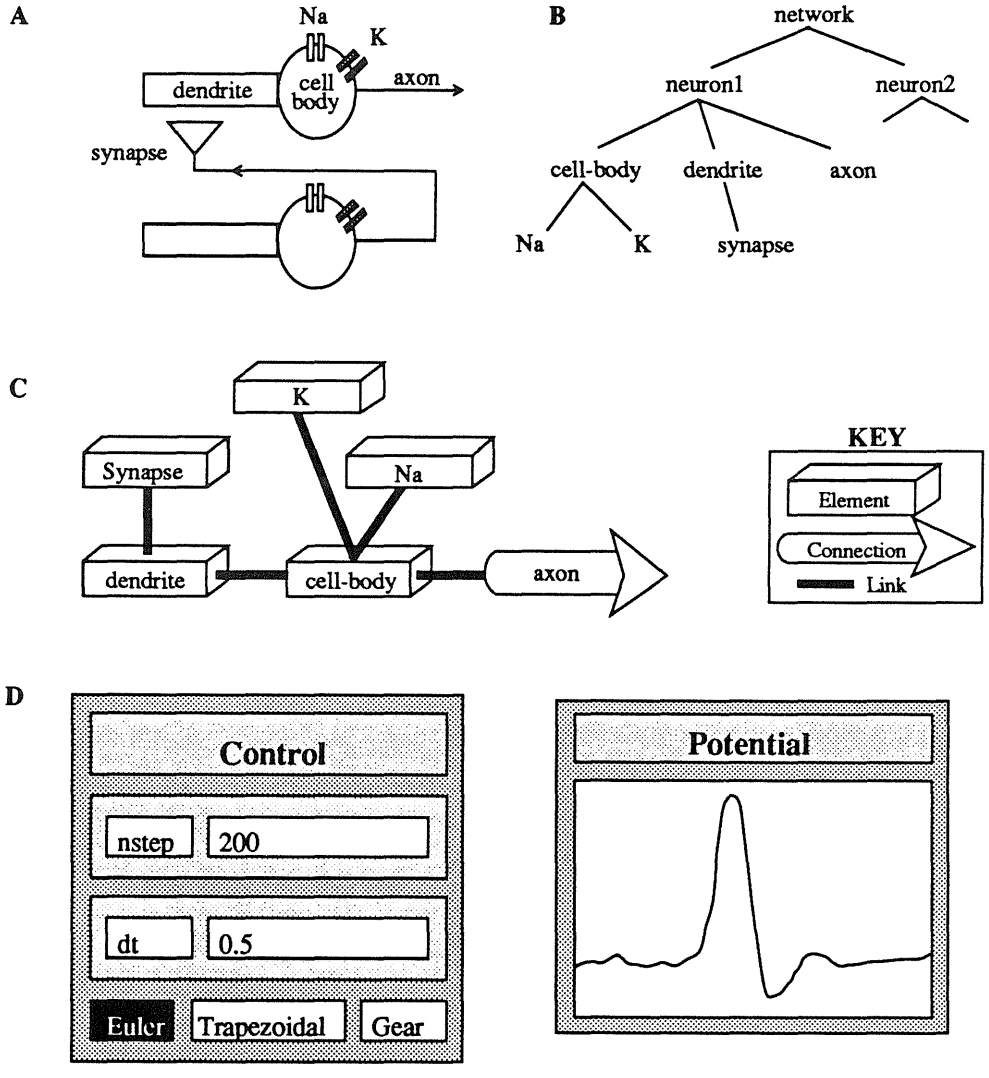

Figure 3. Implementation of a two neuron model in GENESIS. (A) Schematic diagram of compartmentally modeled neurons. Each cell in this simple model has a passive dendritic compartment, an active cell-body, and an output axon. There is a synaptic input to the dendrite of one cell and two ionic channels on the cell body. (B) Hierarchical representation of the components of the simulation as maintained in GENESIS. The cell-body of neuron 1 is referred to as /network/neuron1/cell-body. (C) A representation of the functional links between the basic components of one neuron. (D) Sample interface control and display widgets created using the XODUS toolkit.

of one neuron connects to a synaptic input of the other. Figure 3 shows the basic structure of the model as implemented under GENESIS. In the model, the synapse, channels, dendritic compartments, cell body and axon are each treated as separate computational elements (fig. 3C). Links allow elements to share information (e.g. the Na channel needs to have access to the cell-body membrane

```
Create different types of elements and assign them names.
    create                          neuron1
    create    active_compartment    cell-body
    create    passive_compartment   dendrite
    create    synapse               dendrite/synapse

Establish functional "links" between the elements.
    link      dendrite              to    cell-body
    link      dendrite/synapse      to    dendrite

Set parameters associated with the elements.
    set       dendrite      capacitance     1.0e-6

Make copies of entire element subtrees.
    copy      neuron1             to    neuron2

Establish "connections" between two elements.
    connect   neuron1/axon        to    neuron2/dendrite/synapse

Set up a graph to monitor an element variable
    graph     neuron1/cell-body       potential

Make a control panel with several control "widgets".
    xform     control
    xdialog   nstep   set-nstep   -default 200
    xdialog   dt      set-dt      -default 0.5
    xtoggle   Euler   set-euler
```

Figure 4. Sample script commands for constructing a simulation (see fig. 3)

voltage). Figure 4 shows a portion of the script used to construct this simulation.

SIMULATOR SPECIFICATIONS

Memory requirements of GENESIS.

Currently, GENESIS consists of about 20,000 lines of simulator code and a similar amount of graphics code, all written in C. The executable binaries take up about 1.5 Megabytes. A rough estimate of the amount of additional memory necessary for a particular simulation can be calculated from the sizes and number of modules used in a simulation. Typically, elements use around 100 bytes, connections 16 and messages 20. Widgets use 5-20 Kbytes each.

Performance

The overall efficiency of the GENESIS system is highly simulation specific. To consider briefly a specific case, the most sophisticated biologically based simulation currently implemented under GENESIS, is a model of piriform (olfactory) cortex (Wilson et al., 1986; Wilson and Bower, 1988; Wilson and Bower, 1989). This simulation consists of neurons of four different types. Each neuron contains from one to five compartments. Each compartment can contain several channels. On a SUN 386i with 8 Mbytes of RAM, this simulation with 500 cells runs at 1 second per time step.

Other models that have been implemented under GENESIS

The list of projects currently completed under GENESIS includes approximately ten different simulations. These include models of the olfactory bulb (Bhalla et al., 1988), the inferior olive (Lee and Bower, 1988), and a motor circuit in the invertebrate sea slug Tritonia (Ryckebusch et al., 1989). We have also built several tutorials to allow students to explore compartmental biological models (Hodgkin and Huxley, 1952), and Hopfield networks (Hopfield, 1982).

Access/use of GENESIS

GENESIS and XODUS will be made available at the cost of distribution to all interested users. As described above, new user-defined modules can be linked into the simulator to extend the system. Users are encouraged to support the continuing development of this system by sending modules they develop to Caltech. These will be reviewed and compiled into the overall system by GENESIS support staff. We would also hope that users would send completed published simulations to the GENESIS data base. This will provide others with an opportunity to observe the behavior of a simulation first hand. A current listing of modules and full simulations will be maintained and available through an electronic mail newsgroup, Babel. Enquiries about the system should be sent to GENESIS@caltech.edu or GENESIS@caltech.bitnet.

Acknowledgments

We would like to thank Mark Nelson for his invaluable assistance in the development of this system and specifically for his suggestions on the content of this manuscript. We would also like to recognize Dave Bilitch, Wojtek Furmanski, Christof Koch, innumerable Caltech students and the students of the 1988 MBL summer course on Methods in Computational Neuroscience for their contributions to the creation and evolution of GENESIS (not mutually exclusive). This research was also supported by the NSF (EET-8700064), the NIH (BNS 22205), the ONR (Contract N00014-88-K-0513), the Lockheed Corporation, the Caltech Presidents Fund, the JPL Directors Development Fund, and the Joseph Drown Foundation.

References

D. Anderson. (ed.) Neural information processing systems. American Institute of Physics, New York (1988).

U.S. Bhalla, M.A. Wilson, & J.M. Bower. Integration of computer simulations and multi-unit recording in the rat olfactory system. Soc. Neurosci. Abstr. 14: 1188 (1988).

J.M. Bower. Reverse engineering the nervous system: An anatomical, physiological, and computer based approach. In: An Introduction to Neural and Electronic Networks. Zornetzer, Davis, and Lau, editors. Academic Press (1989)(in press).

A.L. Hodgkin and A.F. Huxley. A quantitative description of membrane current and its application to conduction and excitation in nerve. J.Physiol, (Lond.) 117, 500-544 (1952).

J.J. Hopfield. Neural networks and physical systems with emergent collective computational abilities. Proc. Natl. Acad. Sci. USA. 79, 2554-2558 (1982).

C. Koch and I. Segev. (eds.) Methods in Neuronal Modeling: From Synapses to Networks. MIT Press, Cambridge, MA (in press).

M. Lee and J.M. Bower. A structural simulation of the inferior olivary nucleus. Soc. Neurosci. Abstr. 14: 184 (1988).

M. Nelson, W. Furmanski and J.M. Bower. Simulating neurons and neuronal networks on parallel computers. In: Methods in Neuronal Modeling: From Synapses to Networks. C. Koch and I. Segev, editors. MIT Press, Cambridge, MA (1989)(in press).

S. Ryckebusch, C. Mead and J.M. Bower. Modeling a central pattern generator in software and hardware: Tritonia in sea moss (CMOS). (1989)(this volume).

D.E. Rumelhart, J.L. McClelland and the PDP Research Group. Parallel Distributed Processing. MIT Press, Cambridge, MA (1986).

D. Touretzky. (ed.) Advances in Neural Network Information Processing Systems. Morgan Kaufmann Publishers, San Mateo, California (1989).

M.A. Wilson and J.M. Bower. The simulation of large-scale neuronal networks. In: Methods in Neuronal Modeling: From Synapses to Networks. C. Koch and I. Segev, editors. MIT Press,

Cambridge, MA (1989)(in press).

M.A. Wilson and J.M. Bower. A computer simulation of olfactory cortex with functional implications for storage and retrieval of olfactory information. In: Neural information processing systems. pp. 114-126 D. Anderson, editor. Published by AIP Press, New York, N.Y (1988).

M.A. Wilson, J.M. Bower and L.B. Haberly. A computer simulation of piriform cortex. Soc. Neurosci. Abstr. 12,1358 (1986).

Appendix 1: Parameter variations and their effect on simulated EEG

Introduction

This appendix examines the effects of critical parameter variations on the simulated EEG responses in the network model of piriform cortex.

The model used contained 405 cells (9x15) of the types described in chapter 1. The smaller network size was necessary in order to perform the required simulations considering computational and data storage overhead which rapidly becomes prohibitive.

Field potentials were computed using the methods described in chapters 1 and 2. An 8x5 simulated electrode array was placed at the surface of the cortex. The fields measured from these electrodes were combined to produce a single average measure of the EEG for the population. Power spectra were computed from the average EEG using an FFT with Parzen data windowing (Press et al. 1988). Afferent input was provided through 10 independent fibers each of which were driven by independent poisson distributed random impulse generating processes. The average rate of impulse generation along a single fiber was 200 Hz. The amplitudes of impulses were subject to variation according to the manipulations described.

Inhibitory effects

Oscillatory frequency is modulated through both local and long range interactions. The local modulatory features include the coupling characteristics from pyramidal cells to inhibitory cells as well as from afferent input to inhibitory cells and from inhibitory cells back to pyramidal cells. The model parameters which govern these interactions include the strength of coupling along these pathways as well as the time course of excitatory and inhibitory synaptic conductances.

In the actual cortex, barbiturates are known to potentiate the time course of inhibitory conductance changes through Cl- mediated channels. Figure 1a demonstrates the effect on oscillatory behavior as the open channel time for the Cl- mediated inhibitory process is increased from 7 to 18 msec. With an afferent input level of 0.5 this modification has the effect of reducing peak frequency (fig. 1c) and virtually eliminating structured oscillatory behavior.

Figure 1b demonstrates the effect of increasing feedback inhibition onto feedback interneurons which has the effect of enhancing oscillatory firing of interneurons. The result of this modification is the appearance of more robust EEG oscillations with increased energy in the frequency bands corresponding to the relative duration of inhibitory conducting times as seen in figure 1c.

As mentioned earlier, parameters involved in modifying the gain of in-

hibitory feedback to pyramidal cells have a significant impact on oscillatory behavior. Figure 2a demonstrates the result of changing the relative strength of synaptic activation from feedback interneurons to pyramidal cells for low level (A=.1) afferent input with a Cl- channel open time of 18 msec. Under nominal conditions, the response takes the form of irregular spindles occuring at low frequencies with no significant energy in the 20-80 Hz range (fig. 2b). Reducing the efficacy of feedback inhibitory to pyramidal cell synapses by 0.75 results in the appearance of higher frequency oscillatory components. Further reduction to a level half of the nominal value results in high frequency oscillations reflecting maximal firing of pyramidal cells. This indicates a fairly narrow operating range for the coupling strength of feedback to pyramidal cell inhibitory connections.

Excitatory effects

As discussed in chapter 1, system parameters which modulate network excitability have a significant effect on the generation of oscillatory behavior. In the model these parameters include level of background activity and strength of excitatory coupling.

Figure 3 demonstrates the effect of varying the relative strength of excitatory synaptic connections between pyramidal cells along association fiber pathways. The values shown next to each trace are the factors by which all long range excitatory synaptic weights were multiplied. In the nominal case (1x),

oscillations appear relatively unstructured, with energy peaks near 20 and 45 Hz. Attenuation of association fiber weights by a factor of 0.5 from the nominal value results in a significant reduction in oscillatory behavior. Conversely, increasing relative efficacy by as little as 20 percent results in an increase in energy concentrated in the 40-60 Hz range and the emergence of modest oscillatory bursts 100-200 msec in duration. Increasing relative association fiber efficacy by a factor of 5 results in the appearance of fully oscillatory behavior with enery in the 40-80 Hz range and the appearance of clear burst intervals. This demonstrates the role of positive feedback on the generation of oscillatory bursts.

As seen in earlier chapters, the interaction of excitatory events during these burst cycles is thought to underly the basic computation performed by the olfactory cortex. Consequently, the enhancement of these oscillatory periods with increased excitatory coupling is consistent with the activation or amplification of this computational process.

The enhancement of oscillatory behavior with increases in the strength of excitatory coupling arises from the increase in excitability of cells induced by intrinsic positive feedback. This excitability can also be modulated through afferent input. Figure 4 explores the effects of changing levels of afferent input. A most interesting effect is noted in the case of near baseline input levels. There

is an abrupt transition from the low spontaneous level seen in figure 3 with attenuated association fiber gains, to a fully oscillatory state. Further increases in afferent levels of activation do not significantly alter the oscillatory behavior with peak energy remaining in the 40-60 Hz range in each case. The reason for this modest effect is that afferent input targets both excitatory and inhibitory cells. Thus increasing afferent input increases activity levels on both types resulting in a relatively balanced effect. This result, coupled with the results obtained through adjustment of association fiber gain suggests that with nominally enhanced synaptic efficacy, the system has a tremendous sensitivity to the presence of input but the oscillatory gain is relatively insensitive to absolute input magnitude. Again this is consistent with the idea that the oscillations reflect the action of a computational process which acts on the input rather than being explicitly driven by it. Regulation of the oscillatory behavior can be effectively performed through modulation of intrinsic excitatory pathways which suggests the presence of pharmacological mechanisms which are specific to the intrinsic excitatory connections. As discussed in chapter 2, recent work has uncovered mechanisms which have the requisite specificity (Hasselmo and Bower 1990).

An additional mechanism which could selectively increase pyramidal cell excitability would be selective enhancement of afferent synapses onto pyramidal

cells. This pathway is known to possess physiological and pharmacological properties that distinguish it from association fiber pathways (Haberly and Bower 1986).

Figure 5 shows the results of simulations in which afferent to pyramidal cell synapses were increased up to 10 fold. The effect on oscillatory behavior was modest with little effect on oscillatory frequency or burst production. The inability of purely afferent driven input to produce oscillatory responses comparable to those generated through enhanced association fiber gain is largely a function of the continous nature of the simulated afferent input. While steady bulbar input increases excitability of pyramidal cells, the presence of steady in-phase as well as out of phase activation of pyramidal cells induces an out of phase bias to fire reducing the modulation of spike activity. In the case of enhanced excitatory coupling, positive feedback is not distributed uniformly over time but is modulated at the population frequency. With the appropriate phase relationships between cells (outlined in chapter 1) this activation remains in phase with oscillations of distant cells. Thus, intrinsic positive feedback not only enhances excitability, but does so in a coordinated fashion. The synchronized feedback introduced between cells coupled with the appropriate phase relationship significantly increases the amplification of pyramidal cell activity.

An interesting feature of the simulated oscillatory behavior is its modu-

lation into 100-200 msec bursts. Earlier work presented in chapter 1 indicated that the K+ mediated feedforward inhibitory process was capable of modulating EEG bursts at comparable frequencies. Due to the relatively attenuated feedback contribution from pyramidal cells to feedforward interneurons used in these simulations, K+ mediated inhibition was not responsible for observed modulation. Consequently, additional intrinsic mechanisms must be in place to produce equivalent effects.

Examination of the activity patterns underlying the simulated EEG (fig. 6) suggests that a potential mechanism for burst frequency modulation involves desychronization of pyramidal cell firing leading to disruption of phase relationships and, therefore, of amplified positive feedback. This mechanism could operate in the following manner. As pyramidal cell firing increases, positive feedback initiates burst activity with feedback inhibition modulating the frequency based on the strength and time constants of inhibitory feedback. As excitation increases, the feedback mechanisms for regulating frequency become saturated. The loss of uniform frequency regulation across the cortex results in desynchronized firing which terminates the burst. While this explanation is suggested by these results, further investigation will be required to establish this more firmly.

It is quite interesting to note that the apparent frequency of burst modu-

lation produced through this mechanism is consistent with time contants for the long-duration hyperpolarizing K+ inhibitory process. This provides another example of the tuning of multiple system parameters to single phenomena as was observed in chapter 1 with regard to the timing of propagated excitatory events. Taken in the context of periodic desynchronization of pyramidal cell activity, the K+ inhibition could be seen as explicitly suppressing the desynchronized interburst period which appears to result in its absence. The advantage of this is apparent if one assumes that during the desynchronized state, information is not effectively processed and therefore activity occuring during this period should be ignored.

The general results of these manipulations indicate that the relative efficacy of excitatory association fiber connections is a significant parameter governing the appearance of coordinated oscillatory bursts. The use of intrinsic positive feedback provides an exquisitely high gain amplification mechanism for establishing burst behavior. Thus, these basic results introduce an additional aspect to modulation of synaptic efficacy which goes beyond issues of local dendritic computation. The switching of dynamic modes may have fundamental impact on the very nature of computation performed in the cortex (chapters 1-3). Therefore, these results again emphasize the necessity of considering the structure of computation at all levels of scale and their interactions, a function

ideally suited to simulations of the type described in this work.

REFERENCES

Bower, J.M., Haberly, L.B. Facilitating and nonfacilitating synapses on pyramidal cells: A correlation between physiology and morphology. *Proc. Natl. Acad. Sci. USA* **83**, 1115-1119, 1986.

Hasselmo, M.E., Bower, J.M. Cholinergic suppression specific to intrinsic not afferent fiber synaptic transmission in piriform cortex. submitted to Brain Res. 1990.

Press, W.H., Flannery, B.P., Teukolsky, S.A., Vetterling, W.T. Numerical recipes in C: The art of scientific computing. New York: Cambridge University Press. 1988.

Fig. 1a.

This shows the EEGs produced by continuous afferent stimulation in which the open time for the Cl- mediated inhibitory channel is varied between 7 msec (top), 10 msec (middle), and 18 msec (bottom). The stimulation amplitude is 0.5 and the strength of excitatory association fiber coupling is 1.5 times the nominal level. At 7 msec open time oscillatory behavior is apparent but irregular with peak energy between 40 and 60 Hz. Increasing the duration of Cl- inhibition reduces frequency and results in increasingly irregular behavior.

Fig. 1b.

This shows the effect of increasing the strength of connections between feedback interneurons by a factor of 1.5 on oscillations produced under the same stimulus conditions as those shown in figure 1a.

Fig. 1c.

Comparison of power spectra for EEGs shown in figure 1a (left column) and 1b (right column) showing the enhancement of energy appearing in the 20-60 Hz range due to increased inhibitory modulation of inhibitory cells.

Fig. 2.

This shows the effect on oscillatory behavior of reducing the relative efficacy of synapses from feedback interneurons to pyramidal cells. Afferent input level is 0.1 and excitatory association fiber synapses have been enhanced by a factor of

1.5. The bottom trace shows the nominal response with a relative efficacy of 1. Reduction of inhibitory input by 0.75 (middle trace) results in the appearance of more regular oscillations. Further reduction to 0.5 leads to sustained high frequency oscillations corresponding to uncontrolled pyramidal cell firing.

Fig. 3a.

This shows the effect of increasing efficacy of intrinsic excitatory association fiber synapses. The multiplier shown next to each trace represents the factor by which all long-range association fiber synapses were adjusted. The effect of enhanced excitatory coupling is seen in the uppermost trace as the appearance of regular oscillations modulated into 100-200 msec bursts.

Fig. 3b.

Power spectra for traces shown in figure 3a showing an upward shift in dominant frequency with enhanced association fiber coupling.

Fig. 4a.

This shows the effect of changing afferent input levels on oscillatory behavior. Association fiber coupling gain has been set to 1.2 times the nominal level. Effect of lowest amplitude input is shown in the bottom trace. After 400 msec an abrupt transition is made from low level activity to fully oscillatory behavior due to the effects of intrinsic positive feedback. Further increase in input amplitude (upper traces) has little effect on oscillatory behavior.

Fig. 4b.

Power spectra for traces shown in figure 4a showing little effect on frequency composition with increased input amplitude.

Fig. 5a.

This shows the effect of changing efficacy of synaptic connections from afferent fibers to pyramidal cells. Amplitude of afferent input is 0.1 and association fiber coupling gain has been set to the nominal level. The multiplier shown next to each trace represents the factor by which all afferent to pyramidal cell connections were adjusted. Response with nominal coupling is shown in the bottom trace. Increase in coupling (upper traces) produces a modest improvement in oscillatory behavior which does not improve significantly with further increases.

Fig. 5b.

Power spectra for traces shown in figure 5a showing little effect on frequency composition with selective increase in afferent to pyramidal cell synaptic efficacy.

Fig. 6a.

Activity patterns underlying oscillatory EEG with association fiber gain of 5 and input level of 0.1. The upper trace is the population average EEG (inverted with respect to previous EEGs). Below that are pyramidal population average conductances contributed by the designated pathways. The lower three traces represent population averaged spike activity for pyramidal, feedback, and

feedforward cells. Spike binwidth = 2 msec. Scale factors used in plotting are given for individual traces. Time is given in msec.

Fig. 6b.

Increased resolution display of activity shown in figure 6a.

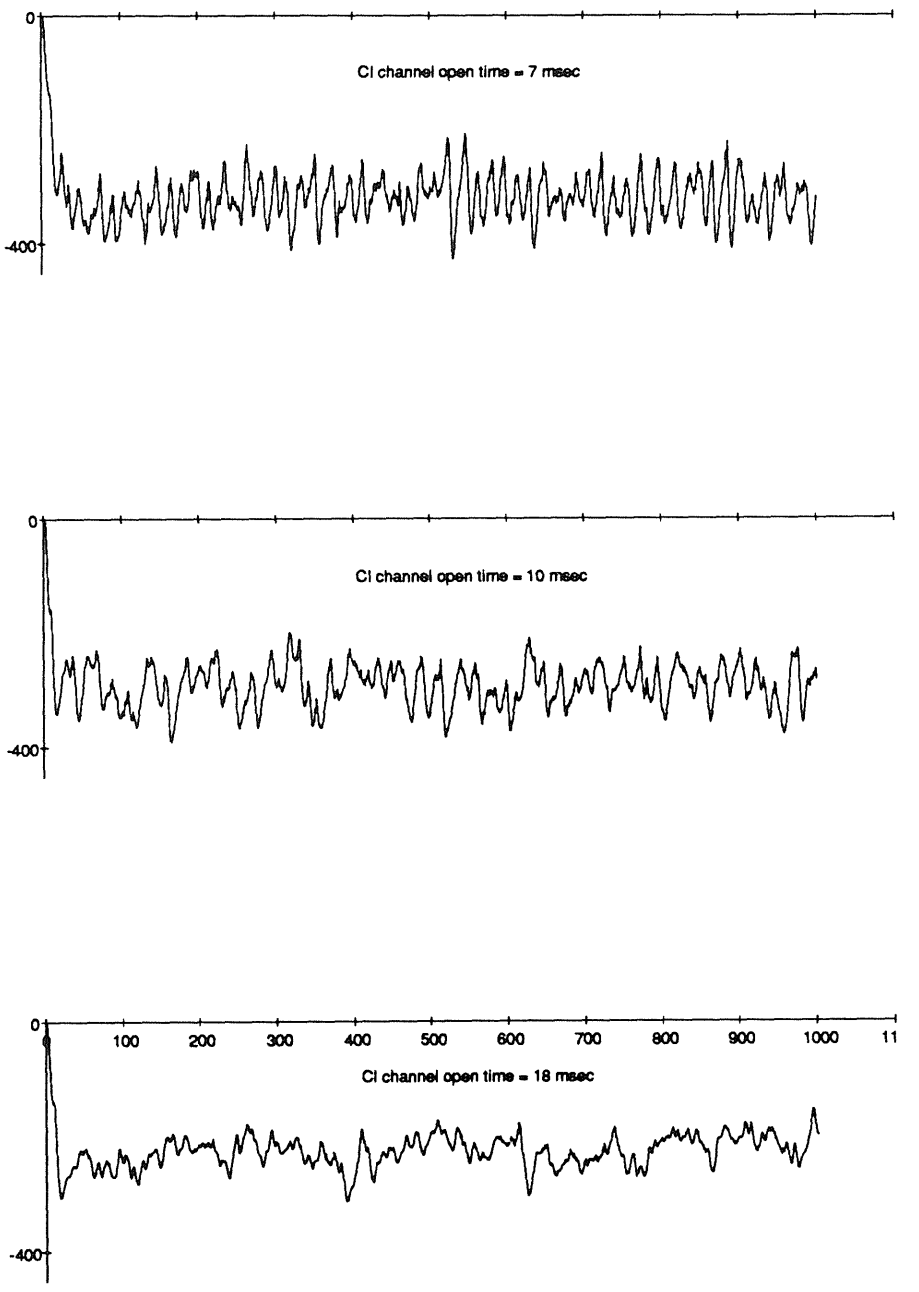
0
Cl channel open time = 7 msec
-400
0
Cl channel open time = 10 msec
-400
0
100
200
300
400
500
600
700
800
900
1000
11
Cl channel open time = 18 msec
-400

Figure 1A

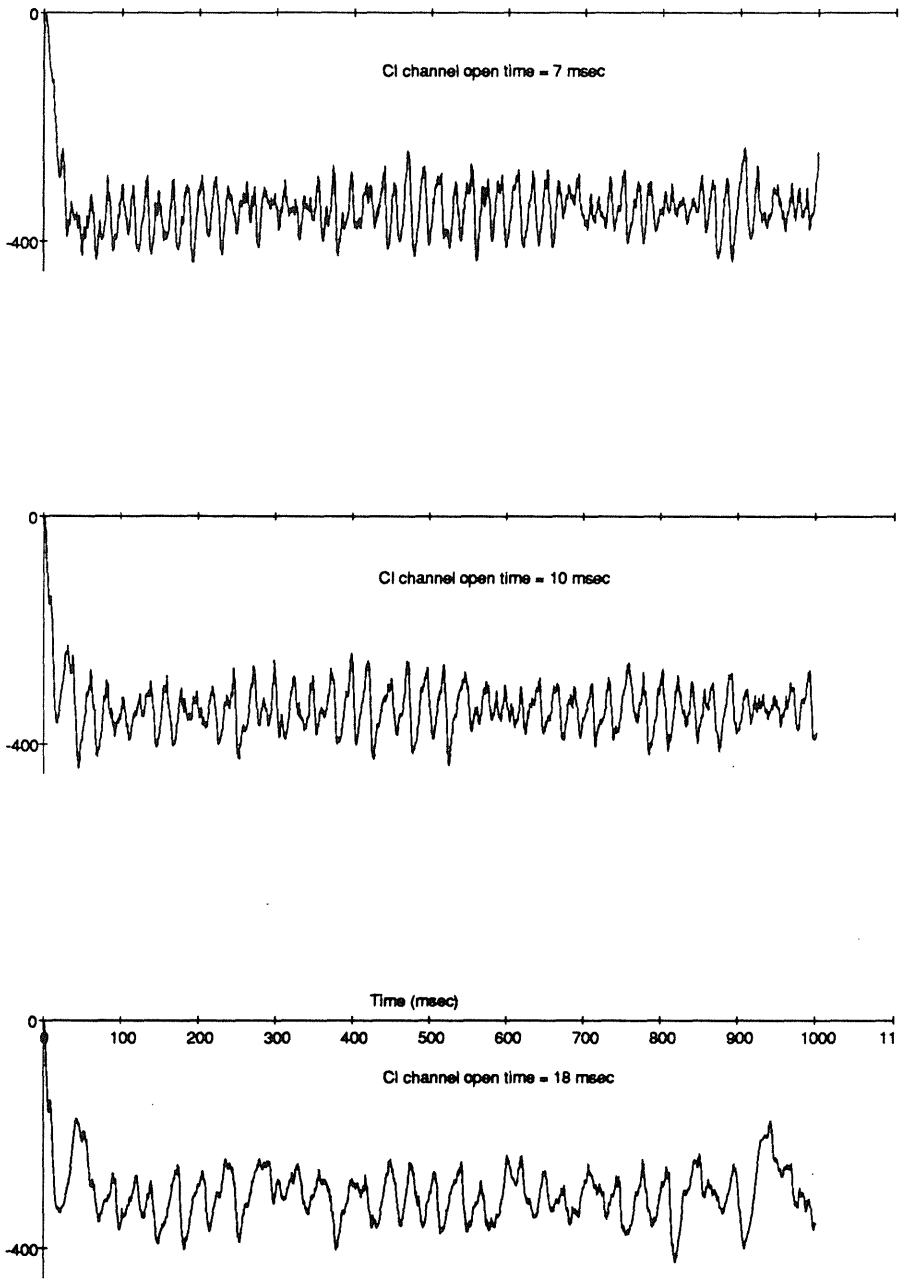
0
Cl channel open time = 7 msec
-400
0
Cl channel open time = 10 msec
-400
Time (msec)
0
100
200
300
400
500
600
700
800
900
1000
11
Cl channel open time = 18 msec
-400

Figure 1B

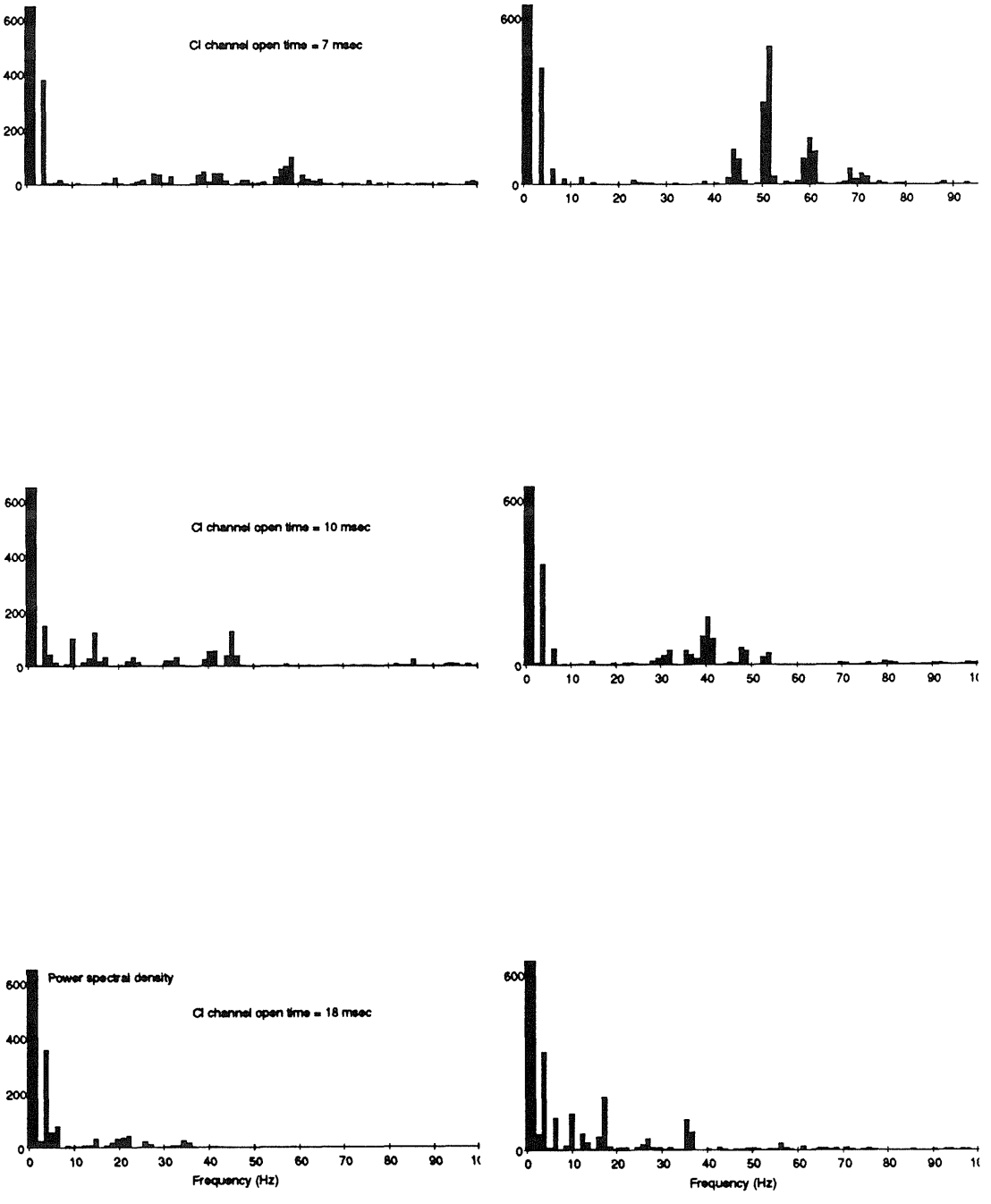
Cl channel open time = 7 msec
Cl channel open time = 10 msec
Power spectral density
Cl channel open time = 18 msec
Frequency (Hz)
Frequency (Hz)

Figure 1C

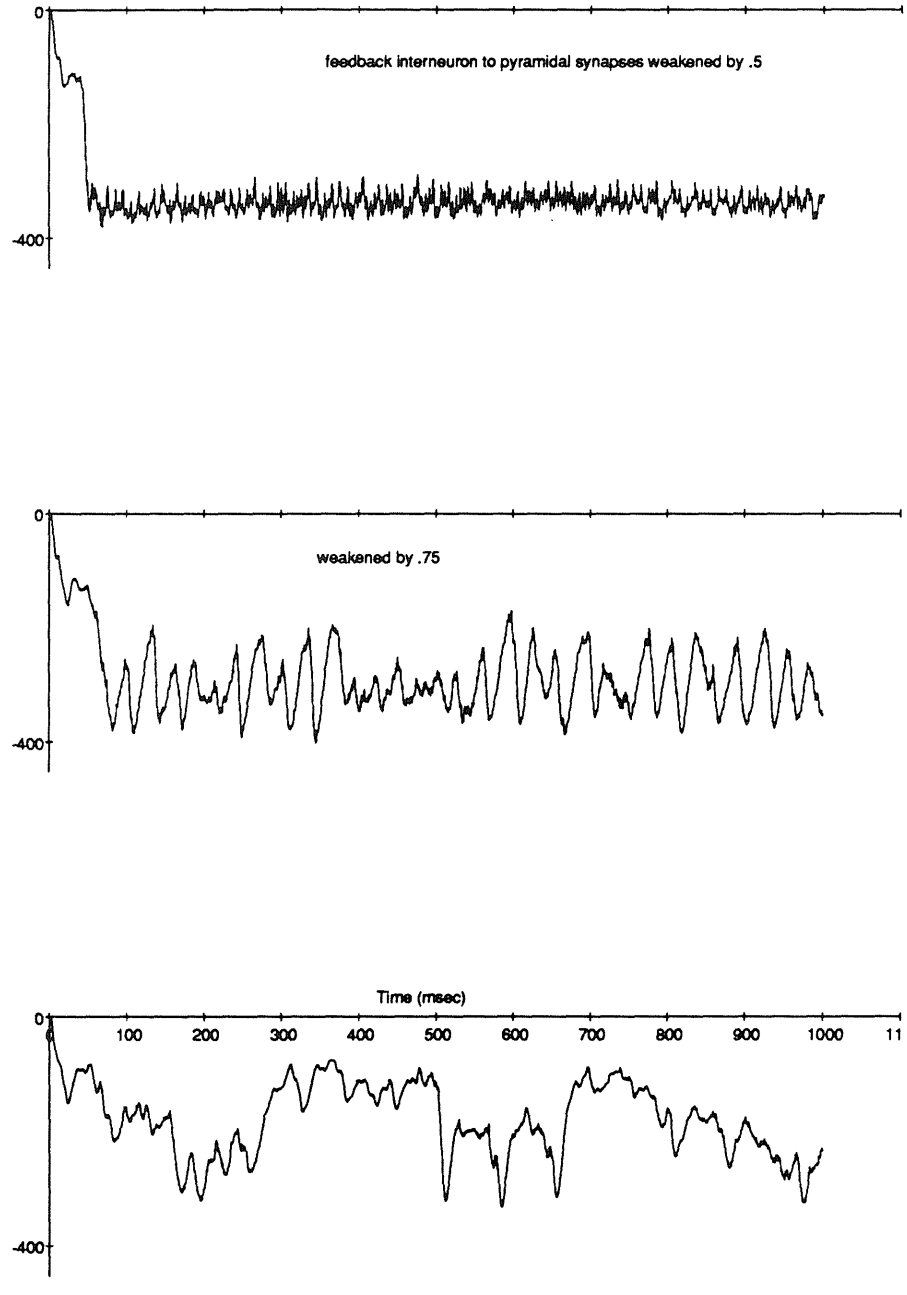
0
feedback interneuron to pyramidal synapses weakened by .5
-400
0
weakened by .75
-400
Time (msec)
0
100
200
300
400
500
600
700
800
900
1000
11
-400

Figure 2

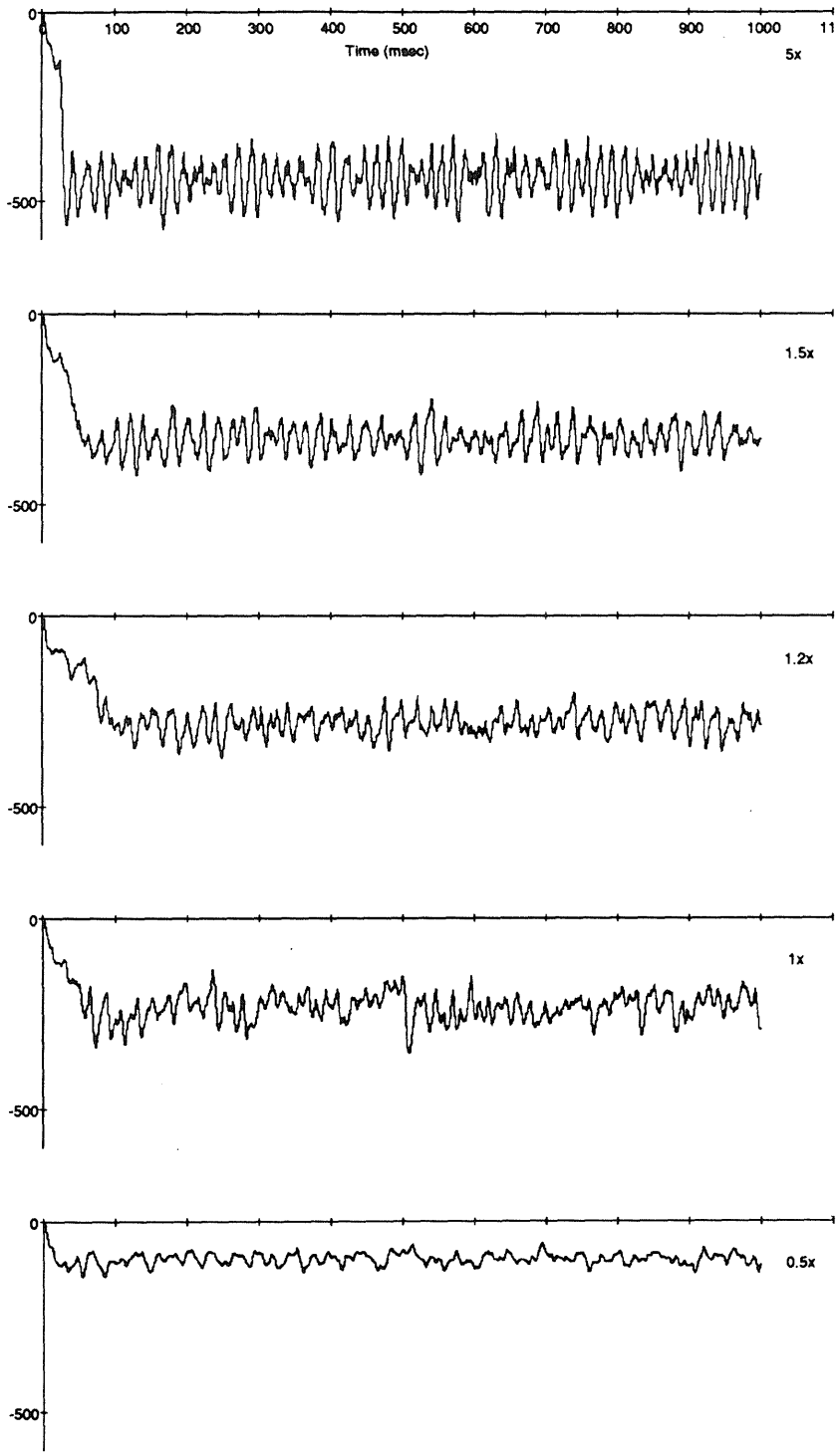
0
100
200
300
400
500
600
700
800
900
1000
11
Time (msec)
5x
-500
0
1.5x
-500
0
1.2x
-500
0
1x
-500
0
0.5x
-500

Figure 3A

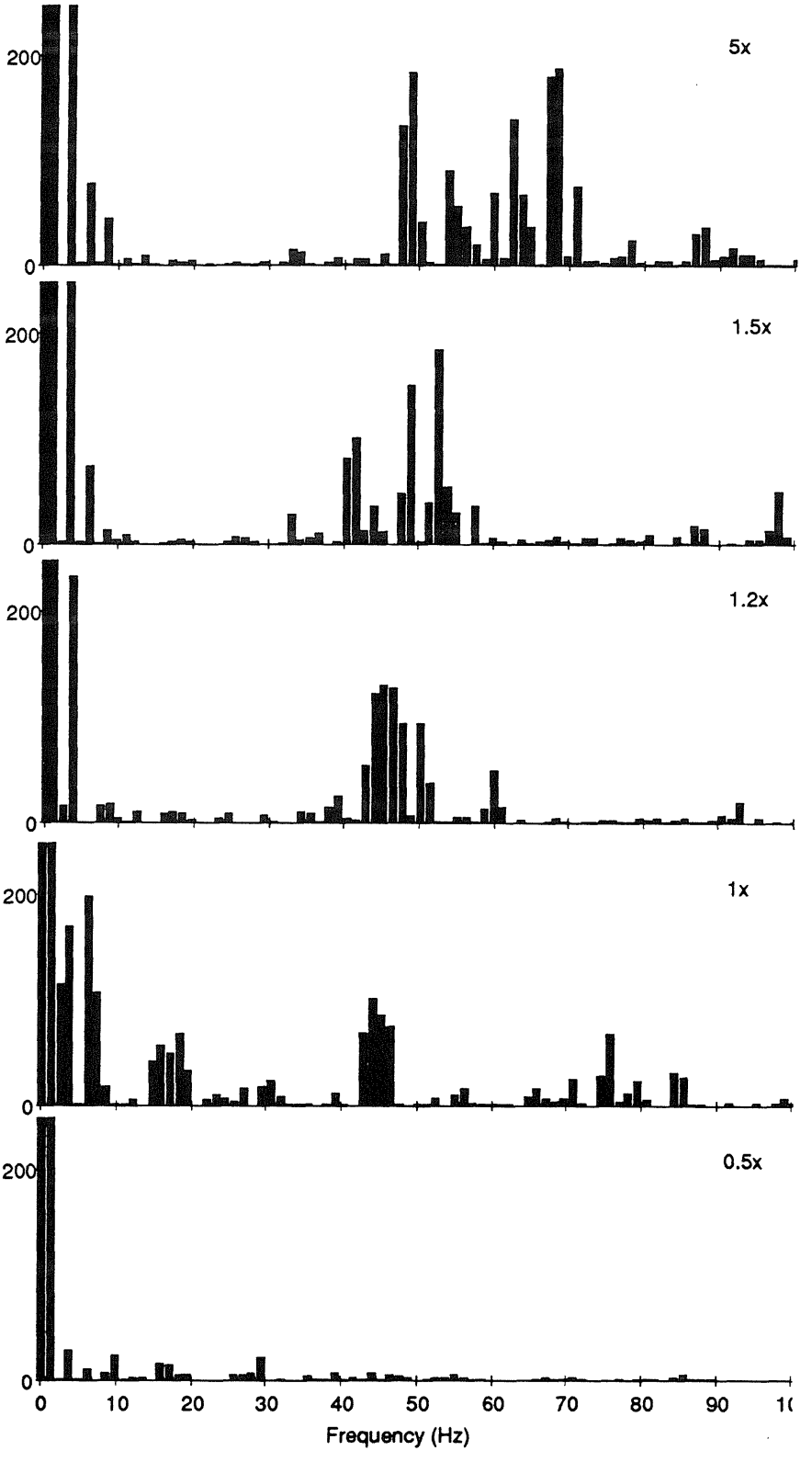

Figure 3b

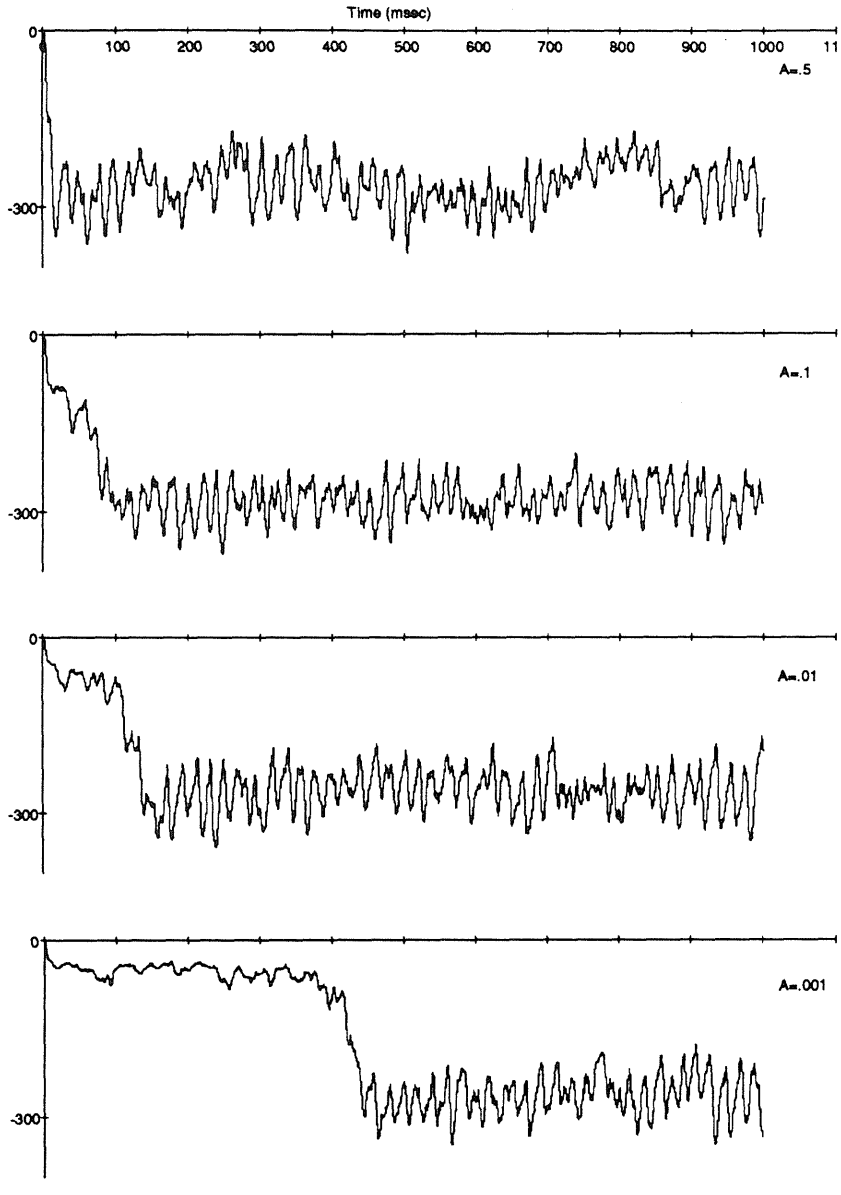
Time (msec)
0
100
200
300
400
500
600
700
800
900
1000
11
A=.5
-300
0
A=.1
-300
0
A=.01
-300
0
A=.001
-300

Figure 4A

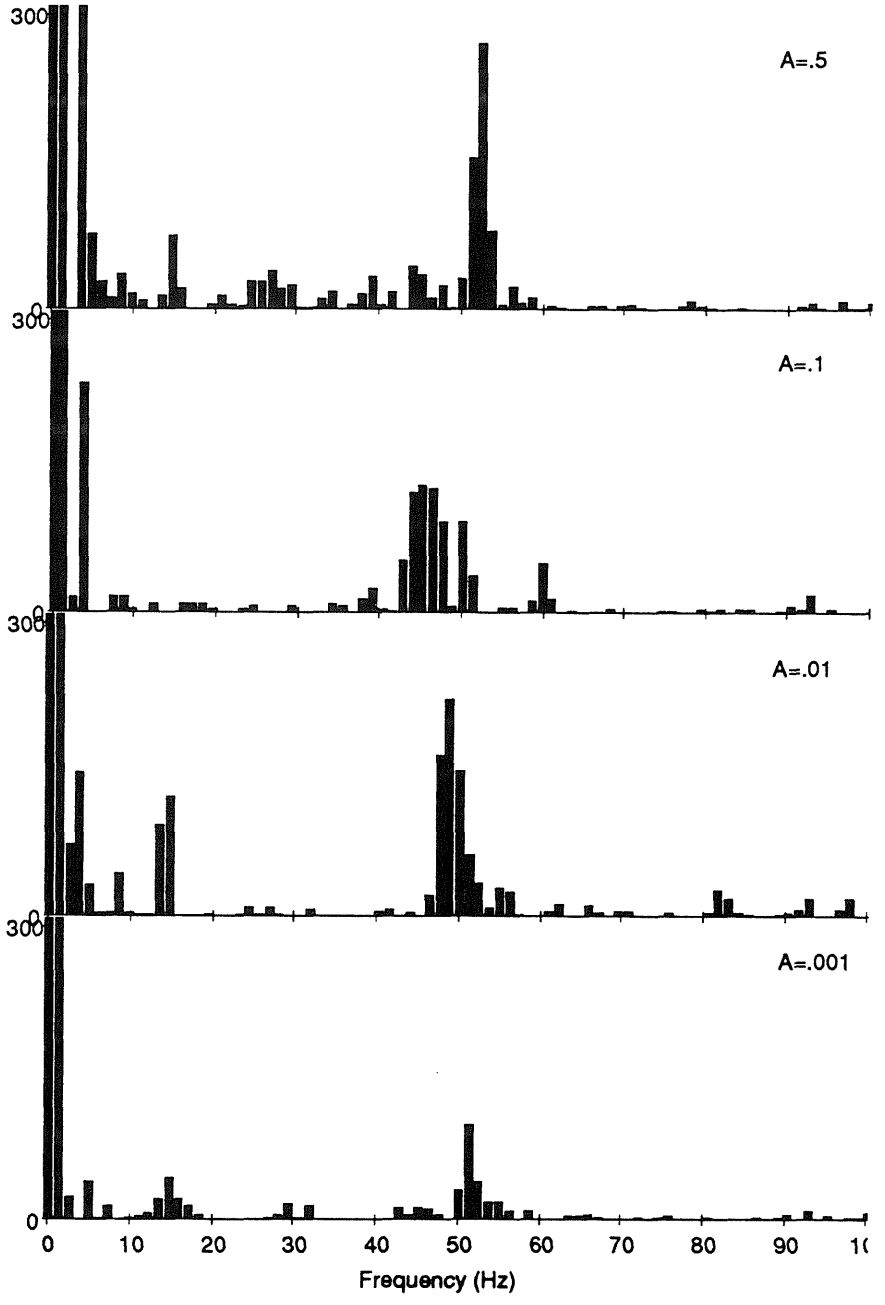
300
A=.5
0
300
A=.1
0
300
A=.01
0
300
A=.001
0
0 10 20 30 40 50 60 70 80 90 1(
Frequency (Hz)

Figure 4B

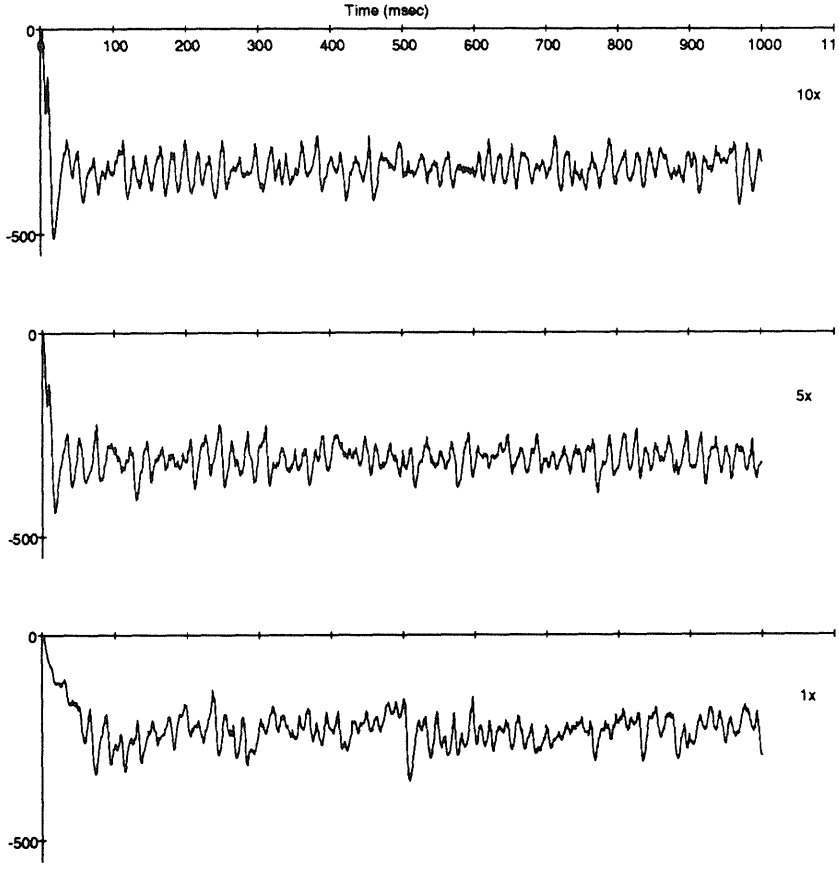
Time (msec)
0
100
200
300
400
500
600
700
800
900
1000
11
10x
-500
0
5x
-500
0
1x
-500

Figure 5A

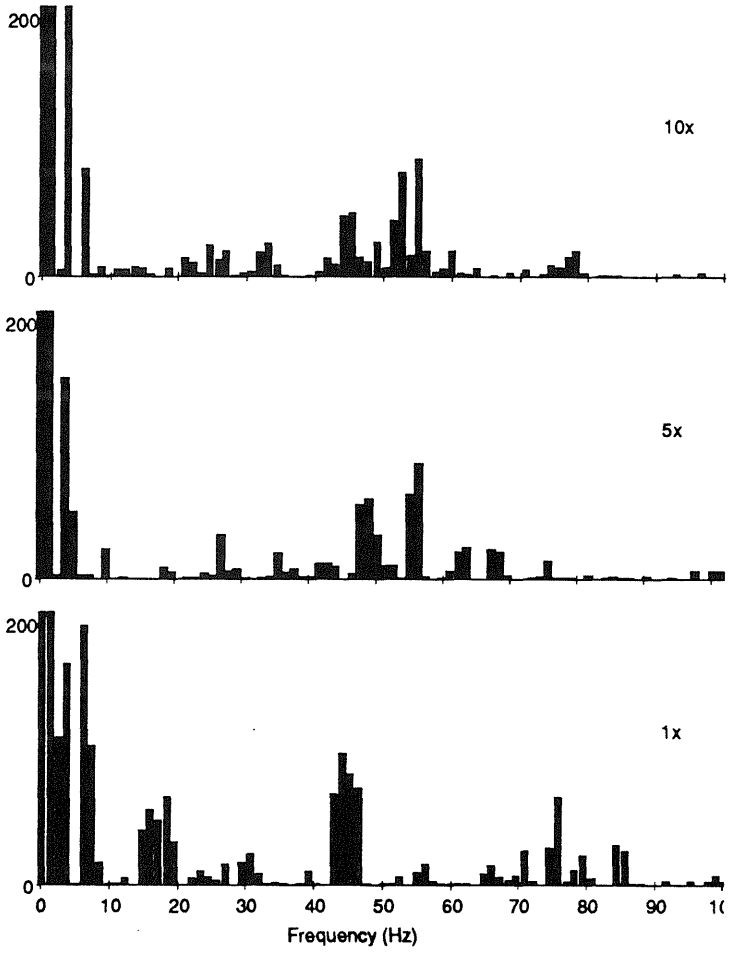

Figure 5B

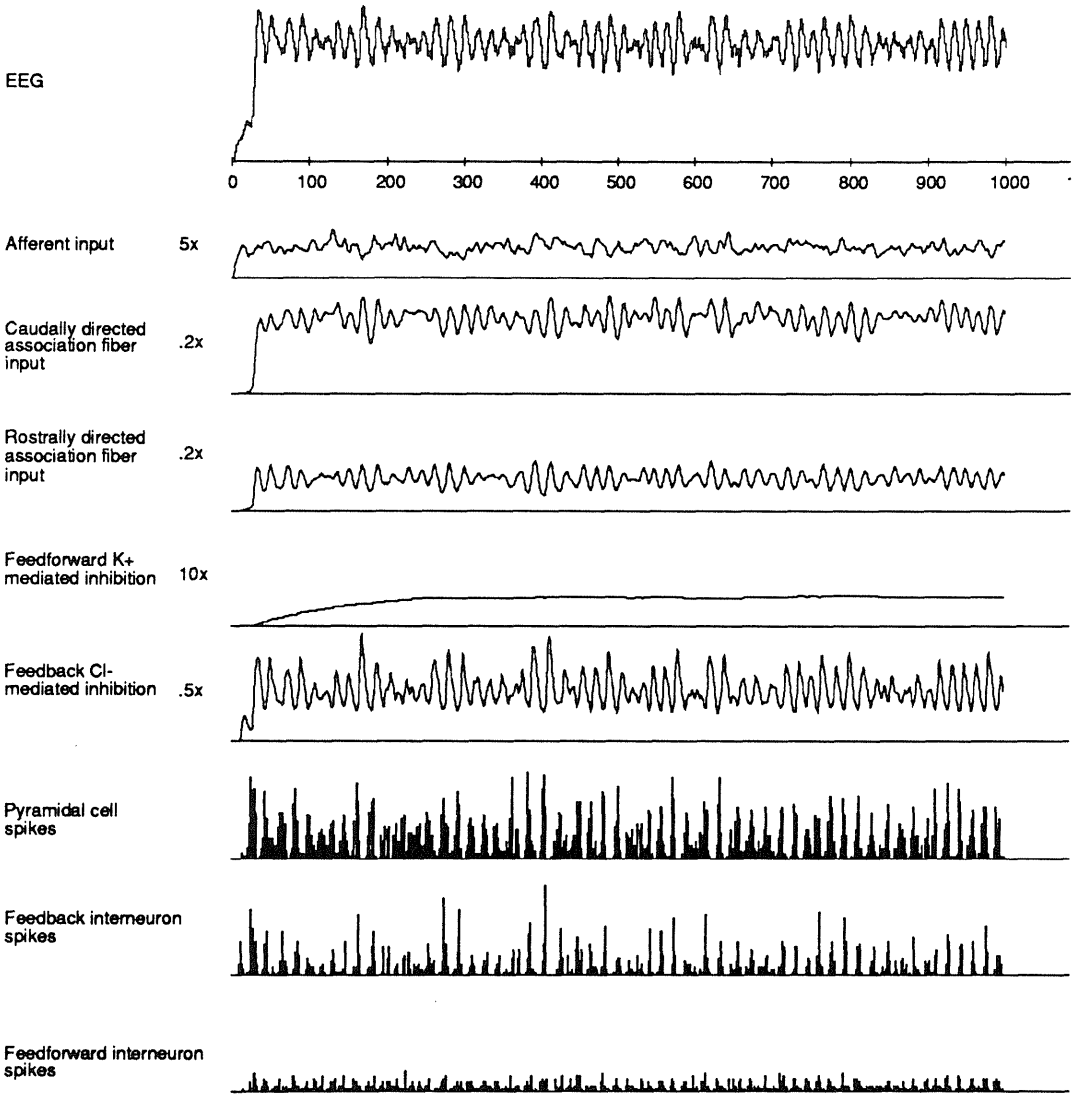
EEG
0
100
200
300
400
500
600
700
800
900
1000
Afferent input
5x
Caudally directed association fiber input
.2x
Rostrally directed association fiber input
.2x
Feedforward K+ mediated inhibition
10x
Feedback Cl- mediated inhibition
.5x
Pyramidal cell spikes
Feedback interneuron spikes
Feedforward interneuron spikes

Figure 6A

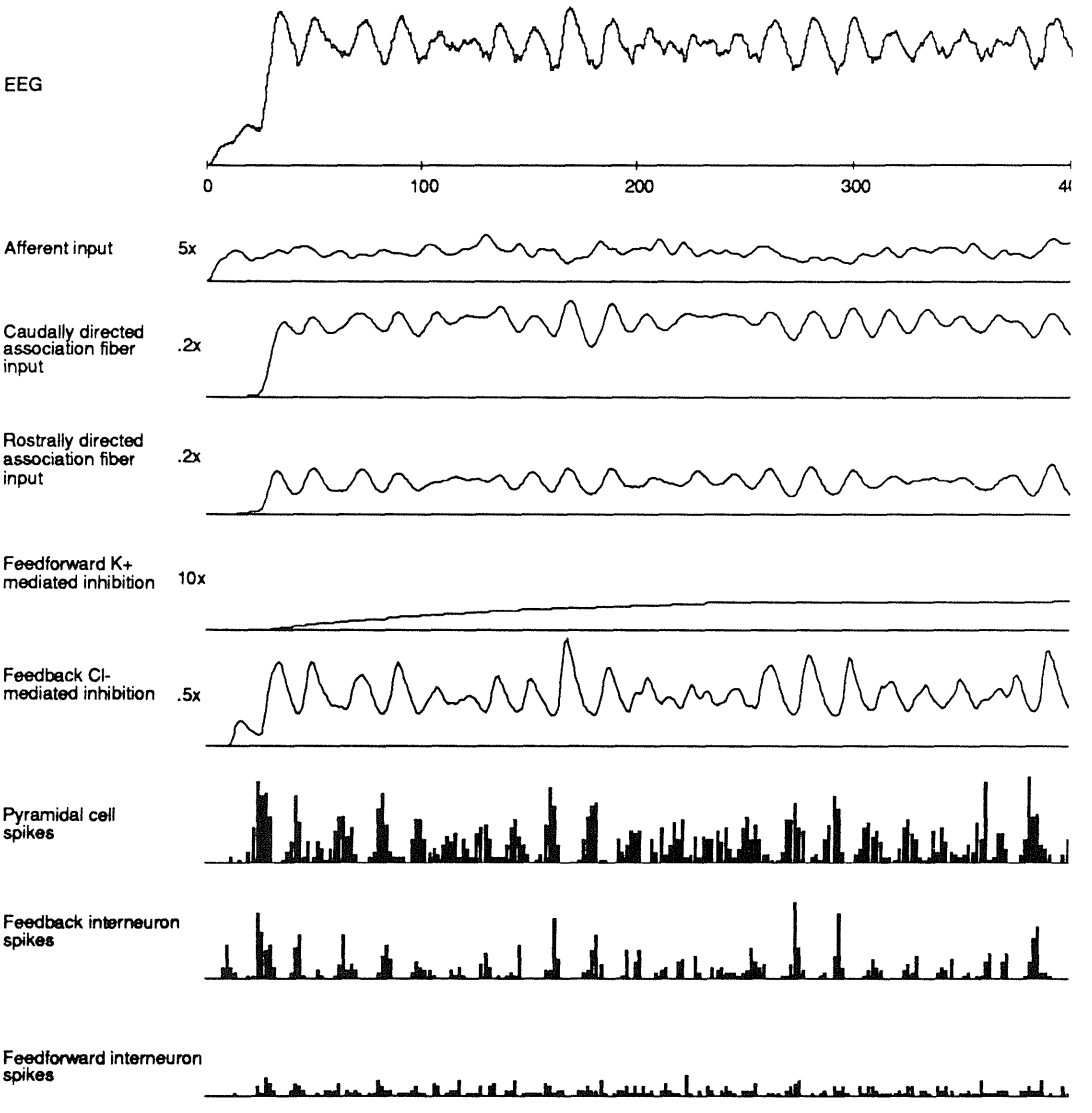
EEG
0
100
200
300
Afferent input
5x
Caudally directed association fiber input
.2x
Rostrally directed association fiber input
.2x
Feedforward K+ mediated inhibition
10x
Feedback Cl- mediated inhibition
.5x
Pyramidal cell spikes
Feedback interneuron spikes
Feedforward interneuron spikes

Figure 6B

Appendix 2: Genesis scripts implementing the model of piriform cortex

This section contains the complete listing of the Genesis scripts used to produce the network simulations described in this work. Given the variations in the configurations of the model used in the different chapters, this appendix contains the "nominal" representation. All others constitute minor variations of parameters which are described in the appropriate chapters.

It should be emphasized that this section is provided as a reference for those who are already familiar with the Genesis simulation system and are interested in the details of the model implementation. The Genesis simulation system used to implement the model was developed during the course of this research at Caltech and is available at no cost via ftp at the internet site genesis.caltech.edu. Potential users should be warned that at the present time the simulator remains a research tool with limited documentation and therefore requires significant effort to successfully master. Continued support and development is planned to improve this status.

piriform.g

```
//genesis
echo " "
echo "***********************************************"
echo "*             PIRIFORM CORTEX                 *"
echo "*                                             *"
echo "*         Written by Matt Wilson              *"
echo "*    California Institute of Technology       *"
echo "*                                             *"
echo "*         GENESIS implementation              *"
echo "*                  8/15/88                    *"
echo "***********************************************"
echo " "

include constants.g     // set local variables
include functions.g     // set up some functions
include protodefs.g     // create some prototype objects
include cells.g         // set up the cells
include pyramidal.g     // create the cell populations
include fb.g
include ff.g
include bulb.g
include connfuncs.g         // set up the connections
include pyrconn.g
include fbconn.g
include ffconn.g
include bulbconn.g
include field.g         // place field potential electrodes
include output.g        // set up the outputs
/*
include theta.g

maketheta
*/
include adjustweights.g
echo " "
echo checking and initializing simulation
echo Piriform cortex simulation loaded.
check
reset               // get a clean start
```

adjustweights.g

```
//genesis
adjustspike          // correct the spike output amplitude for
                  // the time step


scaleweight /pyr/pyramidal[]/RAaxon 3.5
scaleweight /pyr/pyramidal[]/CAaxon 3.5
scaleweight /fb/interneuron[]/axon 15
scaleweight /ff/interneuron[]/axon 20
scaleweight /bulb/mitral[]/axon 3.5
scaleweight /pyr/pyramidal[]/FBaxon 2.25
scaleweight /pyr/pyramidal[]/FFaxon 1.5
```

bulb.g

```
//genesis

if(BULB)
    bulb(/library/mitral)
    createmap   /library/mitral     /bulb   {BULB_NX}  {BULB_NY
}  \
                    {BULB_DX}  {BULB_DY}
end
```

bulbconn.g

```
//genesis
function bulb_connect(path)
str path

    echo
    echo                                AFFERENT INPUT
    echo
    if(MULTI)
    dst = "/pyr/pyramidal[]/soma/Ia_dend/Aff_Na_channel"
    else
    dst = "/pyr/pyramidal[]/soma/Aff_Na_channel"
    end
    echo afferent connections
    region_connect {path} to {dst} \
    with synapse -rel \
    1 1 -100 -100 100 100 \      // do this over all the cells
    1  1 -100 -100 100 100  \    // connect to all the cells
    {PBULB_to_PYR}

    region_connect {path}2  to /ff/interneuron[]/soma/Na_channe
l \
    with synapse -rel \
    1 1 -100 -100 100 100 \      // do this over all the cells
    1 1 -100 -100 100 100 \      // connect to all the cells
    {PBULB_to_FF}

    region_connect {path}3  to /fb/interneuron[]/soma/Na_channe
l \
    with synapse -rel \
    1 1 -100 -100 100 100 \      // do this over all the cells
    1 1 -100 -100 100 100   \    // connect to all the cells
    {PBULB_to_FB}

    //                                AFFERENT DELAYS
    echo afferent delays
    execute AffDelay {path} 45 -uniformvx {VLOT_MAIN_MIN/SCALE}
  \
                        {VLOT_MAIN_MAX/SCALE} \
                    -uniformvy {VLOT_COLL_MIN/SCALE} \
                        {VLOT_COLL_MAX/SCALE}
    execute AffDelay {path}2    45 -uniformvx {VLOT_MAIN_MIN/SC
ALE}  \
                        {VLOT_MAIN_MAX/SCALE} \
                    -uniformvy {VLOT_COLL_MIN/SCALE} \
```

```
                        {VLOT_COLL_MAX/SCALE}
    execute AffDelay {path}3    45 -uniformvx {VLOT_MAIN_MIN/SC
ALE}  \
                        {VLOT_MAIN_MAX/SCALE} \
                    -uniformvy {VLOT_COLL_MIN/SCALE} \
                        {VLOT_COLL_MAX/SCALE}

    //                              AFFERENT WEIGHTS
    echo afferent weights
    aff_weight {path}   45 {WBULB_to_PYR} \
            {LBULB_to_MAIN} {LBULB_to_COLL} {AWBULB_to_PYR}
    aff_weight {path}2  45 {WBULB_to_FF} \
            {LBULB_to_MAIN} {LBULB_to_COLL} {AWBULB_to_FF}
    aff_weight {path}3  45 {WBULB_to_FB} \
            {LBULB_to_MAIN} {LBULB_to_COLL} {AWBULB_to_FB}
end

function parallel(path)
str path

    echo
    echo                                AFFERENT INPUT
    echo
    if(MULTI)
    dst = "/pyr/pyramidal[]/soma/Ia_dend/Aff_Na_channel"
    else
    dst = "/pyr/pyramidal[]/soma/Aff_Na_channel"
    end
    echo afferent connections
    region_connect {path} to {dst} \
    with synapse -rel \
    1 1 -100 -100 100 100 \     // do this over all the cells
    1  1 -1 -1 1 1          // connect to cells in 2x2mm region


    region_connect {path}2  to /ff/interneuron[]/soma/Na_channe
l \
    with synapse -rel \
    1 1 -100 -100 100 100 \     // do this over all the cells
    1  1 -1 -1 1 1          // connect to cells in 2x2mm region


    region_connect {path}3  to /fb/interneuron[]/soma/Na_channe
l \
```

```
    with synapse -rel \
    1 1 -100 -100 100 100 \     // do this over all the cells
    1  1 -1 -1 1 1          // connect to cells in 2x2mm region


    gaussian_weight {path} {WBULB_to_PYR} 1 0       // 1mm sigm
a wmin = 0
    gaussian_weight {path}2 {WBULB_to_FF} 1 0       // 1mm sigm
a
    gaussian_weight {path}3 {WBULB_to_FB} 1 0       // 1mm sigm
a
    set {path}:# delay 0
    set {path}2:# delay 0
    set {path}3:# delay 0
end

// rate is in spikes/sec
function bar(x1,y1,x2,y2,rate)
float x1,y1,x2,y2,rate
    set /bulb/mitral[x>={x1}][y>={y1}][x<={x2}][y<={y2}]/input
rate {rate/1000.0}
end

function baseinput(rate)
float rate
    set /bulb/mitral[]/input rate {rate/1000.0}
end

bulb_connect /bulb/mitral[]/axon
baseinput 10
```

```
//genesis

str string

//=============================================================
===========
//                          PYRAMIDAL CELL
//=============================================================
===========
/*
** this function constructs a pyramidal cell according to the a
rguments
** passed to it
*/
function pyramidal_cell(pathname,multi,spike,connect, \
soma_d,soma_l,dend_d,dend_l)

str pathname
int multi
int spike
int connect
float   soma_d      // um
float   soma_l      // um
float   dend_d      // um
float   dend_l      // um

    float soma_a    =   PI*soma_d*soma_l    // um^2
    float soma_xa   =   PI*soma_d*soma_d/4  // um^2
    float dend_a    =   PI*dend_d*dend_l    // um^2
    float dend_xa   =   PI*dend_d*dend_d/4  // um^2

    create  neutral     {pathname}
    ce  {pathname}
    // passive soma

    create compartment soma
    set soma \
    Em      {PYR_EREST} \               // mV
    Rm      { RM/soma_a } \             // Kohm
    Cm      { CM*soma_a*SCALE } \           // uF
    Ra      { RA*soma_l/soma_xa }           // Kohm

    /*
    ** add a buffer for generating thresholded spike events
```

```
    */
    copy    /library/spike .
    set spike abs_refract 10
    set spike thresh    -40                 // mV
    /*
    ** use the soma potential (or state) to drive the threshold
ed
    ** spike generation buffer
    */
    sendmsg  soma   spike       INPUT Vm

    /*
    ** axons
    */
    foreach string (RA CA LRA LCA FF FB )
    create axon {string}axon
    set {string}axon latency {SYNDELAY}
    sendmsg     spike   {string}axon    BUFFER name
    end

    if(multi)
    push soma
    /*
    ** add a passive dendritic compartments
    */
    create compartment III_dend
        set     III_dend \
        Em  {PYR_EREST} \               // mV
        Rm  {RM/ dend_a} \              // Kohms
        Cm  {CM * dend_a*SCALE} \           // uF
        Ra  {RA * dend_l/dend_xa}           // Kohm

    copy III_dend   deepIb_dend
    copy III_dend   supIb_dend
    copy III_dend   Ia_dend

    /*
    ** and link them
    */
    link_compartment    III_dend        .
    link_compartment    deepIb_dend     .
    link_compartment    supIb_dend      deepIb_dend
    link_compartment    Ia_dend         supIb_dend
    pop
```

```
    end

    if(spike)
    /*
    ** add spike producing channels
    */
    create channelC     SNa_channel
        set SNa_channel \
        Ek  {ENA} \                 // mV
        tau1    { 0.2  * SCALE } \      // msec
        tau2    { 0.2  * SCALE } \      // msec
        gmax    {SGMAX_NA*fAC*soma_a}       // mS
    create  channelC    SK_channel
        set SK_channel \
        Ek  {EK} \                  // mV
        tau1    { 1 * SCALE } \         // msec
        tau2    { 1 * SCALE } \         // msec
        gmax    {SGMAX_K*fAC*soma_a}        // mS
    /*
    ** use the spike output as activation for the channels
    */
    sendmsg  spike SNa_channel      ACTIVATION state
    sendmsg  spike SK_channel       ACTIVATION state
    singlelink_channel      SNa_channel     soma
    singlelink_channel      SK_channel  soma
    end

    if(connect)
    /*
    ** add synaptically activated channels
    */
    if(multi)
        push soma/Ia_dend
        copy    /library/Na_channel     Aff_Na_channel
        set Aff_Na_channel      gmax    {DISTAL_GMAX_NA} // mS/
synapse
        link_channel Aff_Na_channel     .
        pop

        push soma/supIb_dend
        copy    /library/Na_channel     CA_Na_channel
        set CA_Na_channel       gmax    {DISTAL_GMAX_NA}
        link_channel    CA_Na_channel   .
        pop
```

```
    push soma/deepIb_dend
    copy    /library/Na_channel     RA_Na_channel
    set RA_Na_channel       gmax    {DISTAL_GMAX_NA}
    link_channel    RA_Na_channel   .
    pop

    push soma/III_dend
    copy    /library/Na_channel     Local_Na_channel
    set Local_Na_channel    gmax    {LOCAL_GMAX_NA}
    link_channel    Local_Na_channel .
    pop

    push soma/Ia_dend
    copy    /library/K_channel  K_channel
    set K_channel       gmax    {GMAX_K}
    link_channel    K_channel   .
    pop

    push soma
    copy    /library/Cl_channel     Cl_channel
    set Cl_channel      gmax    {GMAX_CL}
    link_channel    Cl_channel  .
    pop
else
    push soma
    copy    /library/Na_channel     Aff_Na_channel
    set Aff_Na_channel      gmax    {DISTAL_GMAX_NA}
    link_channel    Aff_Na_channel      .

    copy    /library/Na_channel     CA_Na_channel
    set CA_Na_channel       gmax    {DISTAL_GMAX_NA}
    link_channel    CA_Na_channel       .

    copy    /library/Na_channel     RA_Na_channel
    set RA_Na_channel       gmax    {DISTAL_GMAX_NA}
    link_channel    RA_Na_channel       .

    copy    /library/Na_channel     Local_Na_channel
    set Local_Na_channel    gmax    {LOCAL_GMAX_NA}
    link_channel    Local_Na_channel    .

    copy    /library/K_channel  K_channel
    set K_channel       gmax    {GMAX_K}
```

```
        link_channel    K_channel       .

        copy        /library/Cl_channel     Cl_channel
        set Cl_channel      gmax    {GMAX_CL}
        link_channel    Cl_channel      .
        pop
    end // multi
    end     // connect
    if(multi)
    push soma
    /*
    ** set dendritic positions relative to the soma
    */
    position III_dend   I I R100e-3 // 100um deep to the soma
    position deepIb_dend    I I R-100e-3    // 100um super to t
he soma
    position supIb_dend     I I R-200e-3    // 200um super to t
he soma
    position Ia_dend    I I R-300e-3    // 300um super to the s
oma
    pop
    end     // multi
end // pyramidal_cell

//=============================================================
===========
//                          INTERNEURON
//=============================================================
===========
function interneuron(pathname,soma_d,soma_l,Cl,multaxon)
str pathname
float   soma_d      // um
float   soma_l      // um
int Cl      // flag for incorporating a Cl channel
int multaxon    // flag for additional axon

    float soma_a    =   PI*soma_d*soma_l    // um^2
    float soma_xa   =   PI*soma_d*soma_d/4  // um^2

    create  neutral {pathname}
    ce  {pathname}

    /*
    ** soma
```

```
    */
    create compartment  soma
    set soma \
    Em      {I_EREST} \                 // mV
    Rm      {I_RM / soma_a} \           // Kohms
    Cm      {I_CM * soma_a * SCALE} \       // uF
    Ra      {I_RA * soma_l / soma_xa}           // Kohm
    /*
    ** channels
    */
    copy    /library/Na_channel soma
    set soma/Na_channel     gmax        {I_GMAX_NA}
    link_channel        soma/Na_channel     soma

    if(Cl)
    copy    /library/Cl_channel soma
    set soma/Cl_channel     gmax        {I_GMAX_CL}
    link_channel        soma/Cl_channel     soma
    end
    copy    /library/Cl_channel soma
    set soma/Cl_channel     gmax        {I_GMAX_CL*NSYN_FB_from
_FB}
    link_channel        soma/Cl_channel     soma

    /*
    ** add spike producing channels
    */
    create channelC SNa_channel
    set SNa_channel \
    Ek      {ENA} \             // mV
    tau1        { 0.2 * SCALE } \       // msec
    tau2        { 0.2 * SCALE }\        // msec
    gmax        {SGMAX_NA*fAC*soma_a}       // mS
    create channelC SK_channel
    set SK_channel \
    Ek      {EK} \              // mV
    tau1        { 1 * SCALE } \         // msec
    tau2        { 1  * SCALE } \        // msec
    gmax        {SGMAX_K*fAC*soma_a}        // mS
    /*
    ** use the spike output as activation for the channels
    */
    singlelink_channel      SNa_channel     soma
    singlelink_channel      SK_channel  soma
```

```
    singlelink_channel      soma/Cl_channel     soma

    copy    /library/spike  .
    set spike thresh -40
    set spike abs_refract 10
    sendmsg  soma   spike       INPUT Vm
    sendmsg  spike SNa_channel      ACTIVATION state
    sendmsg  spike SK_channel       ACTIVATION state
    sendmsg  spike soma/Cl_channel      ACTIVATION state

    create  axon    axon
    set axon latency {SYNDELAY}
    sendmsg     spike   axon    BUFFER name
    if(multaxon)
    create  axon    fbaxon
    set fbaxon latency {SYNDELAY}
    sendmsg     spike   fbaxon  BUFFER name
    end
end // interneuron

//=============================================================
===========
//                          BULBAR INPUT
//=============================================================
===========
function bulb(path)
str path

    create      neutral {path}
    ce ^
    create random input
    set input min_amp 3
    set input max_amp 6
    set input rate 1        // spikes/msec
    create axon axon
    sendmsg     input   axon    BUFFER name
    create axon axon2
    sendmsg     input   axon2   BUFFER name
    create axon axon3
    sendmsg     input   axon3   BUFFER name
end
```

connfuncs.g

```
//genesis
function propagation_velocity(path,velocity)
str path
float velocity
    execute RadialDelay  {path} { 1.0/velocity }
end

function gausspropagation_velocity(path,min,max,mean,sd)
str path
float min,max
float mean,sd
    execute RadialDelay  {path} -gaussian {1.0/mean} {1.0/sd} {
1.0/max} {1.0/min}
end

function rangepropagation_velocity(path,min_velocity,max_veloci
ty)
str path
float min_velocity
float max_velocity
    execute RadialDelay  {path} -uniform { 1.0/max_velocity } {
1.0/min_velocity}
end

function exponential_weight(path,maxweight,lambda,minval)
str     path
float   maxweight
float   lambda
float   minval
    execute ExpWeight {path} {-1.0/lambda} {maxweight} {minval}

end

function gaussian_weight(path,maxweight,lambda,minval)
str     path
float   maxweight
float   lambda
float   minval
    execute GaussianWeight {path} {lambda} {maxweight} {minval}

end

function aff_weight(path,angle,max,mlambda,clambda,min)
str     path
```

```
float   angle
float   maxweight
float   mlambda
float   clambda
float   min
    execute AffWeight {path} {angle} {max} {-1.0/mlambda} {-1.0
/clambda} {min}
end
```

constants.g

```
//genesis


prompt      "piriform !"        // set the prompt
setclock    0       0.1 // set the basic simulation step size
setclock    1       0.5 // set the output step size
setclock    2       1.0 // set the alternate output step size
randomseed -new

int     MULTI       =   1
int     CONNECT     =   1
int     INTERNEURON =   1
int     SPIKE       =   1
int     BULB        =   1
int     FIELD       =   1
int     T_NOISE     =   0
int     LOCAL_FF    =   1
int     DISINHIB    =   0

// time scale factor
float   SCALE       =   1e-3        // convert msec to sec
float   SCALE       =   1       // no conversions

// ============================================================
=========
//                          NETWORK DIMENSIONS
// ============================================================
=========

// cortical dimensions
float   CORTEX_X    =   10.0            // mm
float   CORTEX_Y    =   6.0         // mm

//                        PYRAMIDAL POPULATION

int PYR_NX      =   25          // # neurons in x
int PYR_NY      =   15          // # neurons in y
int PYR_NX      =   50          // # neurons in x
int PYR_NY      =   30          // # neurons in y

echo Pyramidal array dimensions {PYR_NX} by {PYR_NY}

// cell spacing
float   PYR_DX      =   CORTEX_X / PYR_NX   // mm/cell
```

```
float   PYR_DY      =   CORTEX_Y / PYR_NY   // mm/cell

//                          FB INTERNEURON POPULATION

int FB_NX       =   1.0*PYR_NX      // # neurons in x
int FB_NY       =   1.0*PYR_NY      // # neurons in y

echo FB interneuron array dimensions {FB_NX} by {FB_NY}

float   FB_DX       =   CORTEX_X/FB_NX      // mm/cell
float   FB_DY       =   CORTEX_Y/FB_NY      // mm/cell

//                          FF INTERNEURON POPULATION

int FF_NX       =   1.0*PYR_NX      // # neurons in x
int FF_NY       =   1.0*PYR_NY      // # neurons in y

echo FF interneuron array dimensions {FF_NX} by {FF_NY}

float   FF_DX       =   CORTEX_X/FF_NX      // mm/cell
float   FF_DY       =   CORTEX_Y/FF_NY      // mm/cell

//                          AFFERENT POPULATION

int BULB_NX     =   10          // # neurons in x
int BULB_NY     =   10          // # neurons in y

echo Bulbar dimensions {BULB_NX} by {BULB_NY}

// shrink the scales to that of the LOT input dimensions

float   BULB_DX     =   1e-3                // mm/fiber
float   BULB_DY     =   1e-3                // mm/fiber

//                          PATHWAY EXTENTS

float   RPYR_to_LOCAL       =   0.5             // mm
float   RPYR_to_FB      =   2.0             // mm
float   RPYR_to_FF      =   0.5             // mm
float   RFB_to_PYR      =   1.0             // mm
float   RFF_to_PYR      =   0.5             // mm
float   RPYR_to_RDIST       =   10.0            // mm
float   RPYR_to_CDIST       =   10.0            // mm
```

```
// ================================================================
=========
//                              CONNECTION DENSITY
// ================================================================
=========
// connection probabilities
float   PPYR_to_RLOCAL      =   0.2
float   PPYR_to_CLOCAL      =   0.2
float   PPYR_to_RDIST       =   0.02
float   PPYR_to_CDIST       =   0.02
float   PPYR_to_FB      =   0.2
if(LOCAL_FF)
    float   PPYR_to_FF      =   0.2
else
    float   PPYR_to_FF      =   0.02
end
float   PFB_to_PYR      =   1.0
float   PFF_to_PYR      =   0.2
float   PBULB_to_PYR        =   0.1
float   PBULB_to_FF     =   0.1
float   PBULB_to_FB     =   0.1

// synaptic target count    (synapses/path)
float   NSYN_PYR_from_BULB  =   1200
float   NSYN_PYR_from_CA    =   1200
float   NSYN_PYR_from_RA    =   700
float   NSYN_PYR_from_FB    =   200
float   SDSYN_PYR_from_FB   =   20  // standard deviation
float   NSYN_PYR_from_FF    =   25
float   SDSYN_PYR_from_FF   =   3   // standard deviation
float   NSYN_PYR_from_CLOCAL    =   30
float   NSYN_PYR_from_RLOCAL    =   30

float   NSYN_FB_from_PYR    =   800
float   SDSYN_FB_from_PYR   =   80  // standard deviation

float   NSYN_FB_from_FB     =   80
float   SDSYN_FB_from_FB    =   8   // standard deviation

float   NSYN_FF_from_PYR    =   200
float   SDSYN_FF_from_PYR   =   20  // standard deviation

float   NSYN_FB_from_BULB   =   75
```

```
float   NSYN_FF_from_BULB   =   200

// source cell count        (src_cells)
float   NBULB_to_PYR    =   PBULB_to_PYR*BULB_NX*BULB_NY
float   NBULB_to_FF =   PBULB_to_FF*BULB_NX*BULB_NY
float   NBULB_to_FB =   PBULB_to_FB*BULB_NX*BULB_NY

// network space constants
float   LPYR_to_RLOCAL      =   5.0     // mm
float   LPYR_to_CLOCAL      =   5.0     // mm
float   LPYR_to_CA      =   5.0     // mm
float   LPYR_to_RA      =   5.0     // mm
float   LPYR_to_FB      =   5.0     // mm
float   LPYR_to_FF      =   5.0     // mm
float   LFB_to_PYR      =   5.0     // mm
float   LFB_to_FB       =   5.0     // mm
float   LFF_to_PYR      =   5.0     // mm
float   LBULB_to_MAIN       =   20.0        // mm
float   LBULB_to_COLL       =   10.0        // mm


//  target path       target  path  src
float   WBULB_to_FF     =   NSYN_FF_from_BULB/NBULB_to_FF
float   WBULB_to_FB     =   NSYN_FB_from_BULB/NBULB_to_FB
float   WBULB_to_PYR        =   NSYN_PYR_from_BULB/NBULB_to_PYR


// asymptotic connection level      (fractional synapses/src_ce
ll)
float   AWPYR_to_RLOCAL     =   0.2
float   AWPYR_to_CLOCAL     =   0.2
float   AWPYR_to_CA     =   0.4
float   AWPYR_to_RA     =   0.4
float   AWPYR_to_FB     =   0.2
float   AWPYR_to_FF     =   0.2
float   AWFB_to_PYR     =   0.2
float   AWFB_to_FB      =   0.2
float   AWFF_to_PYR     =   0.2
float   AWBULB_to_FF        =   0.2*WBULB_to_FF
float   AWBULB_to_FB        =   0.2*WBULB_to_FB
float   AWBULB_to_PYR       =   0.2*WBULB_to_PYR

// velocities               (m/s)
float   VPYR_CA         =   0.37
```

```
float   SD_VPYR_CA      =   0.03
float   VPYR_CA_MIN     =   0.25
float   VPYR_CA_MAX     =   0.48

float   VPYR_RA         =   0.85
float   SD_VPYR_RA      =   0.13
float   VPYR_RA_MIN     =   0.45
float   VPYR_RA_MAX     =   1.25

float   VPYR_FF         =   1.0
float   SD_VPYR_FF      =   0.06
float   VPYR_FF_MIN     =   0.8
float   VPYR_FF_MAX     =   1.2

float   VPYR_FB         =   1.0
float   SD_VPYR_FB      =   0.06
float   VPYR_FB_MIN     =   0.8
float   VPYR_FB_MAX     =   1.2

float   VLOT_MAIN       =   7.0
float   SD_VLOT_MAIN        =   0.06
float   VLOT_MAIN_MIN       =   6.8
float   VLOT_MAIN_MAX       =   7.2

float   VLOT_COLL       =   1.6
float   SD_VLOT_COLL        =   0.06
float   VLOT_COLL_MIN       =   1.4
float   VLOT_COLL_MAX       =   1.8

float   VFB_PYR         =   1.0
float   SD_VFB_PYR      =   0.06
float   VFB_PYR_MIN     =   0.8
float   VFB_PYR_MAX     =   1.2

float   VFF_PYR         =   1.0
float   SD_VFF_PYR      =   0.06
float   VFF_PYR_MIN     =   0.8
float   VFF_PYR_MAX     =   1.2

// ============================================================
=========
//                          CELL DIMENSIONS
// ============================================================
=========
```

```
float   PI      =   3.14159

// pyramidal cell dimensions

float   PYR_SOMA_D  =   20              // um
float   PYR_SOMA_L  =   70              // um
float   PYR_SOMA_A  =   PI*PYR_SOMA_D*PYR_SOMA_L    // um^2
float   PYR_SOMA_XA =   PI*PYR_SOMA_D*PYR_SOMA_D/4  // um^2
float   PYR_DEND_D  =   4               // um
float   PYR_DEND_L  =   120             // um
float   PYR_DEND_A  =   PI*PYR_DEND_D*PYR_DEND_L    // um^2
float   PYR_DEND_XA =   PI*PYR_DEND_D*PYR_DEND_D/4  // um^2

// interneuron dimensions
float   GLOB_SOMA_D =   10              // um
float   GLOB_SOMA_L =   10              // um

float   FUS_SOMA_D  =   15              // um
float   FUS_SOMA_L  =   15              // um

// ============================================================
=========
//                          PHYSIOLOGICAL PARAMETERS
// ============================================================
=========

//                          IONIC EQUILIBRIUM POTENTIALS
float   EKA         =   0               // mV
float   ENA         =   55              // mV
float   ECL         =   -65             // mV
float   EK      =   -90             // mV
float   PYR_EREST   =   -55             // mV
float   I_EREST     =   -55             // mV


//                              UNIT CONDUCTANCES
//              (mS/channel)
float   UNIT_GNA    =   8e-9
float   UNIT_GK     =   4e-9
float   UNIT_GCL    =   20e-9

float   SUNIT_GNA   =   8e-9
float   SUNIT_GK    =   4e-9
```

```
//                              CHANNEL LIFETIMES
//                (msec)
float   TAU_CL          =   18

//                              CHANNEL DENSITIES
//                (channel/um^2)
float   RHO_NA          =   30
float   RHO_CL          =   20
float   RHO_K           =   30
float   SRHO_NA         =   330
float   SRHO_K          =   72
float   IRHO_NA         =   15
float   IRHO_CL         =   7

//                              SYNAPTIC AREA
//                (um^2/synapse)
float   ASYN_LOCAL_NA   =   0.12        // d=.40
float   ASYN_DISTAL_NA  =   0.43        // d=.74
float   ASYN_CL         =   0.62        // d=.89
float   ASYN_K          =   0.43        // d=.74

float   IASYN_NA        =   0.29
float   IASYN_CL        =   0.62        // d=.89

//                              ACTIVE AREA
// fraction of somatic area containing active channels
float   fAC         =   0.04


//                              PEAK CONDUCTANCE
// peak_g = unit_g * channel_density * synaptic_area
//                (mS/synapse)
float   I_GMAX_NA       =   UNIT_GNA * IRHO_NA * IASYN_NA
float   I_GMAX_CL       =   UNIT_GCL * IRHO_CL * IASYN_CL
float   LOCAL_GMAX_NA   =   UNIT_GNA * RHO_NA * ASYN_LOCAL_NA
float   DISTAL_GMAX_NA  =   UNIT_GNA * RHO_NA * ASYN_DISTAL_NA
float   GMAX_K          =   UNIT_GK * RHO_K * ASYN_K
float   GMAX_CL         =   UNIT_GCL * RHO_CL * ASYN_CL

float   SGMAX_NA        =   SUNIT_GNA * SRHO_NA     // mS/um^2
float   SGMAX_K         =   SUNIT_GK * SRHO_K       // mS/um^2

//                              MEMBRANE PARAMETERS
```

constants.g

```
float   RM        =   4e+8                // Kohm-um^2
float   RA        =   0.10e+4             // Kohm-um
float   CM        =   2.0e-8              // uF/um^2

float   I_RM          =   2.0e+8              // Kohm-um^2
float   I_RA          =   RA                  // Kohm-um
float   I_CM          =   CM                  // uF/um^2

float   SYNDELAY  =   0.8                 // msec
float   FFDELAY   =   8.0                 // msec
```

fb.g

```
//genesis
echo creating the fb population
create  neutral /fb

if(DISINHIB)
    interneuron(/interneuron,{FUS_SOMA_D},{FUS_SOMA_L},1,1)
else
    interneuron(/interneuron,{FUS_SOMA_D},{FUS_SOMA_L},0,0)
end

createmap /interneuron  /fb {FB_NX}  {FB_NY} {FB_DX}  {FB_DY}
delete /interneuron
position /fb I I 800e-3

echo setting fb thresholds
randomfield /fb/interneuron[]/spike  thresh -gaussian -35 7

if(T_NOISE)
    // ======================================================
==
    //                      TRANSMITTER NOISE
    // ======================================================
==
    create funcgen /fb/Nanoise
    set ^ mode 3 amplitude 1 x {350*getclock(0)}
    sendmsg ^ /fb/interneuron[]/soma/Na_channel  \
    RAND_ACTIVATION output x        // prob amplitude

end
```

```
//genesis

echo
echo                                    FB INTERNEURONS
echo


//                                    FB to PYR CONNECTIONS
echo fb to pyr connections
region_connect /fb/interneuron[]/axon to /pyr/pyramidal[]/soma/
Cl_channel \
    with synapse -rel \
    1 1 -100 -100 100 100 \     // do this over all the cells
    1 1 {-RFB_to_PYR} {-RFB_to_PYR} \
    {RFB_to_PYR} {RFB_to_PYR} \     // connect to local area of
 cells
    {PFB_to_PYR}

//                                    FB to PYR DELAYS
echo fb to pyr delays
gausspropagation_velocity /fb/interneuron[]/axon \
    { VFB_PYR_MIN / SCALE } {VFB_PYR_MAX/SCALE} \
    {VFB_PYR/SCALE} {SD_VFB_PYR/SCALE}

/*
** counts the convergent synapses onto a single ff interneuron
*/
float pyr_sum = \
expsum(/fb/interneuron[x>={CORTEX_X/2 - RFB_to_PYR}][y>={CORTEX
_Y/2 - RFB_to_PYR}][x<={CORTEX_X/2 + RFB_to_PYR}][y<={CORTEX_Y/
2 + RFB_to_PYR}],\
{-1.0/LFB_to_PYR},1,{AWFB_to_PYR},{CORTEX_X/2},{CORTEX_Y/2})

float wpyr = NSYN_PYR_from_FB/(pyr_sum*PFB_to_PYR)

//                                    FB to PYR WEIGHTS
echo fb to pyr weights
exponential_weight /fb/interneuron[]/axon   {wpyr} \
                          {LFB_to_PYR} \
                          {AWFB_to_PYR*wpyr}

if(DISINHIB)
    //                                FB to FB CONNECTIONS
    echo fb to fb connections
```

```
    region_connect /fb/interneuron[]/fbaxon to /fb/interneuron[
]/soma/Cl_channel \
        with synapse -rel \
        1 1 -100 -100 100 100 \     // do this over all cells
        1 1 {-RFB_to_PYR} {-RFB_to_PYR} \
        {RFB_to_PYR} {RFB_to_PYR} \     // connect to local are
a
        {PFB_to_PYR}

    //                              FB to FB DELAYS
    echo fb to pyr delays
    gausspropagation_velocity /fb/interneuron[]/fbaxon \
    { VFB_PYR_MIN / SCALE } {VFB_PYR_MAX/SCALE} \
    {VFB_PYR/SCALE} {SD_VFB_PYR/SCALE}


    //                              FB to FB WEIGHTS
    echo fb to fb weights
    exponential_weight /fb/interneuron[]/fbaxon     1 \
                           {LFB_to_FB} \
                           {AWFB_to_FB}
    normalize_synapses /fb/interneuron[]/fbaxon /fb/interneuron
[]/soma/Cl_channel \
    -gaussian {NSYN_FB_from_FB} {SDSYN_FB_from_FB}
end

/*
** perform synapse normalization
** this will adjust the number of convergent synapses per targe
t
** to within a given range.
** This will compensate for edge imbalances in synaptic enervat
ion
** generated as a result of synaptic distribution based on numb
ers of
** divergent synapses per source
*/
normalize_synapses /fb/interneuron[]/axon /pyr/pyramidal[]/soma
/Cl_channel \
    -gaussian {NSYN_PYR_from_FB} {SDSYN_PYR_from_FB}
```

ff.g

```
//genesis
echo creating ff population
create      neutral     /ff

interneuron(/interneuron, {GLOB_SOMA_D},{GLOB_SOMA_L},0,0)
set /interneuron/axon latency {FFDELAY}
createmap /interneuron  /ff {FF_NX}  {FF_NY}  {FF_DX}  {FF_DY}

delete /interneuron
position /ff I I 200e-3

echo setting ff thresholds
randomfield /ff/interneuron[]/spike  thresh -gaussian -35 7

if(T_NOISE)
    // ============================================================
==
    //                      TRANSMITTER NOISE
    // ============================================================
==
    create funcgen /ff/Nanoise
    set ^ mode 3 amplitude 1 x {150*getclock(0)}
    sendmsg ^ /ff/interneuron[]/soma/Na_channel  \
    RAND_ACTIVATION output x        // prob amplitude

end
```

```
//genesis
echo
echo                                    FF INTERNEURONS
echo
//                                  FF to PYR CONNECTIONS
echo ff to pyr connections
if(MULTI)
    dst = "/pyr/pyramidal[]/soma/Ia_dend/K_channel"
else
    dst = "/pyr/pyramidal[]/soma/K_channel"
end
region_connect /ff/interneuron[]/axon   to {dst} \
    with synapse -rel \
    1 1 -100 -100 100 100 \     // do this over all the cells
    1 1 {-RFF_to_PYR} {-RFF_to_PYR} \
    {RFF_to_PYR} {RFF_to_PYR} \ // connect to local area of cel
ls
    {PFF_to_PYR}

//                                  FF to PYR DELAYS
echo ff to pyr delays
gausspropagation_velocity /ff/interneuron[]/axon \
    {VFF_PYR_MIN/SCALE} {VFB_PYR_MAX/SCALE} \
    {VFF_PYR/SCALE} {SD_VFF_PYR/SCALE}

//                                  FF to PYR WEIGHTS
echo ff to pyr weights

/*
** counts the convergent synapses onto a single ff interneuron
*/
float pyr_sum = \
expsum(/ff/interneuron[x>={CORTEX_X/2 - RFF_to_PYR}][y>={CORTEX
_Y/2 - RFF_to_PYR}][x<={CORTEX_X/2 + RFF_to_PYR}][y<={CORTEX_Y/
2 + RFF_to_PYR}],\
{-1.0/LFF_to_PYR},1,{AWFF_to_PYR},{CORTEX_X/2},{CORTEX_Y/2})

float wpyr = NSYN_PYR_from_FF/(pyr_sum*PFF_to_PYR)

exponential_weight /ff/interneuron[]/axon   {wpyr} \
                        {LFF_to_PYR} \
                        {AWFF_to_PYR*wpyr}

normalize_synapses /ff/interneuron[]/axon {dst} \
```

-gaussian {NSYN_PYR_from_FF} {SDSYN_PYR_from_FF}

functions.g

```
//genesis

// ================================
//      link in a new compartment
// ================================
function link_compartment
    sendmsg  $1  $2     RAXIAL      Ra previous_state
    sendmsg   $2  $1    AXIAL       previous_state
end

// ================================
//      link in a new channel
// ================================
function link_channel(chan,comp)
    sendmsg   {chan}  {comp}    CHANNEL     Gk Ek
    sendmsg   {comp}  {chan}    VOLTAGE     Vm
end

function singlelink_channel(chan,comp)
    sendmsg   {chan}  {comp}    CHANNEL     Gk Ek
end

// ================================
//   somatic current injection (uA)
// ================================
function inject(neuron,value)
str neuron
float value
    set {neuron}/soma inject value
end

// ================================
//   modify spike output based on
//   integration step to give constant
//   impulse area
// ================================
function adjustspike
    set /##[TYPE=spike] output_amp {1.0/getclock(0)}
end

// ================================
//   sets baseline LOT input rates
// ================================
function baseline(min,max,rate)
```

```
    float min,max,rate
    str path

    path  = "/bulb/mitral[]/input"
    set {path} min_amp {min} max_amp {max} rate {rate}
end

// ================================
//   simulate shock to the LOT
// ================================
function shock(value)
str path
float value
float oldrate,oldmin,oldmax
    baseline {value} {value} 1000   // shock
    step
    // baseline 0.05 0.1 0.4        // 400 Hz noise
    baseline 0 0 0
end

function pcsave(file)
str file
    save /##[TYPE=compartment] {file}
    save /##[TYPE=channelC] {file} -append
    save /##[TYPE=channelC2] {file} -append
end
```

field.g

```
//genesis

function field_electrode(path,target,x,y,z,r,rz)
str path
str target
float x,y,z,r,rz
    create efield {path}
    set ^ scale 1e5 x {x} y {y} z {z}
    sendmsg \
    {target}/##[TYPE=compartment][x>={x-r}][y>={y-r}][x<={x+r}]
[y<={y+r}] \
    ^ CURRENT Im 0.0
    call ^ RECALC
end

function move_electrode(path,x,y,z)
str path
float x,y,z
    set {path} x {x} y {y} z {z}
    call {path} RECALC
end

function electrode_array(path,xmin,ymin,xmax,ymax,xspacing,yspa
cing,z)
str path
float xmin,ymin
float xmax,ymax
float xspacing,yspacing
float z
float x,y
int count = 0

    for(y=ymin;y<ymax;y=y+yspacing)
    for(x=xmin;x<xmax;x=x+xspacing)
        field_electrode /field[{count}] {path} {x} {y} {z} {abs
(z)+0.5} 1
        echo -n .
        count = count+1
    end
    end
    echo
    return(count)
end
```

```
if(FIELD && MULTI)
    // construct the electrode array
    // arrange the spacing so that each electrode consistently
lies
    // at consistent distances between neurons
    echo setting up {CORTEX_X}x{CORTEX_Y}mm field electrode arr
ay

    // X dimension
    // try for something as close to 1 mm spacing as possible
    float dxtrodes = round({1.0/PYR_DX})*PYR_DX
    // figure out how many of these will fit in cortex_x mm
    int nxtrodes = trunc({CORTEX_X/dxtrodes})

    // Y dimension
    // try for something as close to 1 mm spacing as possible
    float dytrodes = round({1.0/PYR_DY})*PYR_DY
    // figure out how many of these will fit in cortex_y mm
    int nytrodes = trunc({CORTEX_Y/dytrodes})
    echo {nxtrodes} x {nytrodes} electrode array
    echo {electrode_array(/pyr,{PYR_DX/2.0},{PYR_DY/2.0},{CORTE
X_X},{CORTEX_Y},{dxtrodes},{dytrodes},0)} electrodes
end
```

output.g

```
//genesis
str name
int clock = 1

echo setting up disk outputs

function disk(diskpath,srcpath,field)
    create xviewdata /output/{diskpath}
    set /output/{diskpath} \
    leave_open  1 \
    flush       1
    sendmsg {srcpath} /output/{diskpath} SAVE {field}
    useclock /output/{diskpath} {clock}
    echo {diskpath}
end

function disk2(diskpath,srcpath,field)
    create disk_out /output/{diskpath}
    set /output/{diskpath} \
    leave_open  1 \
    flush       1
    sendmsg {srcpath} /output/{diskpath} SAVE {field}
    useclock /output/{diskpath} 1
    echo {diskpath}
end

/*
** DISK OUTPUT
** write out the intracellular membrane potentials to disk
** for all elements in /pyr
*/
disk    pyr_Vm      /pyr/pyramidal[]/soma   Vm
disk    fb_Vm   /fb/interneuron[]/soma  Vm
disk    ff_Vm   /ff/interneuron[]/soma  Vm

clock = 2
/*
** CONDUCTANCES
*/
if(MULTI)
    str base = "/pyr/pyramidal[]/soma"
    disk    pyr_gAff    {base}/Ia_dend/Aff_Na_channel       Gk
    disk    pyr_gRA     {base}/deepIb_dend/RA_Na_channel    Gk
    disk    pyr_gCA     {base}/supIb_dend/CA_Na_channel     Gk
```

```
    disk    pyr_gLocal  {base}/III_dend/Local_Na_channel    Gk
    disk    pyr_gFB     {base}/Cl_channel           Gk
    disk    pyr_gFF     {base}/Ia_dend/K_channel        Gk
else
    disk    pyr_gAff    /pyr/pyramidal[]/Aff_Na_channel     Gk
    disk    pyr_gRA     /pyr/pyramidal[]/RA_Na_channel      Gk
    disk    pyr_gCA     /pyr/pyramidal[]/CA_Na_channel      Gk
    disk    pyr_gLocal  /pyr/pyramidal[]/Local_Na_channel   Gk
    disk    pyr_gFB     /pyr/pyramidal[]/Cl_channel         Gk
    disk    pyr_gFF     /pyr/pyramidal[]/K_channel      Gk
end

/*
** CURRENTS
*/
if(MULTI)
    str base
    disk    soma_Im     /pyr/pyramidal[]/soma   Im
    foreach base (Ia supIb deepIb III)
    disk    {base}_Im   /pyr/pyramidal[]/soma/{base}_dend   Im
    end
    str base
    foreach base (Ia supIb deepIb III)
    disk    {base}_Vm   /pyr/pyramidal[]/soma/{base}_dend   Vm
    end
end

/*
** FIELD POTENTIALS
*/
if(FIELD && MULTI)
    disk    efield      /field[]    field
    useclock /output/efield 0
end
```

protodefs.g

```
//genesis
create neutral /library
disable /library

//=============================================================
==========
//                                  CHANNELS
//=============================================================
==========
create      channelC2   /library/Na_channel
    set         /library/Na_channel \
    Ek      {EKA} \
    tau1        { 1.0 * SCALE } \   // msec
    tau2        { 3.0 * SCALE }     // msec
create      channelC2   /library/K_channel
    set         /library/K_channel \
    Ek      { EK } \
    tau1        { 10.0 * SCALE } \  // msec
    tau2        { 100.0 * SCALE }   // msec
create      channelC2   /library/Cl_channel
    set         /library/Cl_channel \
    Ek      {ECL} \
    tau1        { 1.0 * SCALE } \   // msec
    tau2        { 7.0 * SCALE }     // msec

//=============================================================
==========
//                            SPIKE DETECTOR
//=============================================================
==========
create      spike       /library/spike
    set /library/spike \
    thresh      -40 \               // mV
    abs_refract { 10 * SCALE } \        // msec
    output_amp      1
```

```
//genesis
str dst

echo
echo "                                PYRAMIDAL CELLS"
echo

// ============================================================
=======
//                                    CONNECTIONS
// ============================================================
=======

//                                CAUDAL CONNECTIONS
echo caudal connections
if(MULTI)
    dst = "/pyr/pyramidal[]/soma/supIb_dend/CA_Na_channel"
else
    dst = "/pyr/pyramidal[]/soma/CA_Na_channel"
end
/*
** spatial units are in mm
*/
region_connect /pyr/pyramidal[]/CAaxon  to {dst} \
    with synapse -rel \
    1 1 -100 -100 100 100 \     // do this over all the cells
    2 1 0 {-RPYR_to_CDIST} \    // connect to cells caudal to i
t
    {RPYR_to_CDIST} {RPYR_to_CDIST} \
    -1 {-RPYR_to_LOCAL} {-RPYR_to_LOCAL} \
    {RPYR_to_LOCAL} {RPYR_to_LOCAL} \ //  dont connect to the l
ocal region
    {PPYR_to_CDIST}


//                                ROSTRAL CONNECTIONS
echo rostral connections
if(MULTI)
    dst = "/pyr/pyramidal[]/soma/deepIb_dend/RA_Na_channel"
else
    dst = "/pyr/pyramidal[]/soma/RA_Na_channel"
end
region_connect /pyr/pyramidal[]/RAaxon to {dst} \
    with synapse -rel \
```

```
    1 1 -100 -100 100 100 \     // do this over all the cells
    2 1 {-RPYR_to_RDIST} {-RPYR_to_RDIST} \
    {-PYR_DX}  {RPYR_to_RDIST} \    // connect to cells rostral
 to it
    -1 {-RPYR_to_LOCAL} {-RPYR_to_LOCAL} \
    {RPYR_to_LOCAL} {RPYR_to_LOCAL} \  // dont connect to the l
ocal region
    {PPYR_to_CDIST}

//                              LOCAL CONNECTIONS
echo local connections
if(MULTI)
    dst = "/pyr/pyramidal[]/soma/III_dend/Local_Na_channel"
else
    dst = "/pyr/pyramidal[]/soma/Local_Na_channel"
end
region_connect /pyr/pyramidal[]/LRAaxon to {dst} \
    with synapse -rel \
    1 1 -100 -100 100 100 \         // do this over all the cel
ls
    2 1 {-RPYR_to_LOCAL} {-RPYR_to_LOCAL} \
    {-PYR_DX} {RPYR_to_LOCAL} \     //  connect to the local re
gion
     -1 0 0 0 0  \              //  dont connect to itself
    {PPYR_to_RLOCAL}

region_connect /pyr/pyramidal[]/LCAaxon to {dst} \
    with synapse -rel \
    1 1 -100 -100 100 100 \     // do this over all the cells
    2 1 0 {-RPYR_to_LOCAL} \
    {RPYR_to_LOCAL} {RPYR_to_LOCAL}  \  //  connect to the loca
l region
    -1 0 0 0 0 \            //  dont connect to itself
    {PPYR_to_CLOCAL}

//                              PYR to FF CONNECTIONS
echo pyr to ff connection
if(LOCAL_FF)
region_connect /pyr/pyramidal[]/FFaxon  to /ff/interneuron[]/so
ma/Na_channel \
    with synapse -rel \
    1 1 -100 -100 100 100 \     // do this over all the cells
    1 1 {-RPYR_to_FF} {-RPYR_to_FF} \
    {RPYR_to_FF} {RPYR_to_FF} \ // connect to a local area of c
```

```
ells
    {PPYR_to_FF}
else
region_connect /pyr/pyramidal[]/FFaxon  to /ff/interneuron[]/so
ma/Na_channel \
    with synapse -rel \
    1 1 -100 -100 100 100 \     // do this over all the cells
    2 1 -100 -100 \
    100  100 \      // connect to all cells
    -1 {-RPYR_to_LOCAL} {-RPYR_to_LOCAL} \
    {RPYR_to_LOCAL} {RPYR_to_LOCAL} \  // dont connect to the l
ocal region
    {PPYR_to_FF}
end
//                              PYR to FB CONNECTIONS
echo pyr to fb connection
region_connect /pyr/pyramidal[]/FBaxon  to /fb/interneuron[]/so
ma/Na_channel \
    with synapse -rel \
    1 1 -100 -100 100 100 \     // do this over all the cells
    1 1 {-RPYR_to_FB} {-RPYR_to_FB} \
    {RPYR_to_FB} {RPYR_to_FB}  \    // connect to a local area
of cells
    {PPYR_to_FB}

// ============================================================
=======
//                                  DELAYS
// ============================================================
=======
// velocities in m/s or mm/msec

//                              CAUDAL DELAYS
echo caudal delays
gausspropagation_velocity /pyr/pyramidal[]/CAaxon \
    {VPYR_CA_MIN/SCALE} {VPYR_CA_MAX/SCALE} \
    {VPYR_CA/SCALE} {SD_VPYR_CA/SCALE}

//                              ROSTRAL DELAYS
echo rostral delays
gausspropagation_velocity /pyr/pyramidal[]/RAaxon \
    {VPYR_RA_MIN/SCALE} {VPYR_RA_MAX/SCALE} \
    {VPYR_RA/SCALE} {SD_VPYR_RA/SCALE}
```

```
//                              LOCAL DELAYS
echo local delays
gausspropagation_velocity /pyr/pyramidal[]/LRAaxon \
    {VPYR_RA_MIN/SCALE} {VPYR_RA_MAX/SCALE} \
    {VPYR_RA/SCALE} {SD_VPYR_RA/SCALE}
gausspropagation_velocity /pyr/pyramidal[]/LCAaxon \
    {VPYR_CA_MIN/SCALE} {VPYR_CA_MAX/SCALE} \
    {VPYR_CA/SCALE} {SD_VPYR_CA/SCALE}

//                              PYR to FF DELAYS
echo pyr to ff delays
gausspropagation_velocity /pyr/pyramidal[]/FFaxon \
    {VPYR_FF_MIN/ SCALE } {VPYR_FF_MAX/SCALE} \
    {VPYR_FF/SCALE} {SD_VPYR_FF/SCALE}

//                              PYR to FB DELAYS
echo pyr to fb delays
gausspropagation_velocity /pyr/pyramidal[]/FBaxon \
    {VPYR_FB_MIN/ SCALE } {VPYR_FB_MAX/SCALE} \
    {VPYR_FB/SCALE} {SD_VPYR_FB/SCALE}


// ============================================================
=======
//                                  WEIGHTS
// ============================================================
=======
/*
** use an exponential distribution with distance for weights
** which represent the number of synaptic contacts
** the arguments are (peakweight spaceconstant minweight)
** The space constant is in mm.
*/

/*
** counts the convergent synapses onto a single pyramidal cell
*/
float cloc_sum = \
expsum(/pyr/pyramidal[x<={CORTEX_X/2}][y<={CORTEX_Y}],\
{-1.0/LPYR_to_CLOCAL},1,{AWPYR_to_CLOCAL},{CORTEX_X/2},{CORTEX_
Y/2})

float cloc_sum = \
expsum(/pyr/pyramidal[x>={CORTEX_X/2 - RPYR_to_LOCAL}][y>={CORT
```

```
EX_Y/2 - RPYR_to_LOCAL}][x<={CORTEX_X/2}][y<={CORTEX_Y/2 + RPYR
_to_LOCAL}],\
{-1.0/LPYR_to_CLOCAL},1,{AWPYR_to_CLOCAL},{CORTEX_X/2},{CORTEX_
Y/2})

float rloc_sum = \
expsum(/pyr/pyramidal[x>={CORTEX_X/2}][y>={CORTEX_Y/2 - RPYR_to
_LOCAL}][x<={CORTEX_X/2+RPYR_to_LOCAL}][y<={CORTEX_Y/2 + RPYR_t
o_LOCAL}],\
{-1.0/LPYR_to_RLOCAL},1,{AWPYR_to_RLOCAL},{CORTEX_X/2},{CORTEX_
Y/2})

float caloc_sum = \
expsum(/pyr/pyramidal[x>={CORTEX_X/2 - RPYR_to_LOCAL}][y>={CORT
EX_Y/2 - RPYR_to_LOCAL}][x<={CORTEX_X/2}][y<={CORTEX_Y/2 + RPYR
_to_LOCAL}],\
{-1.0/LPYR_to_CA},1,{AWPYR_to_CA},{CORTEX_X/2},{CORTEX_Y/2})

float raloc_sum = \
expsum(/pyr/pyramidal[x>={CORTEX_X/2}][y>={CORTEX_Y/2 - RPYR_to
_LOCAL}][x<={CORTEX_X/2+RPYR_to_LOCAL}][y<={CORTEX_Y/2 + RPYR_t
o_LOCAL}],\
{-1.0/LPYR_to_RA},1,{AWPYR_to_RA},{CORTEX_X/2},{CORTEX_Y/2})

float ca_sum = \
expsum(/pyr/pyramidal[x<={CORTEX_X/2}][y<={CORTEX_Y/2 + RPYR_to
_CDIST}][x>={CORTEX_X/2 - RPYR_to_CDIST}][y>={CORTEX_Y/2 - RPYR
_to_CDIST}],\
{-1.0/LPYR_to_CA},1,{AWPYR_to_CA},{CORTEX_X/2},{CORTEX_Y/2}) -
caloc_sum

float ra_sum = \
expsum(/pyr/pyramidal[x>={CORTEX_X/2}][y<={CORTEX_Y/2 + RPYR_to
_RDIST}][x<={CORTEX_X/2 + RPYR_to_RDIST}][y>={CORTEX_Y/2 - RPYR
_to_RDIST}],\
{-1.0/LPYR_to_RA},1,{AWPYR_to_RA},{CORTEX_X/2},{CORTEX_Y/2}) -
raloc_sum

/*
** counts the convergent synapses onto a single fb interneuron
*/
float fb_sum = \
expsum(/pyr/pyramidal[x>={CORTEX_X/2 - RPYR_to_FB}][y>={CORTEX_
Y/2 - RPYR_to_FB}][x<={CORTEX_X/2 + RPYR_to_FB}][y<={CORTEX_Y/2
```

```
 + RPYR_to_FB}],\
{-1.0/LPYR_to_FB},1,{AWPYR_to_FB},{CORTEX_X/2},{CORTEX_Y/2})

/*
** counts the convergent synapses onto a single ff interneuron
*/
float ff_sum = \
expsum(/pyr/pyramidal[x>={CORTEX_X/2 - RPYR_to_FF}][y>={CORTEX_
Y/2 - RPYR_to_FF}][x<={CORTEX_X/2 + RPYR_to_FF}][y<={CORTEX_Y/2
 + RPYR_to_FF}],\
{-1.0/LPYR_to_FF},1,{AWPYR_to_FF},{CORTEX_X/2},{CORTEX_Y/2})

float wca = NSYN_PYR_from_CA/(ca_sum*PPYR_to_CDIST)
float wra = NSYN_PYR_from_RA/(ra_sum*PPYR_to_RDIST)
float wrloc = NSYN_PYR_from_RLOCAL/(rloc_sum*PPYR_to_RLOCAL)
float wcloc = NSYN_PYR_from_CLOCAL/(cloc_sum*PPYR_to_CLOCAL)
float wfb = NSYN_FB_from_PYR/(fb_sum*PPYR_to_FB)
float wff = NSYN_FF_from_PYR/(ff_sum*PPYR_to_FF)

//                              CAUDAL WEIGHTS
echo caudal weights
exponential_weight /pyr/pyramidal[]/CAaxon  {wca} \
                        {LPYR_to_CA} \
                        {AWPYR_to_CA*wca}

//                              ROSTRAL WEIGHTS
echo rostral weights
exponential_weight /pyr/pyramidal[]/RAaxon  {wra} \
                        {LPYR_to_RA} \
                        {AWPYR_to_RA*wra}

//                              LOCAL WEIGHTS
echo local weights
exponential_weight /pyr/pyramidal[]/LRAaxon     {wrloc} \
                        {LPYR_to_RLOCAL} \
                        {AWPYR_to_RLOCAL*wrloc}

exponential_weight /pyr/pyramidal[]/LCAaxon     {wcloc} \
                        {LPYR_to_CLOCAL} \
                            {AWPYR_to_CLOCAL*wcloc}

//                              PYR to FF WEIGHTS
echo pyr to ff weights
exponential_weight /pyr/pyramidal[]/FFaxon  {wff} \
```

```
                        {LPYR_to_FF} \
                        {AWPYR_to_FF*wff}

//                              PYR to FB WEIGHTS
echo pyr to fb weights
exponential_weight /pyr/pyramidal[]/FBaxon  {wfb} \
                        {LPYR_to_FB} \
                        {AWPYR_to_FB*wfb}

/*
** normalize local interneuron weights
*/
normalize_synapses /pyr/pyramidal[]/FBaxon /fb/interneuron[]/so
ma/Na_channel \
    -gaussian {NSYN_FB_from_PYR} {SDSYN_FB_from_PYR}

normalize_synapses /pyr/pyramidal[]/FFaxon /ff/interneuron[]/so
ma/Na_channel \
    -gaussian {NSYN_FF_from_PYR} {SDSYN_FF_from_PYR}
```

pyramidal.g

```
//genesis
echo creating pyramidal cells
/*
** create the pyramidal population element on the root
*/
create      neutral     /pyr

// ============================================================
//                      PYRAMIDAL CELL ARRAY
// ============================================================

pyramidal_cell(/pyramidal,{MULTI},{SPIKE},{CONNECT},\
{PYR_SOMA_D},{PYR_SOMA_L},{PYR_DEND_D},{PYR_DEND_L})

createmap   /pyramidal  /pyr    {PYR_NX} {PYR_NY} {PYR_DX} {PYR
_DY}
delete /pyramidal
position /pyr I I 350e-3

// ============================================================
//                      PYRAMIDAL CELL THRESHOLDS
// ============================================================

randomfield /pyr/pyramidal[]/spike  thresh -gaussian -40 3

// ============================================================
//                      TRANSMITTER NOISE
// ============================================================

if(T_NOISE)
    create funcgen /pyr/Affnoise
    set ^ mode 3 amplitude 1e-3 x {100/getclock(0)}
    sendmsg ^ /pyr/pyramidal[]/soma/Ia_dend/Aff_Na_channel  \
    RAND_ACTIVATION output x
end
```

theta.g

```
//genesis

function maketheta

    create funcgen /bulb/theta
    push /bulb/theta
    set mode        0   // sine wave
    set amplitude   0.15    // peak amplitude
    set frequency   5e-3    // 5 Hz
    set dc_offset   .2  // base amplitude

    sendmsg . /bulb/mitral[]/input MINMAX output output
    baseline 0 0 1      // 1000 Hz firing rate
    pop
end
```

Appendix 3: Genesis scripts for the CSD model of piriform cortex

This section contains the complete listing of the Genesis scripts used to produce the current source density simulations described in chapter 2.

It should be emphasized that this section is provided as a reference for those who are already familiar with the Genesis simulation system and are interested in the details of the model implementation.

csd.g

```
//genesis
clean -f
echo " "
echo "*********************************************"
echo "*       PIRIFORM PYRAMIDAL CSD PROFILE      *"
echo "*                                           *"
echo "*         Written by Matt Wilson            *"
echo "*    California Institute of Technology     *"
echo "*                                           *"
echo "*         GENESIS implementation            *"
echo "*                  9/15/89                  *"
echo "*********************************************"
echo " "

int MATRIX      =   1

include constants.g     // set local variables
include functions.g     // set up some functions
include cells.g         // set up the cell generation functions

include pyramidal.g     // create a pyramidal cell
include file.g
include stimulate.g
if(MATRIX)
    include matrix.g
end

echo checking and initializing simulation
check
reset
echo " "
echo CSD simulation loaded.
```

cells.g

```
//genesis

function multiple_link(src,target,n)
int i
int n
    for(i=1;i<n;i=i+1)
    link_compartment    {src}[{i-1}]    {src}[{i}]
    end
    if({target} != "NONE")
    link_compartment    {src}[{n-1}]        {target}
    end
end

function make_compartment(path,l,d,n)
float l,d
int i,n
float a =   PI*d*l/n    // um^2
float xa =  PI*d*d/4    // um^2


    for(i=0;i<n;i=i+1)
    create compartment {path}[{i}]
    set ^ \
        Em  {PYR_EREST} \           // mV
        Rm  {RM/ a} \           // Kohms
        Cm  {CM * a*SCALE} \        // uF
        Ra  {RA * l/(n*xa)}             // Kohm
    end
end

str s
function presynaptic(comp,channel)
    foreach s ({EL({comp}[])})
    create playback {s}/{channel}/pre
    sendmsg {s}/{channel}/pre {s}/{channel} ACTIVATION state
    end
end

str cname

function createNa(channel,gmax,compartment)
str channel,compartment
float gmax
```

```
    foreach cname ({EL({compartment}[])})
    create channelC2        {cname}/{channel}
    set ^ \
        Ek  {EKA} \             // mV
        tau1    {1.0*SCALE} \       // msec
        tau2    {3.0*SCALE } \      // msec
        gmax    {gmax}          // mS
    link_channel    {cname}/{channel}       {cname}
    end
end

function createK(channel,gmax,compartment)
str channel,compartment
float gmax

    foreach cname ({EL({compartment}[])})
    create channelC2        {cname}/{channel}
    set ^ \
        Ek  {EK} \              // mV
        tau1    {10.0*SCALE} \      // msec
        tau2    {100.0*SCALE } \    // msec
        gmax    {gmax}          // mS
    link_channel    {cname}/{channel}       {cname}
    end
end

//                          CHANNEL LIFETIMES
// mouse spinal neurone - Study and Barker PNAS USA, 1981,78:11
, 7180-7184
// GABA tau_Cl = 18.3 msec
// GABA+PB tau_Cl = 30-130 msec

function createCl(channel,gmax,compartment)
str channel,compartment
float gmax

    foreach cname ({EL({compartment}[])})
    create channelC2        {cname}/{channel}
    set ^ \
        Ek  {ECL} \             // mV
        tau1    {1.0*SCALE} \       // msec
        tau2    {7.0*(PENTOBARB +1)*SCALE } \   // msec
        gmax    {gmax}          // mS
    link_channel    {cname}/{channel}       {cname}
```

```
    end
end

str string

//=================================================================
==========
//                          PYRAMIDAL CELL
//=================================================================
==========
/*
** this function constructs a pyramidal cell according to the a
rguments
** passed to it
*/
function pyramidal_cell(pathname)

str pathname
int i

    float soma_a    =   PI*soma_D*soma_L    // um^2

    create  neutral     {pathname}
    ce  {pathname}

    // soma
    make_compartment(soma,{soma_L},{soma_D},{soma_L/cpt_size})

    // upper soma
    make_compartment(uppersoma,{uppersoma_L},{uppersoma_D},{upp
ersoma_L/cpt_size})

    // lower soma
    make_compartment(lowersoma,{lowersoma_L},{lowersoma_D},{low
ersoma_L/cpt_size})

    if(ACTIVE)
    // add two voltage dependent conductances
    copy    /library/HH_Na_channel soma
    copy    /library/HH_K_channel soma
    link_hhchannel  HH_Na_channel   soma
    link_hhchannel  HH_K_channel    soma
    else
    /*
```

```
    ** add a buffer for generating thresholded spike events
    */
    create spike spike
    set spike abs_refract 10 output_amp 1
    set spike thresh    100                 // mV
    sendmsg  lowersoma  spike       INPUT Vm
    end


    /*
    ** add a passive dendritic compartments
    */
    make_compartment(III,{III_L},{III_D},{III_L/cpt_size})
    make_compartment(deepIb,{deepIb_L},{deepIb_D},{deepIb_L/cpt
_size})
    make_compartment(supIb,{supIb_L},{supIb_D},{supIb_L/cpt_siz
e})
    make_compartment(Ia,{Ia_L},{Ia_D},{Ia_L/cpt_size})

    /*
    ** and link them
    */
    multiple_link(Ia,supIb,{Ia_L/cpt_size})
    multiple_link(supIb,deepIb,{supIb_L/cpt_size})
    multiple_link(deepIb,uppersoma,{deepIb_L/cpt_size})
    multiple_link(uppersoma,soma,{uppersoma_L/cpt_size})
    multiple_link(soma,lowersoma,{soma_L/cpt_size})
    multiple_link(lowersoma,III,{lowersoma_L/cpt_size})
    multiple_link(III,NONE,{III_L/cpt_size})

    /*
    ** add synaptically activated channels
    */
    if(EXTRA)
    createCl(Cl,{GMAX_CL},Ia)
    end

    createNa(Na,{DISTAL_GMAX_NA},Ia)
    createNa(Na,{DISTAL_GMAX_NA},supIb)
    createNa(Na,{DISTAL_GMAX_NA},deepIb)
    createNa(Na,{LOCAL_GMAX_NA},III)

    createK(K,{GMAX_K},Ia)
    createK(K,{GMAX_K},supIb)
```

```
createK(K,{GMAX_K},deepIb)

createCl(Cl,{GMAX_CL},Ia)
createCl(Cl,{GMAX_CL},supIb)
createCl(Cl,{GMAX_CL},deepIb)

createCl(Cl,{GMAX_CL},soma)
createCl(Cl,{GMAX_CL},lowersoma)
createCl(Cl,{GMAX_CL},uppersoma)


if(!ACTIVE)
/*
** add spike producing channels
*/
create channelC     SNa_channel
    set SNa_channel \
    Ek  {ENA} \              // mV
    tau1    { 0.2  * SCALE } \      // msec
    tau2    { 0.2  * SCALE } \      // msec
    gmax    {SGMAX_NA*fAC*soma_a}       // mS
create  channelC    SK_channel
    set SK_channel \
    Ek  {EK} \               // mV
    tau1    { 1 * SCALE } \         // msec
    tau2    { 1 * SCALE } \         // msec
    gmax    {SGMAX_K*fAC*soma_a}        // mS
/*
** use the spike output as activation for the channels
*/
sendmsg  spike SNa_channel      ACTIVATION state
sendmsg  spike SK_channel       ACTIVATION state
singlelink_channel      SNa_channel     lowersoma
singlelink_channel      SK_channel  lowersoma
end

/*
* create the simulated presynaptic inputs
*/
presynaptic(Ia,Na)
presynaptic(supIb,Na)
presynaptic(deepIb,Na)
presynaptic(III,Na)
```

```
    presynaptic(Ia,K)
    presynaptic(supIb,K)
    presynaptic(deepIb,K)

    presynaptic(Ia,Cl)
    presynaptic(supIb,Cl)
    presynaptic(deepIb,Cl)

    presynaptic(soma,Cl)
    presynaptic(lowersoma,Cl)
    presynaptic(uppersoma,Cl)
end // pyramidal_cell
```

constants.g

```
//genesis

prompt      "CSD !"          // set the prompt
if(MATRIX)
    setclock    0       0.1 // set the basic simulation step si
ze
else
    setclock    0       0.005   // set the basic simulation ste
p size
end
setclock    1       0.5 // set the output step size
randomseed -new
float   PI      =   3.14159

int     ACTIVE      =   0
int     EXTRA       =   0
float       PENTOBARB   =   2

// time scale factor
float   SCALE       =   1e-3        // convert msec to sec
float   SCALE       =   1       // no conversions

// ============================================================
=========
//                              CELL DIMENSIONS
// ============================================================
=========

float   cpt_size    =   10              // um

float   Ia_D        =   4               // um
float   Ia_L        =   120             // um

float   supIb_D     =   4               // um
float   supIb_L     =   130             // um

float   deepIb_D    =   4               // um
float   deepIb_L    =   130             // um

float   uppersoma_D =   10              // um
float   uppersoma_L =   60              // um

float   soma_D      =   15              // um
float   soma_L      =   20              // um
```

```
float   lowersoma_D =   10              // um
float   lowersoma_L =   40              // um

float   III_D       =   4               // um
float   III_L       =   100             // um

int ntotal = (Ia_L + supIb_L + deepIb_L + uppersoma_L + soma_L
+ lowersoma_L \
        + III_L)/cpt_size

// ============================================================
=========
//                          PHYSIOLOGICAL PARAMETERS
// ============================================================
=========

//                      IONIC EQUILIBRIUM POTENTIALS
float   EKA         =   0               // mV
float   ENA         =   55              // mV
float   ECL         =   -65             // mV
float   EK      =   -90             // mV
float   EREST       =   -70             // mV
float   PYR_EREST   =   -70             // mV

// Kandel,Schwartz, Principles of Neuroscience, 2nd ed.  pg 83
// gNa 8-18 pS,  gK 4-12 pS
// squid giant axon - Conti et al.(1975),J.Physiol(Lond),248,45
-82
// gNa = 4pS
// squid giant axon - Conti and Neher(1980),Nature(Lond),285,14
0-143
// gK = 18pS
// mouse spinal neurone - Study and Barker(1981),PNAS USA,78:11
,7180-7184
// GABA gCl = 18pS +- 5
// mouse spinal neurone - Mathers and Barker(1982),Int.Rev.Neur
obiol,23,1-34
// gCl = 18pS
// rat hippocampal neurone - Segal and Barker(1984),J.Neurophys
.,51:3,500-515
// gCl = 20pS response to GABA, muscimol, and glycine
//                          UNIT CONDUCTANCES
//              (mS/channel)
```

```
float   UNIT_GNA     =   8e-9
float   UNIT_GK      =   4e-9
float   UNIT_GCL     =   20e-9

float   SUNIT_GNA    =   8e-9
float   SUNIT_GK     =   4e-9

// squid giant axon - Conti et al.(1975),J.Physiol(Lond),248,45
-82
// rhoNa = 330 channels/um^2
// squid giant axon - Conti and Neher(1980),Nature(Lond),285,14
0-143
// rhoK = 72 channels/um^2
//                              CHANNEL DENSITIES
//               (channel/um^2)
float   RHO_NA       =   30
float   RHO_CL       =   15
float   RHO_K        =   30
float   SRHO_NA      =   330
float   SRHO_K       =   72

//                              SYNAPTIC AREA
// Haberly and Presto(1986),J.Comp.Neurol,248,464-474
// basal spine d = .40um
// distal spine d = .74um
// presynaptic to dendritic spines d = .61um
// presynaptic to dendritic shafts d = .89um
// presynaptic to initial segment d = .89um
//
// using synaptic contact area A = pi*d^2/4
//               (um^2/synapse)
float   ASYN_LOCAL_NA   =   0.12         // d=.40
float   ASYN_DISTAL_NA  =   0.43         // d=.74
float   ASYN_CL      =   0.62         // d=.89
float   ASYN_K       =   0.43         // d=.74

//                              ACTIVE AREA
// fraction of somatic area containing active channels
float   fAC      =   0.1

// muse spinal neurone - Study and Barker PNAS USA, 1981,78:11,
 7180-7184
// GABA gCl_peak = 112nS
//                              PEAK CONDUCTANCE
```

```
// peak_g = unit_g * channel_density * synaptic_area
//                (mS/synapse)
float   LOCAL_GMAX_NA   =   UNIT_GNA * RHO_NA * ASYN_LOCAL_NA
float   DISTAL_GMAX_NA  =   UNIT_GNA * RHO_NA * ASYN_DISTAL_NA
float   GMAX_K      =   UNIT_GK * RHO_K * ASYN_K
float   GMAX_CL     =   UNIT_GCL * RHO_CL * ASYN_CL

float   SGMAX_NA    =   SUNIT_GNA * SRHO_NA     // mS/um^2
float   SGMAX_K     =   SUNIT_GK * SRHO_K       // mS/um^2

//                          MEMBRANE PARAMETERS
float   RM      =   2.7e+8              // Kohm-um^2
float   RA      =   0.10e+4             // Kohm-um
float   CM      =   3.0e-8              // uF/um^2
```

field.g

```
//genesis

function field_electrode(path,target,x,y,z,r,rz)
str path
str target
float x,y,z,r,rz
    create efield {path}
    set ^ scale 1e5 x {x} y {y} z {z}
    sendmsg \
    {target}/##[TYPE=compartment][x>={x-r}][y>={y-r}][x<={x+r}]
[y<={y+r}] \
    ^ CURRENT Im 0.0
    call ^ RECALC
end

function move_electrode(path,x,y,z)
str path
float x,y,z
    set {path} x {x} y {y} z {z}
    call {path} RECALC
end

function electrode_array(path,xmin,ymin,xmax,ymax,xspacing,yspa
cing,z)
str path
float xmin,ymin
float xmax,ymax
float xspacing,yspacing
float z
float x,y
int count = 0

    for(y=ymin;y<ymax;y=y+yspacing)
    for(x=xmin;x<xmax;x=x+xspacing)
        field_electrode /field[{count}] {path} {x} {y} {z} {abs
(z)+0.5} 1
        echo -n .
        count = count+1
    end
    end
    echo
    return(count)
end
```

```
if(FIELD && MULTI)
    // construct a 10x6mm electrode array
    echo setting up 10x6mm field electrode array
    echo {electrode_array(/pyr,{PYR_DX/2.0},{PYR_DY/2.0},10,6,1
,1,0)} electrodes
end
```

functions.g

```
//genesis

// ================================
//      link in a new compartment
// ================================
function link_compartment(comp1,comp2)
    if(MATRIX)
    sendmsg  $1  $2     RAXIAL      Ra Vm
    sendmsg   $2  $1    AXIAL       Vm
    else
    if(get({comp1},object->name) == "symcompartment")
        sendmsg  $1  $2     RAXIAL      Ra previous_state
        sendmsg   $2  $1    RAXIAL2     Ra previous_state
    else
        sendmsg  $1  $2     RAXIAL      Ra previous_state
        sendmsg   $2  $1    AXIAL       previous_state
    end
    end
end

// ================================
//      link in a new channel
// ================================
function link_channel(chan,comp)
    sendmsg   {chan}  {comp}    CHANNEL     Gk Ek
    sendmsg   {comp}  {chan}    VOLTAGE     Vm
end

function singlelink_channel(chan,comp)
    sendmsg   {chan}  {comp}    CHANNEL     Gk Ek
end

function link_hhchannel(chan,comp)
    sendmsg   {chan}  {comp}    CHANNEL     Gk Ek
    sendmsg   {comp}  {chan}    VOLTAGE     Vm
    sendmsg   {comp}  {chan}    EREST       Erest
end

// ================================
//   somatic current injection (uA)
// ================================
function inject(neuron,value)
str neuron
float value
```

```
    set {neuron}/soma inject value
end

// ================================
//   modify spike output based on
//   integration step to give constant
//   impulse area
// ================================
function adjustspike
    set /##[TYPE=spike] output_amp {1.0/getclock(0)}
end

// ================================
//   sets baseline LOT input rates
// ================================
function baseline(min,max,rate)
    float min,max,rate
    str path

    path  = "/bulb/mitral[]/input"
    set {path} min_amp {min} max_amp {max} rate {rate}
end

// ================================
//   simulate shock to the LOT
// ================================
function shock(value)
str path
float value
float oldrate,oldmin,oldmax
    baseline {value} {value} 1000   // shock
    step
    // baseline 0.05 0.1 0.4        // 400 Hz noise
    baseline 0 0 0
end

function timestamp(file)
    sh "date > RUNID"
    cat {file} > RUNFILE
    echo -n "// run date : " >> RUNFILE
    cat RUNID >> RUNFILE
end
```

file.g

```
//genesis

if (exists(/pyramidal/Vm))
    delete /pyramidal/Vm
end
create xviewdata /pyramidal/Vm
set ^ leave_open 1\
    flush 1
useclock ^ 1
sendmsg /pyramidal/Ia[] ^ SAVE Vm
sendmsg /pyramidal/supIb[] ^ SAVE Vm
sendmsg /pyramidal/deepIb[] ^ SAVE Vm
sendmsg /pyramidal/uppersoma[] ^ SAVE Vm
sendmsg /pyramidal/soma[] ^ SAVE Vm
sendmsg /pyramidal/lowersoma[] ^ SAVE Vm
sendmsg /pyramidal/III[] ^ SAVE Vm

if (exists(/pyramidal/Im))
    delete /pyramidal/Im
end
create xviewdata /pyramidal/Im
set ^ leave_open 1\
    flush 1
useclock ^ 1
sendmsg /pyramidal/Ia[] ^ SAVE Im
sendmsg /pyramidal/supIb[] ^ SAVE Im
sendmsg /pyramidal/deepIb[] ^ SAVE Im
sendmsg /pyramidal/uppersoma[] ^ SAVE Im
sendmsg /pyramidal/soma[] ^ SAVE Im
sendmsg /pyramidal/lowersoma[] ^ SAVE Im
sendmsg /pyramidal/III[] ^ SAVE Im

if (exists(/pyramidal/GEX))
    delete /pyramidal/GEX
end
create xviewdata /pyramidal/GEX
set ^ leave_open 1\
    flush 1
useclock ^ 1
sendmsg /pyramidal/Ia[]/Na ^ SAVE Gk
sendmsg /pyramidal/supIb[]/Na ^ SAVE Gk
sendmsg /pyramidal/deepIb[]/Na ^ SAVE Gk
sendmsg /pyramidal/uppersoma[] ^ SAVE x
sendmsg /pyramidal/soma[] ^ SAVE x      // placeholder
```

```
sendmsg /pyramidal/lowersoma[] ^ SAVE x
sendmsg /pyramidal/III[]/Na ^ SAVE Gk

if (exists(/pyramidal/GINH))
    delete /pyramidal/GINH
end
create xviewdata /pyramidal/GINH
set ^ leave_open 1\
    flush 1
useclock ^ 1
sendmsg /pyramidal/Ia[]/K ^ SAVE Gk
sendmsg /pyramidal/supIb[]/K ^ SAVE Gk
sendmsg /pyramidal/deepIb[]/K ^ SAVE Gk
sendmsg /pyramidal/uppersoma[]/Cl ^ SAVE Gk
sendmsg /pyramidal/soma[]/Cl ^ SAVE Gk
sendmsg /pyramidal/lowersoma[]/Cl ^ SAVE Gk
sendmsg /pyramidal/III[] ^ SAVE x       // placeholder
```

plot.g

```
//genesis

openfile RUNID r
str runid = readfile(-1,RUNID)
closefile RUNID

// singleep Im -d -o defield
// singleep Im -d -z 500 -o sefield

radialep Im -d -r 2000 -z 500 -o defield
radialep Im -d -r 2000 -z 0 -o sefield

echo /plotname deep_efield > tmp
echo /yscale 50e-4 >> tmp
echo /xaxisoffset 2e-4 >> tmp
echo /xrastaxis 1 >> tmp
xy defield -dx .5 >> tmp

echo /plotname surface_efield > tmp2
echo /yscale 50e-4 >> tmp2
echo /xaxisoffset 2e-4 >> tmp2
echo /xrastaxis 1 >> tmp2
xy sefield -dx .5 >> tmp2
echo fields written

str s
int i = 0
int depth
str Imtitle = "tplot"
str Vmtitle = "vtplot"
echo /graphtitle {chr(34)} Im vs t : {runid} {chr(34)} > {Imtit
le}
echo /graphtitle {chr(34)} Vm vs t : {runid} {chr(34)} > {Vmtit
le}
for(depth=0;depth<ntotal;depth=depth+2)
    echo /newplot >> {Imtitle}
    echo /plotname {depth} >> {Imtitle}
    echo /yscale -1 >> {Imtitle}
    echo /xaxisoffset {-7e-5*i} >> {Imtitle}
    echo /xrastaxis 1 >> {Imtitle}
    asciidata Im -c {depth} -old -xy >> {Imtitle}
    i = i+1
end
int i = 0
```

```
for(depth=0;depth<ntotal;depth=depth+8)
    echo /newplot >> {Vmtitle}
    echo /plotname {depth} >> {Vmtitle}
    echo /xaxisoffset {-30*i} >> {Vmtitle}
    echo /xrastaxis 1 >> {Vmtitle}
    asciidata Vm -c {depth} -old -xy >> {Vmtitle}
    i = i+1
end
echo {Imtitle} and {Vmtitle} written

Imtitle = "zplot"
Vmtitle = "vzplot"
echo /graphtitle {chr(34)} Im vs z : {runid} {chr(34)} > {Imtit
le}
echo /graphtitle {chr(34)} Vm vs z : {runid} {chr(34)} > {Vmtit
le}
for(i=3;i<60;i=i+3)
    echo /newplot >> {Imtitle}
    echo /plotname {i} >> {Imtitle}
    echo /yscale -5e4 >> {Imtitle}
    echo /xaxisoffset {-i} >> {Imtitle}
    echo /xrastaxis 1 >> {Imtitle}
    asciidata Im -t {i} -old -xy >> {Imtitle}

    echo /newplot >> {Vmtitle}
    echo /plotname {i} >> {Vmtitle}
    echo /xaxisoffset {-i*10} >> {Vmtitle}
    echo /xrastaxis 1 >> {Vmtitle}
    asciidata Vm -t {i} -old -xy >> {Vmtitle}
end

echo {Imtitle} and {Vmtitle} written
```

matrix.g

```
//genesis
schedule
addschedule Simulate /##[CLASS=matrix] -action PROCESS
addschedule Simulate /##[] -action RESULTS
create matrixsolver /mat
set /##[TYPE=compartment] method 10     // backward euler
    // register state vars with solver
setupmatrix /pyramidal/##[TYPE=compartment] /mat
call /mat SETUP                         // construct the matric
es
```

pyramidal.g

```
//genesis

echo creating a pyramidal cell
// ============================================================
//                      PYRAMIDAL CELL ARRAY
// ============================================================

pyramidal_cell(/pyramidal)

position /pyramidal I I 350e-3
```

savedata.g

```
//genesis
if(argc < 1)
    echo usage: savedata directory
    return
end
echo saving data to directory $1
mkdir $1
cp Im Vm GEX GINH RUNID RUNFILE $1
touch LOGFILE
echo -n $1 " : " >> LOGFILE
cat RUNID >> LOGFILE

echo done
```

stimb.g

```
// genesis

int MULTIPLE = 0
int SUPERCL = 0

clearstim
float amp = 10.0
float amp2 = 0.0
float amp3 = 0.0
float iamp = amp*2
float iamp2 = amp2*2
float iamp3 = amp3*2

set /pyramidal/Ia[]/K tau1 10
set /pyramidal/supIb[]/K tau1 10
set /pyramidal/deepIb[]/K tau1 10

//compartment   channel time    amplitude   reps    intvl   tau

// ------------------------------------------------------------
------------
expstim Ia  Na  1.0     {1.0*amp}   10  0.1 5

expstim supIb   Na  6.0     {1.0*amp}   20  0.5 10
expstim deepIb  Na  8.0     {0.6*amp}   30  1.0 10
expstim III Na  5.0     {0.8*amp}   20  0.5 5
expstim uppersoma Cl    5.0     {0.3*iamp}  20  0.5 5
expstim soma    Cl  5.0     {0.6*iamp}  20  0.5 5
expstim lowersoma Cl    5.0     {3.0*iamp}  20  0.5 5
expstim Ia  K   5.0     {0.3*amp}   20  0.5 5
expstim supIb   K   5.0     {0.3*amp}   20  0.5 5

if(SUPERCL)
expstim Ia  Cl  5.0     {0.0*iamp}  20  0.5 5
expstim supIb   Cl  5.0     {0.2*iamp}  20  0.5 5
expstim deepIb  Cl  5.0     {0.2*iamp}  20  0.5 5
end

if(MULTIPLE)

expstim supIb   Na  31.0    {1.0*amp2}  20  0.5 10
expstim deepIb  Na  33.0    {0.6*amp2}  30  1.0 10
expstim III Na  30.0    {0.8*amp2}  20  0.5 5
expstim uppersoma Cl    30.0    {0.3*iamp2} 20  0.5 5
```

```
expstim soma    Cl  30.0    {0.6*iamp2} 20  0.5 5
expstim lowersoma Cl    30.0    {3.0*iamp2} 20  0.5 5
expstim Ia  K   30.0    {0.2*amp2}  20  0.5 5
expstim supIb   K   30.0    {0.2*amp2}  20  0.5 5
expstim deepIb  K   30.0    {0.2*amp2}  20  0.5 5

expstim supIb   Na  56.0    {1.0*amp3}  20  0.5 10
expstim deepIb  Na  58.0    {0.6*amp3}  30  1.0 10
expstim III Na  55.0    {0.8*amp3}  20  0.5 5
expstim uppersoma Cl    55.0    {0.3*iamp3} 20  0.5 5
expstim soma    Cl  55.0    {0.6*iamp3} 20  0.5 5
expstim lowersoma Cl    55.0    {3.0*iamp3} 20  0.5 5
expstim Ia  K   55.0    {0.2*amp3}  20  0.5 5
expstim supIb   K   55.0    {0.2*amp3}  20  0.5 5
expstim deepIb  K   55.0    {0.2*amp3}  20  0.5 5

end

timestamp stimb.g
```

stimulate.g

```
// genesis

function clearstim
    set /##[TYPE=playback] start 0 end 0 current 0
end

str s
function stim(path,channel,t,amp,reps,intvl)
float t,amp
int reps
float   intvl
int i
// deliver a pulse
    for(i=0;i<reps;i=i+1)
    foreach s ({EL(/pyramidal/{path}[]/{channel}/pre)})
        putevent {s} {t+i*intvl} {amp/getclock(0)}
        putevent {s} {t+getclock(0)+i*intvl} 0
    end
    end
end

function expstim(path,channel,t,amp,reps,intvl,tau)
float t,amp
int reps
float   intvl
float   tau
int i

// deliver a pulse
    for(i=0;i<reps;i=i+1)
    foreach s ({EL(/pyramidal/{path}[]/{channel}/pre)})
        putevent {s} {t+i*intvl} {exp({-i*intvl/tau})*amp/getcl
ock(0)}
        putevent {s} {t+getclock(0)+i*intvl} 0
    end
    end
end
```

tau.g

```
//genesis

float val
float logval
float maxval=0
float minval=-999
int count=0

touch nul.log nul.val
rm nul.log nul.val

// extract the data from the Vm file

simdump Vm -c 0 > Vm0

openfile Vm0 r
// read in 100 msec
// find the maxval
for(count=0;count<200;count=count+1)
    val = readfile(Vm0)
    if(val < maxval)
    maxval = val
    end
    if(val > minval)
    minval = val
    end
end

openfile Vm0 r
for(count=0;count<200;count=count+1)
    val = 1.0 - ((readfile(Vm0) - minval)/(maxval -minval))
    logval = log({val})
    echo {val} >> nul.val
    echo {logval} >> nul.log
end
closefile Vm0
```